1-1-2012

Natural Convection And Soret Effect In A Multi-Layered Liquid And Porous System

Hussam K. Jawad
Ryerson University

NATURAL CONVECTION AND SORET EFFECT IN A MULTI-LAYERED LIQUID AND POROUS SYSTEM

by

(Hussam K. Jawad, B.Sc. in Mechanical Engineering,

Baghdad University, Iraq, 1988)

A thesis

presented to Ryerson University

in partial fulfillment of the

requirement for the degree of

(Master of Applied Science)

in the Program of

(Mechanical Engineering)

Toronto, Ontario, Canada, 2012

Author Declaration

I hereby declare that I am the sole author of this thesis. This is a true copy of the thesis, including any required final revisions, as accepted by my examiners.

I authorize Ryerson University to lend this thesis to other institutions or individuals for the purpose of scholarly research.

I further authorize Ryerson University to reproduce this thesis by photocopying or by other means, in total or in part, at the request of other institutions or individuals for the purpose of scholarly research.

I understand that my thesis may be made electronically available to the public.

ABSTRACT

NATURAL CONVECTION AND SORET EFFECT IN A MULTI-LAYERED LIQUID AND POROUS SYSTEM

Master of Applied Science, 2012

Hussam K. Jawad

Mechanical and Industrial Engineering

Ryerson University

We investigated the onset of natural convection and thermodiffusion in an initially quiescent multi-layer system consisting of a porous layer sandwiched between two layers of a binary mixture, while the whole system is being heated from above. Two different water-alcohol mixtures were used with Soret coefficients of opposite sign. Then in similar situation a hydrocarbon mixture were investigated. It was found that when the Soret coefficient is negative, the lighter species migrates towards the colder surface while the denser species migrates towards the hotter surface. When the Soret coefficient is positive, the lighter species migrates towards the hotter surface while the denser species migrates towards the colder surface. Also, increasing the temperature difference leads to a greater separation of the mixture components because of the increase in the density gradient. In addition, increasing the porosity reduces the separation ratio due to the increased fluid mixing in the pores.

ACKNOWLEDGEMENTS

I would like to sincerely thank Prof. Dr. Ziad Saghir of Ryerson University for his helpful assistance, guidance, and encouragement throughout the completion of this thesis. Without his help, it was quite impossible for the author to complete this thesis. The author also acknowledges the support and useful suggestions of his colleague Mr. Md. Rahman, PhD students of Ryerson University, who helped me during my research. The author would also like to express his appreciation and deep thanks to his mother, wife, and kids. I thank them for their love, patience, and support during all my studies. I would like to dedicate this thesis to them.

TABLE OF CONTENTS

LIST OF TABLES

LIST OF FIGURES

LIST OF Appendices

NOMENCLATURE

B	Buoyancy force
c	Concentration of the fluid
C	Non-dimensional concentration of the fluid
C_B	Concentration of the lighter component at the bottom
C_T	Concentration of the lighter component at the
$(C_p)_f$	Specific heat of liquid at constant pressure (J/Kg.K)
d	Diameter of glass beads (m)
$d1$	Height of the bottom fluid layer (m)
$d2$	Height of the top fluid layer (m)
$d3$	Height of the porous layer (m)
D	Width of the cavity (m)
Da	Darcy number = K/L^2
D_M	Solutal diffusion coefficient (m^2/s)
D_T	Thermal diffusion coefficient ($m^2/s.k$)
g	Gravitational acceleration (m/s^2)
Gr_T	Thermal Grashof number
h	Thickness of the layer (m)
H	Total thickness of the model (m)
J	Mass diffusion flux (kg/m^2 .s)
K	Permeability of porous media (m^2)
k_f	Conductivity of the fluid (W/m.k)
k_s	Conductivity of the solid (porous media) (W/m.k)

k_e	Effective thermal conductivity (W/m.k)
L	Characteristic length of the cavity in Y-direction=$d1+d2+d3$ (m)
Le	Lewis number = D_M/α
M	Mass (g)
MW	Molecular weight (g/mol)
N	Buoyancy ratio = $\beta_C/\beta_T.\Delta T$
N^*	Number of moles (mol)
Nu	Nusselt number
Nu_H	Nusselt number on the hot surface
Nu_C	Nusselt number on the cold surface
Nu_{avg}	Average Nusselt number
p	Pressure (Pa)
P	Non-dimensional pressure = $p.L/\mu.uo$
Pr	Prandtl number = ν/α
q	Separation ratio
Q	Heat transfer rate (J)
Ra_{TL}	Thermal Rayleigh number for fluid layer = $\frac{g.\beta_T.\Delta T.d_{1,2}^3}{\gamma\alpha}$
Ra_{TP}	Thermal Rayleigh number for porous layer = $\frac{g.\beta_T.\Delta c.d_3.K}{\gamma\alpha}$
Ra_{SL}	Solutal Rayleigh number in fluid layer = $\frac{g.\beta_C.\Delta C.d_{1,2}^3}{\gamma\alpha}$
Ra_{SP}	Solutal Rayleigh number in porous layer = $\frac{g.\beta_C.\Delta c.d_3 K}{\gamma\alpha}$

Re Reynolds number = $\frac{\rho_0.u_0.L}{\mu}$

Sc Schmidt number = γ/D_M

S_T Soret coefficient =D_T/D_M (1/k)

t Time (s)

T Temperature (k)

u Velocity component in the x direction (m/s)

u_0 Characteristic velocity = $\sqrt{g.\beta T.\Delta T.L}$ (m/s)

U Non-dimensional velocity component in the X direction = u/uo

v Velocity component in the y direction (m/s)

V Non-dimensional velocity component in the Y direction = v/uo

V_v Volume occupied by voids (cm^3)

V_T Total volume of the porous material (cm^3)

X Non dimensional x coordinate

X^* Molar fraction (%)

Y Non dimensional y coordinate

Greek Symbols

α Thermal diffusivity = $\frac{k_f}{\rho_{0.}(C_p)_f}$ (m^2/s)

β_C Solutal expansion coefficient

β_T Thermal expansion coefficient (1/k)

θ Non-dimensional temperature = $(T-T_C)$ / (T_h-T_C)

τ Non-dimensional time

τ_D	Diffusive characteristic time (s)
τ_{th}	Thermal characteristic time (s)
μ	Dynamic viscosity (kg/m.s)
γ	Kinematic viscosity (m^2/s)
ρ	Density (kg/m^3)
ρ_0	Density of the fluid at reference temperature T_0 (kg/m^3)
$\emptyset$	Porosity

Subscripts

0	Reference
c	Cold
e	Effective
f	Fluid
h	Hot
i	i th component
L	Liquid
p	Porous
s	Solid

CHAPTER 1

Theory and Literature Review

1.1 Introduction

1.1.1 Onset of Natural Convection

A porous media is defined as a material containing interconnected pores. The skeletal part of the material is called the “solid” or “matrix”, and the voids between them (pores) are normally filled with a fluid. Figure 1.1 shows a fluid flow in a porous media. Examples of porous media are prevalent throughout everyday life, ranging from natural substances such as soils, rocks, wood and limestone, biological tissues such as bones and animal fur, and man-made materials such as cements, brick, ceramics and fibreglass.

Natural convection occurs in fluids due to the density gradient created by a temperature difference. This occurs since fluids of different temperatures have different densities. The fluid motion occurring from the mechanism of natural convection is not generated by any external source such as pumps, fans, or compressors. The motion is generated only due to the buoyancy forces induced in the system. When density decreases due to the rise in temperature, the lighter (less dense) components of the fluid rise and the heavier (more dense) components fall, leading to an unstable system that produces fluid motion. Through natural convection, hot fluid particles move from the bottom to the top of the space occupied by the fluid. The instability of the system occurs due to the opposite direction of buoyancy forces and natural convection.

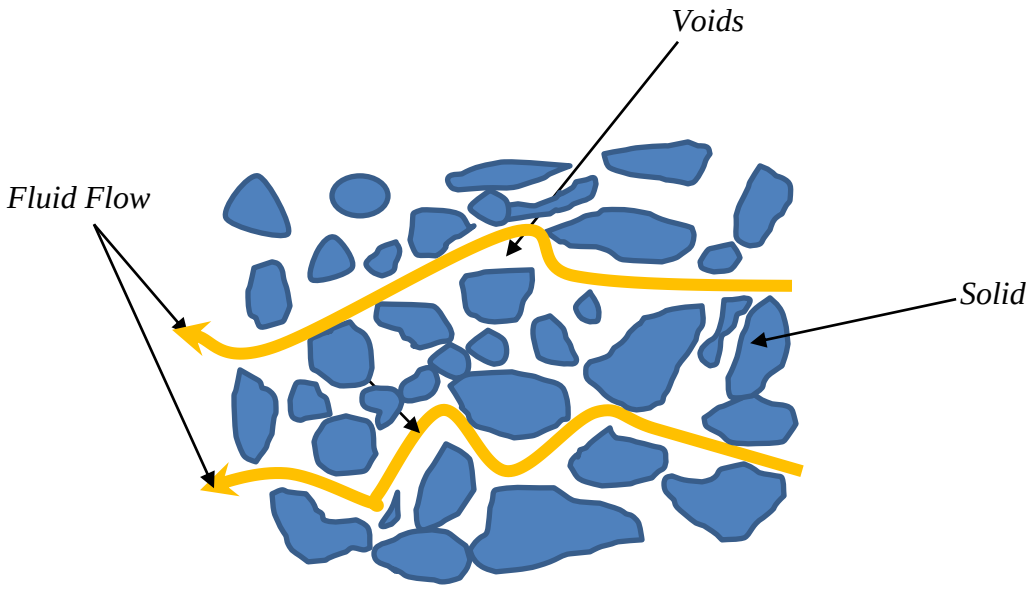

Figure 1.1: Schematic diagram of a fluid flow in a porous media

The buoyancy force is strongly associated with the gravitational acceleration and their relation is expressed as:

$$B = \rho_f . V_f . g$$

Where B, ρ_f, V_f and g are the buoyancy force, fluid density, volume of the displaced fluid, and gravitational acceleration, respectively. Hence, we can understand the impossibility for natural convection to occur in zero gravity environments. The study of natural convection in stacked systems consisting of a porous layer sandwiched between two fluid layers and subjected to heating from the top surface is of great importance due to the common occurrence of the system in many natural and industrial applications, particularly in oil reservoirs.

1.1.2 Onset of Thermosolutal Convection with Soret Effect

The phenomenon of mass flux in a mixture due to a temperature gradient is called the thermosolutal, thermodiffusion, or Soret effect. This phenomenon gained the attention of scientists, researchers, and engineers in the last decade due to its crucial role in many engineering and geophysical applications such as mineral migration and mass transfer in living matters, the analysis and study of compositional variation in hydrocarbon reservoirs, the separation of isotopic and isobaric mixtures [1], and drying processes or solute transfer in the mushy layer during the solidification of binary alloys [2]. The value of the Soret effect in a binary mixture can be obtained from the Soret coefficient (S_T), which represents the ratio of the thermal diffusion coefficient (D_T) to the molecular diffusion coefficient (D_M). This relationship can be stated as the following equation:

$$S_T = -\frac{\beta_C D_T}{\beta_T D_M} \tag{1.1}$$

where β_C is the solutal expansion coefficient and β_T is the thermal expansion coefficient. Convection due to buoyancy has a large influence on the accuracy of S_T, but the inherent flow resistance in a porous media reduces this influence. The separation ratio (q) describes the power of the Soret effect for a mixture, and it can be calculated from the following equation:

$$q = c_0 (1 - c_0) (\beta_C / \beta_T) S_T \tag{1.2}$$

where c_0 is the initial concentration of the mixture.

1.2 Motivations

The phenomenon of heat and mass transfer in a system that contains layers of both fluids and porous media is of great importance because of the common occurrence of the system in many environmental, natural, and industrial applications. Below are some of the applications in which this system occurs:

- Ground water pollution,
- Migration of minerals and mass transport modeling in living matters,
- Geothermal systems, crude oil production,
- Storage of nuclear waste material,
- Solidification of castings,
- Extraction of oil from oil sand and deep oil reservoirs,
- Thermal insulation systems.

1.3 Objectives and Organization of the Thesis

The main objectives of this thesis are to study natural convection and thermodiffusion in an initially quiescent multilayer system consisting of a porous media layer sandwiched between two layers of a binary mixture, where the whole system is heated from above (top horizontal surface). Additionally, I investigate the effect of temperature difference, the sign of the Soret coefficient, and the effect of the porosity of the porous material on the aforementioned phenomena. I performed a series of numerical studies utilizing finite element techniques in order to achieve these objectives.

The thesis is divided into six main parts. First, the theoretical concepts and literature regarding natural convection and thermodiffusion, are discussed in chapter one. The simulations using the algorithm and plots from the visualizing tool are also presented. The dimensional and non-dimensional forms of the governing equations, geometrical and numerical models, and related boundary conditions are introduced in chapter two. In chapter three, natural convection in a multi-layered system of porous media squeezed between two binary fluid layers are discussed in detail, with a full comparison of the effect of heating orientation. To examine the importance of the Soret coefficient, thermodiffusion in water-alcohol mixtures with either negative or positive Soret coefficients are discussed in detail in chapter four. In chapter five, the same study of the Soret effect has been conducted on a hydrocarbon mixture, with the investigation of the relationship between porosity and the Soret effect. Finally, in chapter six, the conclusions and contributions are discussed, and recommendations for future work are suggested.

1.4 Literature Review

As mentioned earlier, the study of natural convection and thermodiffusion in a system consisting of fluid and porous layers has attracted much attention in the scientific community. The groups investigate and identify the most important parameters that affect heat and mass transfer in porous medium during natural convection and thermodiffusion. A detailed review of the related literature provides the framework for the present study. First, the literature on natural convection in systems of porous layers saturated by fluid is reviewed. Thereafter, the literature on thermodiffusion in porous media saturated with binary fluids is presented.

Nield [3] applied linear stability analysis to a two-layer system of a fluid on a porous layer, with a constant heat flux applied from the bottom. For an accurate analysis of interfacial fluid motion between the fluid and the porous media, and relating that to the shear stress in the fluid and slip velocity at the interface area, he used the Beavers-Joseph condition. He proposed the possibility of mass and heat transfer (at the interface) from the low surface-tension area to the area of high surface tension, which is known as the Marangoni Effect. This model is important for studying convection in a system consisting of porous and fluid layers, particularly because it adds in the effects of gravitational and surface tension numbers. This work is the current standard, and its equations are commonly used by engineers and scientists.

Somerton *et al.* [4] studied the onset of convection for a system consisting of a fluid layer overlaying a porous layer saturated with a fluid, with the system heated or cooled from below. The Brinkman extension of Darcy's law was used for calculating a wide range of independent physical parameters, such as the Darcy number, the Rayleigh number, thermal conductivity, effective viscosity, and permeability in the system. The results showed that fluid stability is inversely proportional to the Darcy number, because an increase in the permeability of the porous layer allows more fluid motion. It was found that at a higher thermal conductivity ratio (k_f / k_s) the fluid layer becomes more stable due to the lack of convection rolls. Also, they found that the critical Rayleigh number increases with a stabilizing temperature gradient and decreases with a destabilizing temperature gradient.

Saghir *et al.* [5] investigated the flow structure and mechanism of heat flow for a liquid layer overlaying a porous layer. They studied and analyzed the onset of the convection for two different cases: when the system was heated from the bottom and when a lateral heating was supplied to the system. Their system consisted of a rectangular enclosure filled with a porous

layer underneath a fluid layer, in which they studied the effect of changing the aspect ratio *(AR)* of the system, which is defined as the ratio of the cavity width to its thickness. For the first case (bottom heating) the study found that the *AR* will modify the flow configuration when there is natural convection in the liquid layer, while for the porous layer the *AR* has no effect. Further, large convective motion was present at a low thickness ratio of the liquid layer (defined as the ratio of layer thickness to the total thickness of both layers) and weakens as the thickness ratio increases. For the second case (lateral heating), multi-cellular flow is present for the liquid layer when the *AR* is large. The porous layer acts as an obstacle blocking the flow into the porous media. They concluded that for both cases (bottom or lateral heating), the liquid layer thickness determines whether the flow is mainly in the porous or liquid layer, and for some values of *AR* multi-cell flow patterns occur in addition to the Marangoni convection, both of which enhance the flow in the enclosure.

Pillatsis *et al.* [6] performed a linear stability analysis on a horizontal porous layer (with Darcy flow and the Boussinesq approximation) sandwiched between two fluid layers with the top and bottom boundaries dynamically free and kept at fixed temperatures. They applied the Beavers-Joseph interfacial boundary conditions between the fluid and porous layers. They reported the stability analysis of the same configuration studied by Nield, [3] and compared their results to those of Nield except with free boundary conditions and a constant heat flux. They also discussed their results with respect to the quantitative effects of both thermal (constant heat) and hydrodynamic (free or rigid) boundary conditions. They found that when the boundary between a fluid layer and the porous layer closes, the critical conditions for the onset of convective motion in two different modes were affected. When the boundary is closed, the critical Rayleigh number is reduced due to the slip effect at the interface between the fluid layer and the porous layer.

They also found that for a low-permeability porous layer, the critical Rayleigh number is highly affected by the slipping conditions.

Taslim and Narusawa [7] performed a stability analysis for the onset of convective motion in three systems of horizontal porous and fluid layers in the following configurations:

a. A porous layer sandwiched between two fluid layers with rigid boundaries from the top and bottom,
b. A fluid layer over a porous medium layer, and
c. A fluid layer sandwiched between two layers of porous media.

A detailed examination of the three systems was performed for a wide range of depth ratios (depth of the porous layer / depth of the fluid layer). They also studied the effect of the thermal conductivity ratio, the non-dimensional proportionality constant in the Beavers-Joseph condition, and the square root of the Darcy number on the critical Rayleigh number and the critical wave number. The authors used the slip conditions to predict the critical conditions for the onset of convective motion for various cases when the depth ratio, the square root of the Darcy number, and thermal conductivity ratio all possessed high values. They also found that the critical conditions for the onset of convective motion are highly dependent on the depth ratio and the value of the thermal conductivity. However, these critical conditions are only moderately affected by the square root of the Darcy number.

The phenomenon of crude oil flow through layers of rock, sand, limestone, and shale as well as other geological and industrial applications motivated Vafai and Thiyagaraja [8] to analyze the fluid flow and heat transfer at interface regions between porous and fluid layers. Three different types of interface zones have been selected: (a) the interface between two different porous layers, (b) the interface between porous and fluid layers, and (c) the interface between porous and

impermeable layers. By employing the Forchheimer-Extended Darcy equation in their analyses and taking into account the continuity of shear stress and heat flux, they performed a detailed analysis for the distribution of velocity and temperature for the three zones. This study is considered the fundamental study of interfacial interactions around a saturated porous medium. They established that an analytical solution helps in improving the equations and relationships dealing with porous media. They also found reasonable agreement between analytical and numerical solutions can be achieved for a variety of practical situations.

The Beavers-Joseph condition was one of the first studies describing fluid mechanics at the interface between fluid and porous layers. . Based on this work, Vafai and Kim [9] studied the fluid mechanics at the interface between fluid and porous layers. Their study focused on the effects of Darcy's law and the inertia parameter on the fluid mechanics of this interfacial system. The model that was used in their work consisted of a fluid layer sandwiched between a porous layer from the top and a rigid boundary from the bottom. Their main conclusion was the first exact solution for the fluid mechanics at the interface between the fluid and porous layers. They found that the fluid velocity is affected by:

- The Darcy number: Any decrease in the Darcy number will decrease the permeability of the porous layer, which leads to a lower mass flux through the porous layer.
- The product of multiplying the Reynolds number by the inertia parameter: A higher value of (Re x Inertia Parameter) means greater resistance against the flow in the porous layer, which leads to a higher velocity of the fluid through the open area.

To obtain an exact description of transport phenomena (heat, mass, or momentum) at the interface between fluid and porous layers for any numerical model, it is necessary to specify and select a boundary and/or initial condition. Alazmi and Vafai [10] used the same system

configuration which was used by Vafai and Kim [9] to investigate the differences in heat and mass transfer using different boundary conditions for the interfacial region between fluid and porous layers while employing the Brinkman equation. They used various boundary condition models to investigate the effects of selected physical parameters such as Reynolds number, effective viscosity, porosity, Darcy number, slip coefficient, and inertia parameter on the fluid flow and heat transfer at this interface. They examined the convergence of the models for the applied parameters. They found that the physical parameters have a large effect on the flow velocity, a small effect on the temperature, and even less effect on the Nusselt number.

Umavathi *et al.* [11] studied unsteady (oscillatory) fluid flow and heat transfer in a porous media sandwiched between two viscous fluid layers. The system they modeled consists of three layers: a homogeneous and isotropic porous layer saturated with a viscous fluid and sandwiched between two different fluid layers. They applied boundary and interfacial conditions to find closed-form solutions for each region separately, and then computed numerically the effects of various physical properties such as porosity, periodic frequency, frequency, conductivity ratios, and viscosity ratios on the fluid velocity and temperature. They concluded that an increase in the value of each of porosity, Prandtl number, conductivity ratios, and viscosity ratios causes a reduction in the both temperature and velocity, which in turn restrains the flow. On the other hand, an increase in the frequency parameter and Eckert number values leads to an increase in both the temperature and velocity, which increases the flow. They also found that higher conductivity ratios and viscosity ratios increase the heat transfer rate at the top wall, while decreasing the heat transfer rate at the bottom wall.

Chang [12] studied the stability of thermal convection in a two-layer system with horizontal plane Couette flow. He used a system consisting of a fluid layer over a porous layer saturated with the same fluid sandwiched by two plates. The lower plate was kept warmer than the upper plate, and movement of the upper plate at a constant speed generated shear. He studied the effect of the flow shear and Prandtl number on both longitudinal and transverse convection rolls to provide a general analysis of the stability mechanism for thermal convection in the system. It was found that the onset of instability is controlled by the longitudinal mode and its neutral curve does not depend on the plane Couette flow, Reynolds number, and Pandtl number of the fluid.

Chang [13] extended his previous investigation by examining the thermal convection in a system consisting of a fluid layer over a layer of a porous medium saturated with the same fluid. The system was heated from below and subjected to a horizontally plane Poiseuille flow (a flow with pressure drop through the flowing stream). He investigated the effects of the plane Poiseuille flow on the known instability mechanism of thermal convection in an unstable two-layer system. The author found that for longitudinal rolls at any depth, the onset of the instability ratio and the stability characteristics for the longitudinal rolls are independent of the Reynolds and Prandtl numbers. However, the stability of the transverse mode is strongly dependent on the Reynolds and Prandtl numbers, and it may be the same as for the longitudinal mode when the Reynolds and Prandtl numbers are close to zero. This similarity at low Reynolds and Prandtl numbers explains the stabilizing effects of the plane Poiseuille flow on the fluid layer.

Bukhari [14] applied a numerical linear stability analysis to a bottom-heated system consisting of a horizontal viscous fluid layer sandwiched between porous layers saturated with the same fluid. He computed the stability curves of thermal convection in the viscous fluid using a reciprocal thermal conductivity of 0.7 W/ (m·K), a Darcy number of $4x10^{-6}$ md, a Beavers-Joseph constant

of 0.1, and depth ratios of 0.01 to 0.2. He determined that the Rayleigh and wave numbers are inversely related to the depth ratio: As the depth ratio decreases, for a constant value of the wave number the Rayleigh number increases, and for a constant value of the Rayleigh number the wave number increases.

Chen [15] implemented a linear stability analysis of the convection instability in a system consisting of a porous layer under a fluid layer with flow in the vertical direction. The top wall was kept at constant temperature that was lower than the bottom wall. Since the convection stability is independent of the Prandtl number (*Pr*) in the porous layer while *Pr* has a large effect on the convection stability in the fluid layer, Pr may play an important role in the convection stability of a system consisting of both porous and fluid layers. For this reason, Chen considered the depth ratio, *Pr*, and the through flow strength to be the most important parameters in the study. The author found that in a system consisting of both porous and fluid layers it is possible to enhance both the stabilizing and destabilizing factors for vertical flow. Changing the depth ratio or the strength and direction of the flow gives more accurate control of the buoyantly driven instability in porous and fluid layers. For instance, he found that for a depth ratio of 0.1, where the onset of convection occurs in both fluid and porous layers, the effect of *Pr* is minimal and there is a linear relationship between the flow strength and the critical Rayleigh number. Whereas, for a depth ratio of 0.2, where the onset of convection mainly occurs in the fluid layer, the critical Rayleigh number is proportionally related to the square of the flow strength.

Balasubramanian *et al.* [16] performed a linear stability analysis on thermal convection in a system consisting of a horizontal fluid layer sandwiched between two porous layers of different permeability and thermal properties. They studied the effect on the onset of convection in the fluid layer created by the bounding porous walls, and compared that with the predicted results

obtained from free-free boundaries and rigid-rigid boundaries. They found that the onset of convection for the bounding porous walls is earlier than for rigid-rigid boundaries but later than for free-free boundaries. This result is because the critical Rayleigh number increases when the values in Darcy's law for the lower and upper porous walls increase, and this is the same for the relationship between the critical Rayleigh number and the Biot number for the lower and upper porous walls. They also found that the wave number for adiabatic boundaries is less than for isothermal-isothermal boundaries. From the above results, they concluded the following:

- $\mathrm{Ra}_{\text{free}} \leq \mathrm{Ra}_{\text{porous}} \leq \mathrm{Ra}_{\text{rigid}}$
- $a_{\textit{free-free}} \leq a_{\textit{porous}} \leq a_{\textit{rigid-rigid}}$

Where *Ra* is the Rayleigh number and *a* is the wave number.

Rudraiah *et al.* [17] studied the fluid flow in a sparsely packed porous medium sandwiched between two fluid layers. They specified proper boundary conditions for porous layers of different depths and properties. For this reason, two configurations were used in their study: (a) a thin, sparsely packed porous medium sandwiched between two thick fluid layers, and (b) a thick, sparsely packed porous medium sandwiched between two thin fluid layers. They studied the effect of the porous layer thickness, viscous parameter, and porosity on the mass flow and friction factor in these systems. The authors found that increasing the thickness of porous layer will decrease the mass flow rate, which can be controlled by varying the thickness of porous and fluid layers. However, when the thickness of the porous layer is increased, the friction factor is decreased due to the low resistance to the flow offered by the low density of the porous medium.

Prasad *et al.* [18] conducted flow visualization and heat transfer experiments for buoyancy-driven flow in a cylindrical cavity filled with a fluid-superposed porous layer of beads that was heated from below. The authors observed that the flow is highly complex and active flow

interactions between the fluid and the underlying porous layer were seen even when the Rayleigh number for the porous layer was of the order of unity. Results showed that there was a sharp drop in the critical Rayleigh number from the value of $4Л^2$ when the porous layer thickness was reduced below unity. This is due to the convective flow moving from the porous layer to the fluid layer. They also found that for beads of small diameter the Nusselt number decreases when the thickness ratio increases. For larger size of beads, the Nusselt number decreases with the thickness ratio until the minimum particle size is reached (particle diameter / total height of the cavity), at which point it begins increasing again. The authors show that the Rayleigh number, particle size, thickness ratio, thermal conductivity ratio, and fluid viscosity all have important effects on the heat transfer rate.

V. Prasad [19] extended the above experimental study and conducted a visualized flow field and heat transfer experiment for natural convection in a bottom-heated and top-cooled cylindrical enclosure filled with a fluid over a horizontal porous layer saturated with the same fluid. The purpose of this experiment was to investigate the heat transfer and visualised flow field for a wide range of physical properties such as Rayleigh number, Prandtl number, porous layer height, and thermal conductivity ratio. He used a Plexiglas tube (7-inch. diameter) as a cylindrical enclosure with a bottom end made out of an aluminum plate (0.25'' thick), which was heated by a thermo foil heater fixed underneath the plate. A similar plate fixed to the top end was cooled by circulated water supplied from a constant-temperature circulator to obtain an isothermal surface. In order to reduce the heat loss due to conduction from the bottom end, the enclosure was placed inside a Plexiglas recess (1'' thick plate). A number of thermocouples placed on both sides of the enclosure were used to calculate the approximate heat lost by conduction. The enclosure was insulated and another group of thermocouples were fixed at radial locations. He used different

sizes and materials of spherical beads as the porous layer to fill to the desired height, then filled the cylindrical enclosure with fluid (Dow Corning 200, silicon fluid and ethylene glycol) with maintain the aspect ratio (*AR*) to be equal to one. For the flow visualization, he used very fine aluminum particles (diameter = 5-20 μm) which were lit by a beam of light passing through the center axis of the enclosure, and time exposures were recorded optically by a camera. He observed that the heat transfer rates and convective flow are related to the particle size, Rayleigh number, porous layer height, and thermal conductivity ratio, which shows that the rate of heat transfer in the system can be raised by using porous media with a high thermal conductivity. This result explains why the energy transferred in a system filled with porous media is greater than one filled with fluid when the permeability of the porous media is high and the conductivity ratio is low. He also found that regardless of the thermal conductivity ratio, the relationship between the Nusselt number and the porous medium layer thickness is not simple. However, the Prandtl number has no effect on the convection rate as long as the Prandtl number is large and the permeability of the porous medium is high.

Beckermann *et al.* [20], motivated by natural convection in a solidifying cast, performed a numerical and experimental study to investigate the steady-state convection fluid flow and heat transfer between fluid and porous media. They used a rectangular enclosure partially filled with a fluid-saturated porous medium, and they applied a temperature gradient in the horizontal direction of the system. The porous medium consisted of spherical beads, and a mixture of water and glycerine was the fluid. The interface region between the fluid and the porous layer was permeable to allow the fluid to move between layers. The authors found that the flow penetration into the porous layer increases with an increase in the Darcy number, because larger beads (porous media) have less resistance to the fluid flow, which allows natural convection to occur in

the entire enclosure, while for smaller beads there is almost no penetration into the porous region. They also found that when the fluid penetrates into the porous layer, natural convection in the entire enclosure is different compared to that in fully porous or fluid-filled cells.

P. Nithiarasu *et al.* [21] investigated the effect of porosity on natural convection and heat transfer in a fluid-saturated porous medium using a generalized non-Darcy model with porosity as a separate parameter and applying the Boussineq approximation to the momentum equation. The authors found that at higher Darcy numbers, there is a large effect of the porosity on both the convective flow and heat transfer in the fluid-saturated porous medium. This effect is smaller but not negligible at lower Darcy numbers.

K. Vafai *et al.* [22] studied the effect of a boundary and the inertial forces on fluid flow and heat transfer in a porous medium confined by an external boundary. Specifically, the authors examined the flow through the porous medium near to an impermeable boundary. The authors found three important flow resistances in this model: the bulk damping resistance due to the porous structure, the viscous resistance due to the boundary, and inertial resistance due to the inertial forces. They found that there are minimal effects of the boundary on the flow, but it has a large effect on the heat transfer. They also found that the inertial effects increase with a higher permeability and lower fluid viscosity and that the velocity gradients increase close to the walls, which leads to an increase in the viscous resistance (due to the boundary). Accordingly, the boundary effects are further enhanced when inertial forces increase.

Raptis *et al.* [23] studied the phenomena of natural convection and heat transfer flow of a viscous incompressible fluid passing through a porous layer surrounded by a vertical plane walls. They studied the effect of the Grashof number (Gr) and permeability (K) of the porous layer on the velocity and rate of heat transfer. The authors found that when the permeability of the porous

medium increased, the flow velocity also increased. This phenomenon is more noticeable with a higher value of *Gr*. They also found that the velocity increased when the concentration difference above and below the porous layer increased. They observed that the media porosity plays an important role in reducing the rate of heat transfer, especially in systems with a higher *Gr*.

Kim *et al.* [24] studied the effects of the Darcy number, Prandtl number, and Reynolds number on a local thermal non-equilibrium system consisting of porous media and a fluid, by comparing the temperature of the solid phase with the temperature of the fluid phase when the values of the numbers were varied. The authors used the thermal non-equilibrium test to investigate different problems of convective heat transfer. They found that the local thermal equilibrium condition could be satisfied with high values of porosity, scaled thermal conductivity ratio, and heat transfer coefficient. A porous medium such as metal foam that has low thermal conductivity of the interstitial fluid compared to that of the solid, gives low values of the thermal conductivity ratio. Porous media with low thermal conductivity ratio cause more heat to be transferred by conduction through the solid rather than heat convection through the fluid.

Huke *et al.* [25] conducted two- and three-dimensional numerical investigations on laterally periodic convection structures of binary mixtures (ethanol-water) in the Rayleigh–Bénard system with positive Soret effect. They found that ethanol, which is the lighter component of the mixture, immigrated in the direction of the hot surface. They also found that at a smaller temperature difference, the density gradient causes a larger convective instability than in the case of a pure fluid.

Md. Rahman and Saghir [26] investigated the onset of thermo-solutal (Double Diffusion) convection in a liquid layer over a porous layer in a system heated laterally. They studied two

different cases: the first case was without thermodiffusion (Soret effect) and the second case was in in the presence of the Soret effect. The liquid in this study was water, with either 0.1 or 0.5 mass fraction of isopropanol. Also, different thickness ratios (layers thickness) were selected to study the effect of this ratio on the convection cells produced. The authors observed multiple cells in the fluid layer for the mixture containing 10% isopropanol and 90% water. However, only a single cell was observed for the mixture of 50% isopropanol and 50% water. They also found when the thickness ratio increased, the flow moved to the porous layer. For the case with Soret effect, it was found that the isopropanol components traveled either to the cold or hot side depending on the sign of the Soret effect of the mixture. In addition, there was a strong effect of gravity on the convection due to thermodiffusion.

Eslamian *et al.* [27] developed a dynamic model to investigate the phenomenon of thermodiffusion and to suggest formulas to assist in the estimation of the thermal diffusion factor for binary liquids. They associated the net heat transfer in non-equilibrium thermodynamics with the activation energy of viscous fluid flow, which represents the minimum amount of energy required for a chemical reaction to occur. The authors then proposed the following simple expressions for the estimation of the thermal diffusion factor for binary liquids:

$$\alpha = \frac{E_1^{vis} - E_2^{vis}}{RT} \tag{1.3}$$

and

$$\alpha = 0.5 * \frac{MW_2\, E_1^{vis} - MW_1\, E_2^{vis}}{(MW_1 x_1 + MW_2 x_2)RT} + 0.5 * \frac{E_1^{vis} - E_2^{vis}}{RT} \tag{1.4}$$

where α is the thermal diffusion factor, x_1 and x_2 are the mole fractions of components 1 and 2, MW_1 and MW_2 are the molecular weights of components1 and 2, RT is the approximation of

x_1 $(\partial\mu_1/\partial x_1)$ and E^{vis} is the activation energy of viscous flow of that component in pure form, at the given mixture pressure and temperature.

Mansour *et al.* [28] studied analytically and numerically the combined effect of thermodiffusion and lateral heating on double diffusive natural convection in a horizontal homogeneous and isotropic porous layer using the Darcy model. The porous layer was saturated with a binary, Boussinesq, and incompressible fluid and subjected to uniform heat and mass fluxes on the long sides of the rectangular closure. The results showed that the thermodiffusion could create a higher concentration of solute on the boundary opposite to the side where the mass flux was imposed. Also, they found that the Soret effect may modify significantly the heat transfer in the system by causing a complete disappearance of the flow, hence bringing the system back to a purely conductive state.

Shukla and Firoozabadi [29] presented a model for prediction of the thermal diffusion coefficients in binary fluids using the rules of thermodynamics in irreversible processes. The model was used to predict the coefficients of thermal diffusion at various values of pressure and temperature for hydrocarbon (C_1/C_3, C_1/C_4, C_7/C_{12} and C_7/C_{16}) and non-hydrocarbon ($Ar/C0_2$, N_2/CO_2, H_2/N_2 and H_2/CO_2) fluid mixtures. Comparison with theoretical results showed that the model performed successfully. It was found that the thermodiffusion coefficients are not influenced by pressure or temperature when the model is not near to the critical point.

Davarzani *et al.* [30] determined the effective Darcy-scale coefficients for heat and mass transfer in porous media using a volume averaging technique. The results showed that the effective Soret number differs from the micro-scale value because of the effects of advection. They also showed that for the convective regimes, the effective thermodiffusion coefficient depends on the pore-scale properties (e.g. geometry, conductivity ratio). The study concluded that for low Péclet

numbers the effective Soret number in porous media is the same as for a free fluid, and it is independent of the conductivity ratio. While in convective regimes the effective Soret number decreases. Therefore, a change in the conductivity ratio will change the effective thermodiffusion coefficient in addition to the effective thermal conductivity coefficient.

Benano-Melly *et al.* [31] numerically addressed the problem of thermodiffusion in binary fluid mixtures within a porous medium and subjected to a horizontal thermal gradient. They reproduced Soret number measurement experiments and explained the disagreement observed between numerical and experimental results. Their study showed that multiple convection-roll flow patterns can be developed when solutal and thermal buoyancy forces oppose each other, that is, depending on the value of the Soret number of the binary mixture. It also showed that for a given binary mixture the maximum separation ratio occurs at the larger cell aspect ratio. The authors observed a disagreement between numerical and experimental results when evaluating the optimum permeability for solute separation. They found that dispersion can be responsible for this phenomenon and that it can greatly affect the diffusion and

thermodiffusion coefficients.

Melnikov *et al.* [32] employed a Darcy–Brinkman model to experimentally model the double-diffusive convection with Soret effect in a system consisting of a fluid region adjacent to a porous medium saturated with and laterally sandwiched between the same liquid. For these experiments the liquid possessed a positive Soret effect (50% 1, 2, 3, 4-tetrahydronaphthalene (THN)-dodecane solution). A temperature difference (1, 3, and 5 K) was applied between the sidewalls of the model. The authors found that the concentration field in a pure liquid is uniform in the central region, producing an obvious boundary layer at the interface due to buoyant convection. They also found that when there is a large concentration gradient in the liquid near

the porous region there is strong mass diffusion from the liquid to the porous medium at both the hot and cold sides, which drives the mass transfer that strongly affects the separation of the liquid components.

Bennacer *et al.* [33] studied the phenomenon of natural convection with Soret effect in a binary fluid saturating a shallow, horizontal porous layer. The vertical walls of the model were heated and cooled by uniform heat fluxes with a cross-solutal gradient. They found that when the vertical concentration gradient is stable, steady-state solutions become possible with a range of buoyancy ratios that are dependent on the Soret coefficient.

Mansour *et al.* [34] conducted a numerical analysis to study the Soret effect in fluid flow as well as heat and mass transfer due natural convection in a square porous cavity with a cross concentration and temperature gradients. They found that the Soret effect can affect the heat and mass transfer in the cavity, and it can improve or impair the mass transfer, depending on the flow structure and the sign of the Soret coefficient.

Safi and Benissaad [35] studied numerically the heat and mass transfer in a homogeneous and anisotropic porous medium saturated with a binary fluid mixture. The vertical walls of the rectangular enclosure were subjected to horizontal thermal and concentration gradients. The horizontal walls of the enclosure were adiabatic and impermeable. The Darcy-Brinkman-Forchheimer model was used to describe the flow in the enclosure. The authors discussed the effect of the thermal anisotropic ratio, buoyancy ratio, and Lewis and Darcy numbers on the Nusselt and Sherwood numbers. The results showed that the heat and mass transfer are weak functions of the Darcy number for all conductivity regimes, and the mass transfer is enhanced faster when *Ra* increases. They also showed that for a certain range of the parameters, the heat transfer decreases when the flow penetrates into the porous medium.

CHAPTER 2

Mathematical Formulation and Numerical Approach

2.1 Model Configuration and Boundary Conditions

The schematic diagram for the model used in this study is illustrated in Figure 2.1. It shows a two-dimensional rectangular cavity split into three regions: a porous layer sandwiched between two fluid layers of the same physical specifications. The liquid layers are assumed to be incompressible, Newtonian, and viscous with a thermal expansion coefficient of β_T and solutal expansion coefficient of β_C.

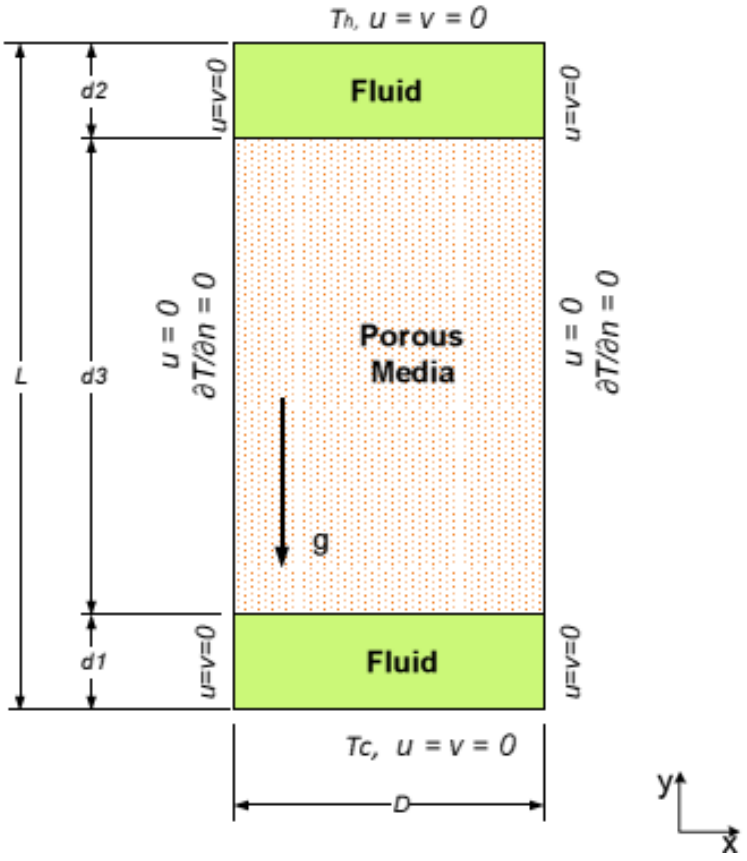

Figure 2.1: Configuration model and boundary conditions of the problem

The width (*D*) of the enclosure is 10 mm with a total height (*L*) of 45 mm. The porous layer has a height (*d3*) of 32.2 mm, while each of the fluid layers (*d1* and *d2*) has a height of 6.40 mm. The physical properties of the liquid are assumed constant. The side (vertical) walls of the enclosure are assumed adiabatic. The temperature of the top wall (T_h) of the enclosure will be greater than the temperature of the bottom wall (T_c), and the temperature difference (ΔT) between them will be 5, 10, or 20 K. It is assumed that the liquid and the porous layers are in thermal equilibrium. The porous medium has a porosity ϕ = 0.39 and thermal conductivity equal to 0.64 W/(m·K), which corresponds to a group of glass beads of 3.25 mm diameter. The Darcy number was calculated by using the Kozeny-Carmen relation:

$$K_e = \frac{d^2}{172.8}\frac{\emptyset^3}{(1-\emptyset)^2} \tag{2.1}$$

2.2 Governing Equations for the Fluid Layer

The flow under consideration is assumed laminar and incompressible. The model is presented in Cartesian coordinates. The complete continuity, momentum balance, energy balance, and mass balance equations were solved simultaneously using the finite element technique. The equations were solved numerically for both liquid layers. The equations presented are for the two-dimensional transient model, but similar equations without the *t* (time) term were used for the steady-state model. The dimensional and non-dimensional equations are explained in detail in appendix (A).

2.2.1 Continuity Equation

The continuity equation of fluid dynamics is a mathematical formula which states that mass is always conserved in fluid systems regardless the complexity or direction of flow:

$$\frac{\partial u}{\partial x} + \frac{\partial v}{\partial y} = 0 \tag{2.2}$$

where u and v are the velocity components in the x and y directions, respectively.

2.2.2 Momentum Balance Equation

The Navier-Stokes equations are used as the momentum balance equations for the flow in the fluid layer. The momentum balance equation in the x-direction is expressed as:

$$\rho\left[\frac{\partial u}{\partial t} + u.\frac{\partial u}{\partial x} + v.\frac{\partial u}{\partial y}\right] = -\frac{\partial p}{\partial x} + \mu\left[\frac{\partial^2 u}{\partial x^2} + \frac{\partial^2 u}{\partial y^2}\right] \tag{2.3}$$

where ρ is the fluid density, p is the pressure, and μ is the fluid viscosity.

In the y-direction, there is a buoyancy-driven flow induced by temperature differences that should be considered in computation, which is represented by the Boussinesq approximation. The Boussinesq approximation states that the density variation in a fluid is small and can be neglected except when it is multiplied by the term of gravitational acceleration (g). The Boussinesq approximation can be expressed as:

$$\rho_f = \rho_0.[\beta_T(T - T_0) - \beta_C\,(c - c_0)] \tag{2.4}$$

where β_T and β_C are the thermal and solutal expansion coefficients, respectively, and ρ_0, T_0 and c_0 are the initial fluid density, temperature, and concentration, respectively. From equation (2.4), it can be noted that the fluid density is a linear function of both fluid temperature and concentration. Similarly, the momentum balance equation in the y–direction can be expressed as:

$$\rho\left[\frac{\partial v}{\partial t}+u.\frac{\partial v}{\partial x}+\ v.\frac{\partial v}{\partial y}\right]=-\frac{\partial p}{\partial y}+\mu\left[\frac{\partial^2 v}{\partial x^2}+\ \frac{\partial^2 v}{\partial y^2}\right]-\rho_0.g[\beta_T(T-T_0)-\beta_C\ (c-c_0)] \qquad (2.5)$$

2.2.3 Energy Balance Equation

Jiang *et al.* [36] expressed the energy conservation equation for a system consisting of a porous layer saturated with a fluid as:

$$\frac{\partial(\rho.Cp)e.T}{\partial t}+u\ \frac{\partial}{\partial x}\left[(\rho Cp)_f\ T\right]+v\ \frac{\partial}{\partial y}\left[(\rho Cp)_f\ T\right]=k_e\ \left[\frac{\partial^2 T}{\partial x^2}+\frac{\partial^2 T}{\partial y^2}\right] \qquad (2.6)$$

where $(\rho Cp)_e$ is the effective volumetric heat capacity of the system and k_e is the effective thermal conductivity of the system. Relationships between these effective physical parameters and the fluid properties and the solid-layer properties are expressed as:

$$(\rho Cp)_e=\ \emptyset\ (\rho Cp)_f f+\ (1-\ \emptyset)(\rho Cp)_p \qquad (2.7)$$

$$k_e\ =\ \emptyset\ k_f+\ (1-\ \emptyset)k_p \qquad (2.8)$$

Substituting Eq (2.7) and (2.8) into (2.6) with porosity (∅) equal to 1 (100%) for a pure fluid, the thermal energy conservation equation for the fluid layer becomes:

$$(\rho Cp)_f\underbrace{\left[\frac{\partial T}{\partial t}+u\ \frac{\partial T}{\partial x}\ +v\ \frac{\partial T}{\partial y}\right]}_{\boldsymbol{(A)}}=k_f\left[\frac{\partial^2 T}{\partial x^2}+\frac{\partial^2 T}{\partial y^2}\right] \qquad (2.9)$$

Term (***A***) is the rate of change of the temperature within the medium due to the convection of fluid into it. Once multiplied by $(\rho Cp)_f$, it becomes the rate of change of thermal energy per unit volume of fluid, due to convection.

2.2.4 Mass Balance Equation

The mass (concentration) balance equation in the fluid layer can expressed as follows [37]:

$$\left[\frac{\partial c}{\partial t} + u\,\frac{\partial c}{\partial x} + v\,\frac{\partial c}{\partial y}\right] = D_M\left[\frac{\partial^2 c}{\partial x^2} + \frac{\partial^2 c}{\partial y^2}\right] + D_T\left[\frac{\partial^2 T}{\partial x^2} + \frac{\partial^2 T}{\partial y^2}\right] \tag{2.10}$$

where c is the concentration, D_M is the molecular diffusion coefficient, and D_T is the thermal diffusion coefficient.

2.3 Governing Equations for the Porous Layer

2.3.1 Continuity Equation

The continuity equation for the porous media region will be same as for the fluid region:

$$\frac{\partial u}{\partial x} + \frac{\partial v}{\partial y} = 0 \tag{2.11}$$

where u and v are the velocity component of the fluid in the x and y directions, respectively.

2.3.2 Momentum Balance Equation

For the momentum balance equation, scientists have found additional forms of Darcy's law. Brinkman [38] found an alternative extension to Darcy's law, which is used to explain the transitional flow between boundaries by adding a viscous term to Darcy's law. For the porous layer, the Brinkman model is an appropriate momentum equation to use; therefore, the Brinkman model is used in this study. The momentum balance equation in the x-direction can be expressed as:

$$\frac{\rho}{\emptyset}\left[\frac{\partial u}{\partial t}\right] + u.\frac{\mu}{K} = -\frac{\partial p}{\partial x} + \mu\left[\frac{\partial^2 u}{\partial x^2} + \frac{\partial^2 v}{\partial y^2}\right] \quad (2.12)$$

where $\emptyset$ is the porosity, μ is the fluid viscosity, and K is the permeability of the porous medium.

The momentum balance equation in the y-direction with the Boussinesq approximation can be expressed as:

$$\frac{\rho}{\emptyset}\left[\frac{\partial u}{\partial t}\right] + v.\frac{\mu}{k} = -\frac{\partial p}{\partial y} + \mu\left[\frac{\partial^2 u}{\partial x^2} + \frac{\partial^2 v}{\partial y^2}\right] - \rho_0 g\left[\beta_T(T - T_0) - \beta_C(c - c_0)\right] \quad (2.13)$$

2.3.3 Energy Balance Equation

The energy balance equation for the porous layer can be expressed as:

$$(\rho Cp)_f \left[\frac{\partial T}{\partial t} + u\,\frac{\partial T}{\partial x} + v\,\frac{\partial T}{\partial y}\right] = k_e \left[\frac{\partial^2 T}{\partial x^2} + \frac{\partial^2 T}{\partial y^2}\right] \quad (2.14)$$

where k_e is the effective thermal conductivity of the system.

2.3.4 Mass Balance Equation

The mass balance equation for the species can be expressed as:

$$\left[\frac{\partial c}{\partial t} + u\,\frac{\partial c}{\partial x} + v\,\frac{\partial c}{\partial y}\right] = D_M \left[\frac{\partial^2 c}{\partial x^2} + \frac{\partial^2 c}{\partial y^2}\right] + D_T \left[\frac{\partial^2 T}{\partial x^2} + \frac{\partial^2 T}{\partial y^2}\right] \quad (2.15)$$

where c is the concentration, D_M is the molecular diffusion coefficient and D_T is the thermal diffusion coefficient.

2.4 Dimensional Analysis

Frank White [39] defined dimensional analysis as*: "a method for reducing the number and complexity of experimental variables that affect a given physical phenomenon, by using a sort of compacting technique."*. The author also stated the Principle of Dimensional Homogeneity (PDH) as: *"If an equation truly expresses a proper relationship between variables in a physical process, it will be dimensionally homogeneous; that is, each of its additive terms will have the same dimensions."* Dimensionless parameters have many advantages, such as a fewer number of variables and a reduction in the number of experiments, simulations, and communications, which saves time and money. Scaling the fundamental variables with respect to typical values and constructing dimensionless parameters provides a measure of the relative importance of the various terms in the equations and identifies the dominant physical phenomena [40]. Examples of some of these dimensionless parameters are illustrated in appendix (B). The dimensionless parameters used to change equations (2.2) to (2.15) to their dimensionless forms are:

$$U = \frac{u}{u_0} \qquad \theta = \frac{T - T_0}{\Delta T} \qquad \tau = \frac{t u_0}{L}$$

$$V = \frac{v}{u_0} \qquad C = \frac{c - c_0}{\Delta c} \qquad N = \frac{\beta_C \, \Delta c}{\beta_T \, \Delta T}$$

$$X = \frac{x}{L} \qquad Re = \frac{\rho_0 u_0 L}{\mu} \qquad Ra_{TL} = \frac{g \beta_T \, \Delta T d_{1,2}^3}{\gamma \alpha}$$

$$Y = \frac{y}{L} \qquad Pr = \frac{\gamma}{\alpha} \qquad Ra_{TP} = \frac{g \beta_T \, \Delta T \, d_3 k}{\gamma \alpha}$$

$$P = \frac{pL}{\mu u_0} \qquad Da = \frac{k}{L^2} \qquad Ra_{SL} = \frac{g\beta_C \Delta c d_{1,2}^3}{\gamma\alpha}$$

$$u_0 = \sqrt{g\beta_T \Delta T L} \qquad Sc = \frac{\gamma}{D_M} \qquad Ra_{TP} = \frac{g\beta_C \Delta c\, d_3 k}{\gamma\alpha}$$

(2.16)

Where U and V are the non-dimensional *x* and *y* components of velocity, respectively, and *X* and *Y* are the non-dimensional *x* and *y* coordinates, respectively. *P* is the non-dimensional pressure term, θ is the non-dimensional temperature term, and τ is non-dimensional time. L, T, and u_0, respectively denote the characteristic length, temperature, and velocity. In non-dimensional analysis, several other parameters appear, such as the Reynolds number *Re*, the Prandtl number *Pr*, the Darcy number *Da*, the thermal Raleigh number for the liquid layer Ra_{TL}, the solutal Raleigh number for the liquid layer Ra_{SL}, the thermal Raleigh number for the porous layer Ra_{TP}, the solutal Raleigh number for the porous layer Ra_{SP}, and the Schmidt number *Sc*. The parameters in equation (2.16) are used in the analysis, which is fully outlined in appendix (A).

2.5 Non-Dimensional Liquid Layer Governing Equations

2.5.1 Continuity Equation:

The dimensionless form for the continuity equation can be expressed as follows:

$$\frac{\partial U}{\partial X} + \frac{\partial V}{\partial Y} = 0 \qquad (2.17)$$

where U and V are the non-dimensional *x* and *y* component of velocity, respectively, *X* and *Y* are the non- dimensional *x* and *y* coordinates, respectively.

2.5.2 Momentum Balance Equations:

The Navier-Stokes equations for the x and y directions are given as follows:

In the X direction:

$$Re\left[\frac{\partial U}{\partial \tau}+U\frac{\partial U}{\partial X}+V\frac{\partial U}{\partial Y}\right]=-\frac{\partial P}{\partial X}+\left[\frac{\partial^2 U}{\partial X^2}+\frac{\partial^2 U}{\partial Y^2}\right] \quad (2.18)$$

where *Re* is the Reynolds number, *P* is the non-dimensional pressure term and, τ is non-dimensional time.

In the Y direction:

$$Re\left[\frac{\partial V}{\partial \tau}+U\frac{\partial V}{\partial X}+V\frac{\partial V}{\partial Y}\right]=-\frac{\partial P}{\partial Y}+\left[\frac{\partial^2 V}{\partial X^2}+\frac{\partial^2 V}{\partial Y^2}\right]-\frac{Gr_T}{Re}[\theta-N.C] \quad (2.19)$$

2.5.3 Energy Balance Equation:

The non-dimensional form of the energy balance for the fluid layers can be stated as:

$$Re.Pr\left[\frac{\partial \theta}{\partial \tau}+U\frac{\partial \theta}{\partial X}+V\frac{\partial \theta}{\partial Y}\right]=\left[\frac{\partial^2 \theta}{\partial X^2}+\frac{\partial^2 \theta}{\partial Y^2}\right] \quad (2.20)$$

where *Pr* is the Prandtl number and θ is the non-dimensional temperature term.

2.5.4 Mass Balance Equation:

The non-dimensional form of the mass balance equation in the fluid layers can be expressed as follows:

$$\left[\frac{\partial C}{\partial \tau}+U\frac{\partial C}{\partial X}+V\frac{\partial C}{\partial Y}\right]=\frac{1}{Re}.\frac{1}{Sc}\left[\frac{\partial^2 C}{\partial X^2}+\frac{\partial^2 C}{\partial Y^2}\right]+\frac{\alpha}{Sc.Re}\left[\frac{\partial^2 \theta}{\partial X^2}+\frac{\partial^2 \theta}{\partial Y^2}\right] \quad (2.21)$$

where C is the non-dimensional concentration term, Sc is the Schmidt number, and α is the thermal diffusivity of the fluid.

2.6 Non-Dimensional Porous Layer Governing Equations

2.6.1 Continuity Equation:

The non-dimensional form of the continuity equation for the porous layer can be stated as the same as the one of the fluid layer:

$$\frac{\partial U}{\partial X} + \frac{\partial V}{\partial Y} = 0 \tag{2.22}$$

where U and V are the non-dimensional x and y components of velocity, respectively, and X and Y are the non-dimensional x and y coordinates, respectively.

2.6.2 Momentum Balance Equations:

The Navier-Stokes Equations for the x and y-directions are given as follows:

In the X-direction:

$$Re\left[\frac{\partial U}{\partial \tau}\right] + \frac{1}{Da}[U] = -\frac{\partial P}{\partial X} + \left[\frac{\partial^2 U}{\partial X^2} + \frac{\partial^2 U}{\partial Y^2}\right] \tag{2.23}$$

where Da is the Darcy number, which is equal to K/H^2.

In the Y-direction:

$$Re\left[\frac{\partial V}{\partial \tau} + U\frac{\partial V}{\partial X} + V\frac{\partial V}{\partial Y}\right] = -\frac{\partial P}{\partial Y} + \left[\frac{\partial^2 V}{\partial X^2} + \frac{\partial^2 V}{\partial Y^2}\right] - \frac{Gr_T}{Re}[\theta - N.C] \tag{2.24}$$

where Gr_T is the thermal Grashof number, and N is the buoyancy factor.

2.6.3 Energy Balance Equation:

The energy balance equation in its dimensionless form can be expressed as:

$$Re.Pr\left[\frac{\partial\theta}{\partial\tau}+U\frac{\partial\theta}{\partial X}+V\frac{\partial\theta}{\partial Y}\right]=G\left[\frac{\partial^2\theta}{\partial X^2}+\frac{\partial^2\theta}{\partial Y^2}\right] \quad (2.25)$$

where G is the non-dimensional thermal conductivity, defined as:

$$G=\frac{k_e}{k_f}=\frac{\emptyset k_f+(1-\emptyset).k_s}{k_f}$$

2.6.4 Mass Balance Equation:

The non-dimensional form of the mass balance equation of the fluid layers can also be utilized to represent the mass balance in the porous layer:

$$\left[\frac{\partial C}{\partial\tau}+U\frac{\partial C}{\partial X}+V\frac{\partial C}{\partial Y}\right]=\frac{1}{Re}.\frac{1}{Sc}\left[\frac{\partial^2 C}{\partial X^2}+\frac{\partial^2 C}{\partial Y^2}\right]+\frac{\alpha}{Sc.Re}\left[\frac{\partial^2\theta}{\partial X^2}+\frac{\partial^2\theta}{\partial Y^2}\right] \quad (2.26)$$

where C is the non-dimensional concentration term, Sc is the Schmidt number, and α is the thermal diffusivity of the fluid.

2.7 Numerical Solution Technique

The finite element method was used in this study. The source code for various cases of our research is shown in Appendix (E). For rigid surface problems, we used the segregated solver, which sequentially solves the governing equations (segregated from one another) by solving each degree of freedom separately. Parameters such as heat flux, mass flux, stream function, and flow rate can be derived from the temperature, pressure, velocity, and species fields, which were

numerically computed. Then, numerical results were plotted graphically with the use of the graphics postprocessor programme FIPOST.

2.7.1 Finite Element Analysis

The full transient Navier-Stokes equations together with the energy and mass transfer equations were solved numerically using the finite element technique. The thermodiffusion coefficients were assumed constant and the PC-SAFT (Perturbed-Chain Statistical Associating Fluid Theory) equation of state was used to evaluate the liquid properties of the non-associating mixture in the model. Galerkin finite-element procedure was applied to the transient Navier-Stokes equations utilizing the implicit time integrator, which is unconditionally stable regardless the size of the time step used. This method was also used in combination with a powerful adaptive time-stepping scheme that dynamically set the size of the time step to maintain a predefined level of temporal accuracy.

The numerical procedure consisted of solving the non-dimensional equations (2.16) to (2.26) using the finite element technique. The finite element technique reduces the infinite number of degrees of freedom in a problem to a finite number by solving a system of equations. For the present two-dimensional model, the computational domain was divided into many small quadrilaterals. To achieve greater accuracy in the results, a finer mesh was applied to the vertical walls of the rectangular cavity and at the free surface where the driving force of the flow was located. The mesh was defined as a finite number of elements, and its variables were evaluated simultaneously. As can be seen in Figure 2.2, the bottom surface of the cavity was defined by key-points 1 and 2, the bottom fluid-porous layer interface by key-points 3 and 4, the top fluid-porous layer interface by key-points 5 and 6 and lastly, the top surface by key-points 7 and 8.

The velocities, temperature, pressure, and species were unknown and were numerically calculated at each node in the meshed cavity.

2.7.2 Mesh Sensitivity Analysis

Accuracy and processing time are essential factors for any simulation process. Therefore, in order to obtain accurate, time-efficient, and cost-effective results, the optimum mesh size (density) has to be selected carefully. For this study, we used a mesh of 31 quadrilateral elements in the *x*-axis by 135 quadrilateral elements in the *y*-axis for the entire analysis. Since a higher temperature gradient and more mass flux are assumed to occur in the fluid layers, a finer mesh was placed in both regions of the liquid layers (top and bottom) as illustrated in Figure 2.3.

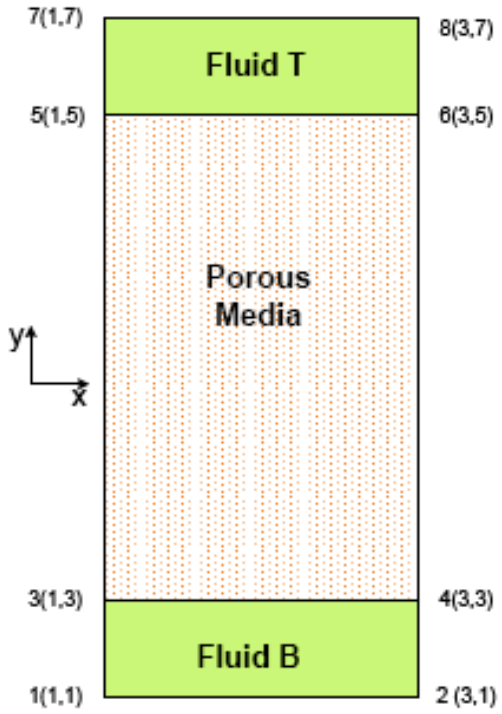

Figure 2.2: Node numbers for key-points

The Nusselt number across the enclosure has been used for the purpose of determining mesh sensitivity because of its direct relationship to the driving force of the simulation in this study. The average Nusselt number has been calculated for different mesh sizes. The average Nusselt number is equal to the average value of the Nusselt number on the both of the hot and cold horizontal surfaces, and it can be expressed as:

$$Nu = \frac{Nu_H + Nu_C}{2} \tag{2.27}$$

where,

$$Nu_H = \int_0^D \frac{\partial \theta}{\partial X} \Big|_{Y=1} . dX \tag{2.28}$$

and

$$Nu_C = \int_0^D \frac{\partial \theta}{\partial X} \Big|_{Y=0} . dX \tag{2.29}$$

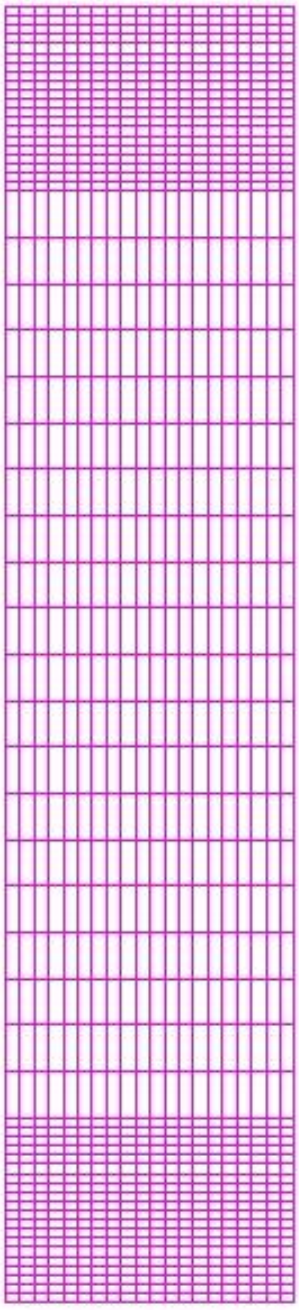

Figure 2.3: Finite element meshes for model defined by 31elements in the x-axis and by 135 elements in the y-axis

Table 2.1 shows the average Nusselt number for each case. It was found that the mesh size of (31 x 135) is the optimum size for this type of study because above this value Nu is constant making it unnecessary to use a finer mesh.

Table 2.1: Calculated average Nusselt number for mesh sensitivity

Number ofNodes	Average Nusselt Number
11 x 43	0.1625
21 x 91	0.1393
31 x 135	0.14
41 x 181	0.13999

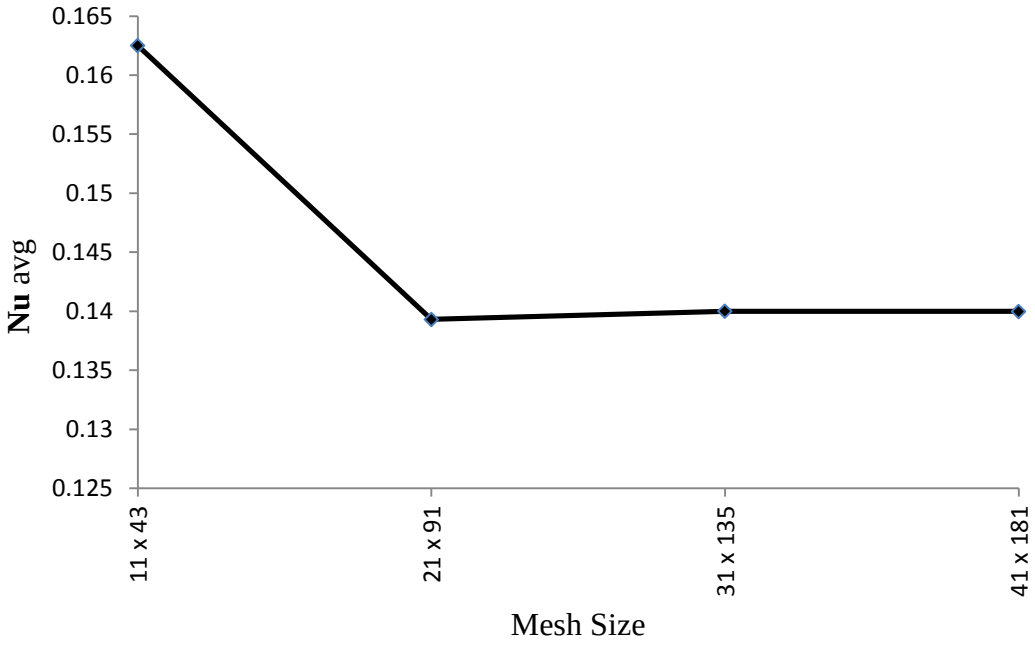

Figure 2.4: Mesh sizes vs. the average Nu number

CHAPTER 3

Natural Convection in a Multi-Layered System of Porous Media and Binary Fluid Layers

3.1 Introduction

Natural convection is a mechanism in which heat and mass transfer occurs in fluids due to the motion generated by a difference in the fluid density due to a temperature gradient. This density difference leads to the generation of a gravitational force called the "buoyancy force," which induces convection rolls. Hence, the buoyancy and gravitational forces play an important role in the onset of natural convection. In a vertical, multi-layered system, natural convection can occur when there is a density difference of the fluids due to a temperature gradient. The temperature gradient in such a system can be produced by heating the system from one of its horizontal sides and cooling from the opposite side, i.e., heating from the bottom side and cooling from the top side or vice versa. In the case of applying heat from the bottom and cooling the top surface, the temperature gradient will lead to a density gradient in the fluid in the same direction of the gravitational force. In this situation, the influence of the buoyancy force will be greater than that of the viscous force, which generates convection swirling patterns. This then causes the system to be in an unstable condition with the temperature distribution evenly disturbed, as shown in Figure 3.1a. The heat and mass are transferred from the bottom layers to the upper layers by means of natural convection.

On the other hand, in the opposite configuration where the temperature of the top surface is greater than that of the bottom surface, the density will not decrease in the same direction of the

gravity forces, which will lead to a reduction of the buoyancy forces. As a result, no patterns of motion will occur in the system and it will be under stable conditions. Such a system, with a temperature distribution stratified (layered), is shown in Figure 3.1b. In a system like this, no convection patterns will be produced, and if any pattern does appear, it is due to the geometry of the cavity. The heat and mass transfer in this case are through a conduction mechanism rather than through convection.

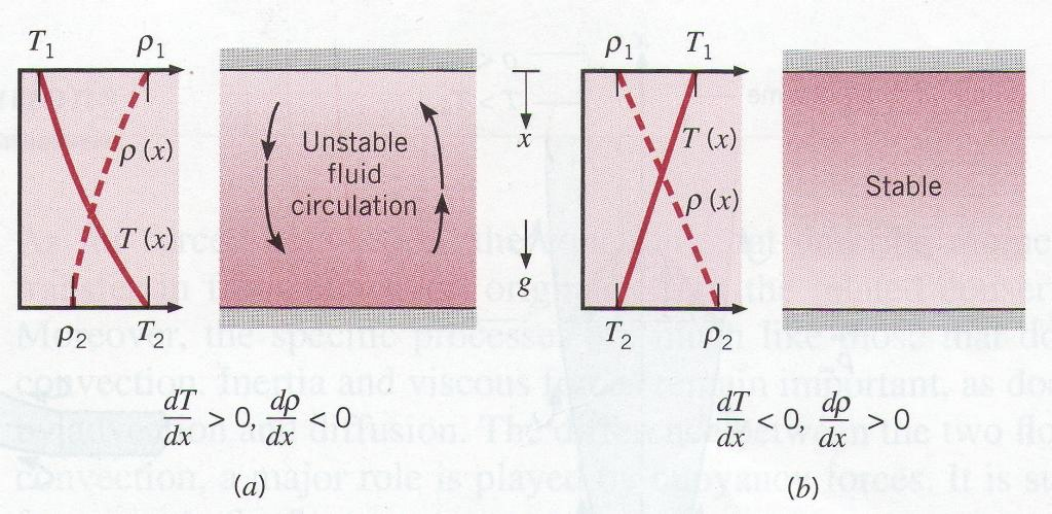

Figure 3.1: Conditions in fluid sandwiched between two horizontal surfaces at different temperatures. (a) Unstable temperature gradient, (b) Stable temperature gradient [41].

To study the patterns of fluid motion that occur during convection, several different techniques have been utilized in order to visualize the flow behaviour. The most common of these techniques is the streamline. Streamlines are defined as *"lines drawn through the flow field in such a manner that the velocity vectors of the fluid at each and every point on the streamline are tangent to the streamline at that instant"* [42]. The stream function is a useful mathematical model that is used to plot streamlines, satisfy, and solve the continuity and momentum equations directly for a single variable. For two-dimensional incompressible flow, the constant value of the

stream function (expressed as Ψ) can be represented by the streamlines and can be calculated by using the following relationships:

$$U = \partial\Psi/\partial Y \text{ and } V = -\partial\Psi/\partial X \quad (3.1)$$

3.2 Natural Convection in a Water-Alcohol Binary Mixture

Our first study was the investigation of natural convection in a system that consists of a layer of a porous material sandwiched between two layers of a water-alcohol binary mixture. The mixture used in this study was 10% isopropanol with 90% water. The physical properties of the mixture of 10% isopropanol with 90% water can be found in appendix (C). The porous material used in this study was a group of glass beads with diameter of 3.25 mm and a thermal conductivity (k_s) of 0.64W/(m·K). The model configuration and the boundary conditions used in this study were similar to those mentioned in Section (2.1) of this thesis. The system was heated from the top surface and was subjected to temperature differences of 5, 10 and 20 K (for each case study separately) between the bottom and the top surfaces. For the comparison, validation, and better understanding of this phenomenon, an identical model but with heating from the bottom surface (with a temperature difference between the bottom and the top surfaces = 20 and 50 K) was numerically simulated. Here we will name it as the Bottom Model (ΔT). One of the important variables, which is directly related to the phenomenon of natural convection, is the Nusselt number (*Nu*). It is a dimensionless number that represents the ratio of convective to conductive heat transport in a system. If the value of *Nu* is equal or less than unity, the conductive heat transfer is the dominant mechanism. If *Nu* is greater than unity, then convection is the dominant heat transfer mechanism. Kim *et al.* [43] carried out calculations in order to evaluate the effects

of the porous material on the heat transfer rate at the horizontal bounding walls. The results for the heat transfer rate were represented in a dimensionless form of the *Nu.* The *Nu* in the bottom layer (which represents the porous layer) can be expressed as:

$$Nu_b = \frac{Q}{K_e\left(\frac{L}{h_p}\right)(T_t - T|y = h_p)} = \left(\frac{K_f}{K_e} + \frac{h_f}{h_p}\right)\frac{h_p}{L}\int_0^{D/H} \frac{\partial\theta}{\partial X}|_{Y=0}.dX \quad (3.2)$$

Moreover, at the top surface (which represents the fluid layer in the mentioned study) it is given by:

$$Nu_t = \frac{Q}{K_e\left(\frac{L}{h_p}\right)(T|y = h_p - T_t)} = \left(\frac{K_f}{K_e} + \frac{h_f}{h_p}\right)\frac{h_p}{L}\int_0^{D/H} \frac{\partial\theta}{\partial X}|_{Y=1}.dX \quad (3.3)$$

where T_t is the temperature of the top layer.

Taking equations (3.2) and (3.3), the model used in this study, and taking into consideration that the *Nu* is neglected in the porous layer since in that layer the mechanism will be conduction, the *Nu* for this system can be expressed as:

$$Nu_H = \int_0^D \frac{\partial\theta}{\partial X}|_{Y=0}.dX \quad (3.4)$$

$$Nu_C = \int_0^D \frac{\partial\theta}{\partial X}|_{Y=1}.dX \quad (3.5)$$

The overall averaged Nusselt number will be:

$$Nu_{avg} = \frac{Nu_H + Nu_C}{2} \quad (3.6)$$

3.2.1 Natural Convection in a Water-Alcohol Binary Mixture Heated from Below

Case 1: Temperature difference $\Delta T = 50$ K

The temperature difference between the top and bottom surfaces considered in this case ($\Delta T = 50$ K) was sufficient to produce strong convection patterns and thus high values of velocity inside both fluid layers. In this case, the fluid was able to penetrate through the porous layer due to the strong convection patterns and the relatively high velocity of these fluids in both the bottom and top layers of the binary fluids. The contours of the streamlines and *x* component of the fluid velocity for this case are shown in Figure 3.2 (a) and (b), respectively. The high values of the velocity inside both fluid layers were responsible for the temperature disturbance of the whole system, as shown in Figure 3.3. The numerically calculated total averaged *Nu* number for this case is 2.854, which is greater than unity, which indicates that convection is the dominant heat transfer mechanism.

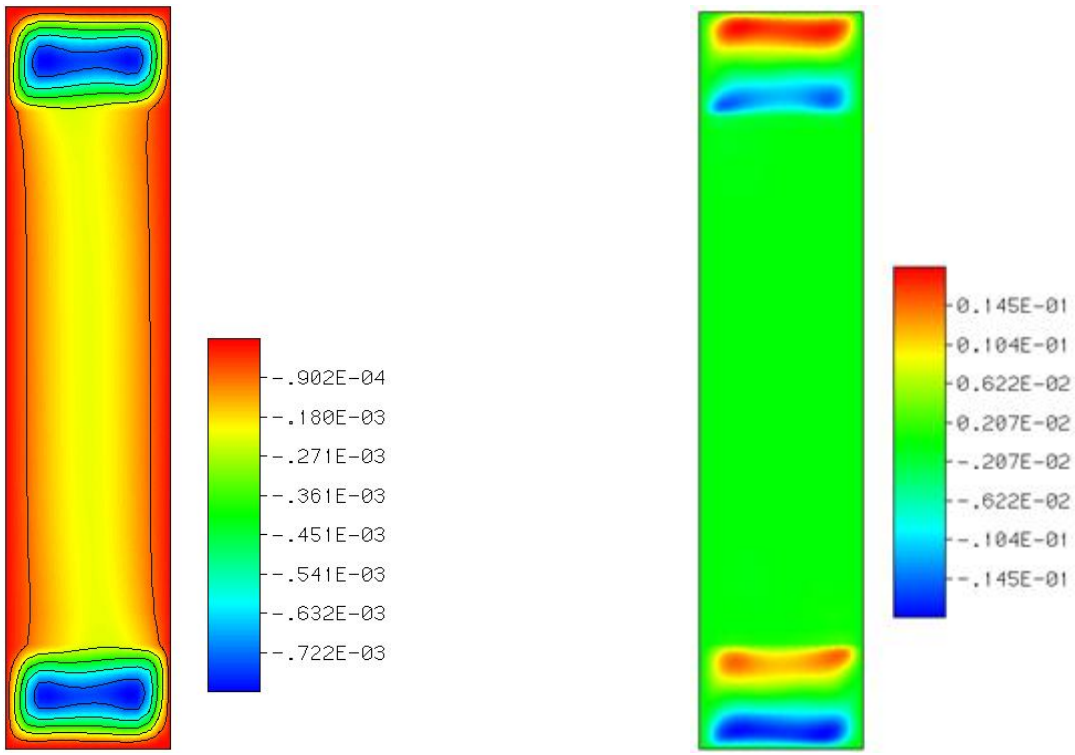

(a) **(b)**

Figure 3.2: The case of heating the system from below at ΔT=50K; (a) contours of stream lines, (b) contours of the x component of fluid velocity

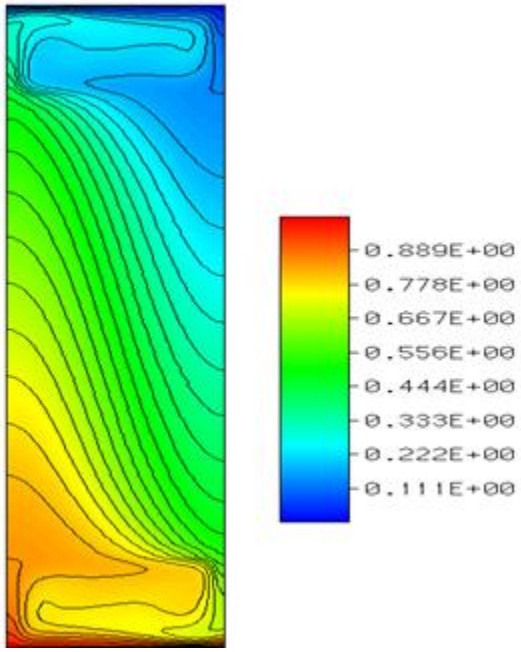

Figure 3.3: Temperature contours for the case of heating the system from below at ΔT=50K.

Case 2: Temperature difference $\Delta T = 20$ K

Figure 3.4a shows the streamline contours for the bottom model (20K). There are noticeable convection patterns in both liquid layers, but the fluid remains within the liquid layers with the porous layer simply acting as a trap or a rigid wall preventing the flow from protruding in. The stream function in this model vary between -0.49959 x 10^{-3} to 0.52485 x 10^{3}. These weak values of the stream function are related to the low velocity inside the model due to the small temperature difference between the bottom and top surfaces, and to the presence of the porous layer between both binary liquid layers. This is expected since the number and values of the convection patterns are inversely proportional to the height of the porous layer. The *x* component of the velocity (*U*) varies between (-0.114 x 10^{-1}) to (0.10987 x 10^{-1}) as shown in Figure 3.4b.

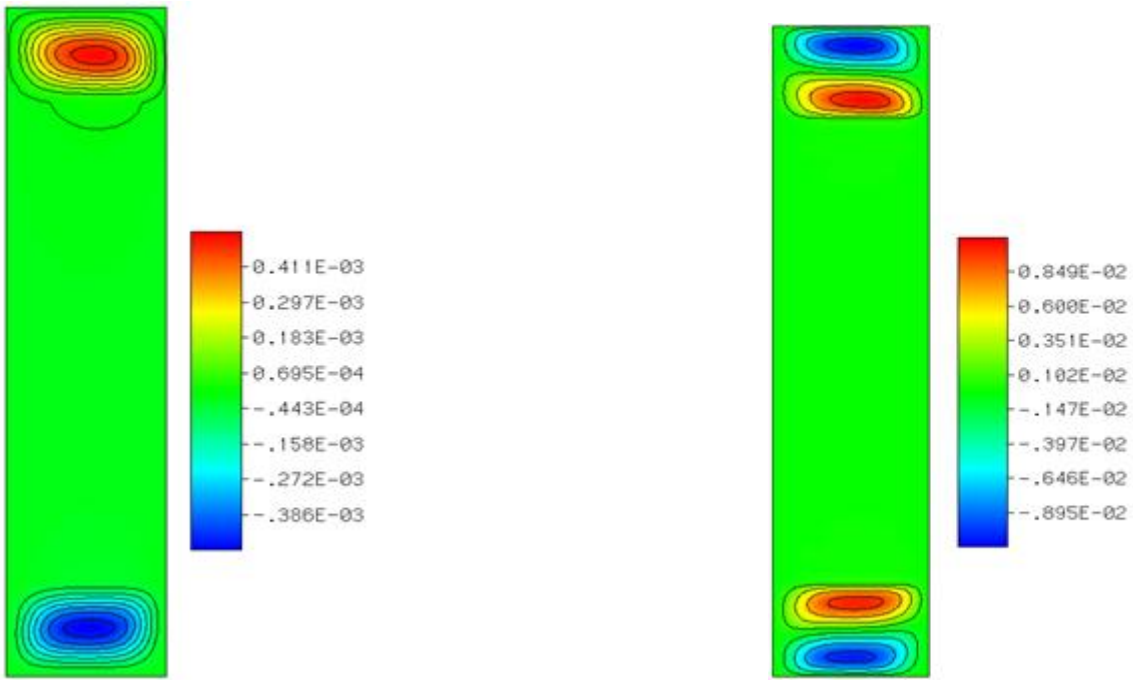

(a) **(b)**

Figure 3.4: The case of heating the system from below at ΔT=20K; (a) contours of stream lines, (b) contours of the x component of fluid velocity

In order to explain what is happening inside this model, a plot of U along the Y-axis of the model is shown in Figure 3.5. The negative values of U indicate the clockwise direction of the flow patterns and the positive values of U indicate the direction of the flow patterns is counterclockwise. There is observable movement in the fluid layers, while in the porous layer the fluid that has saturated the porous medium is steady with a small and constant velocity due to the resistance of the porous medium against the fluid flow.

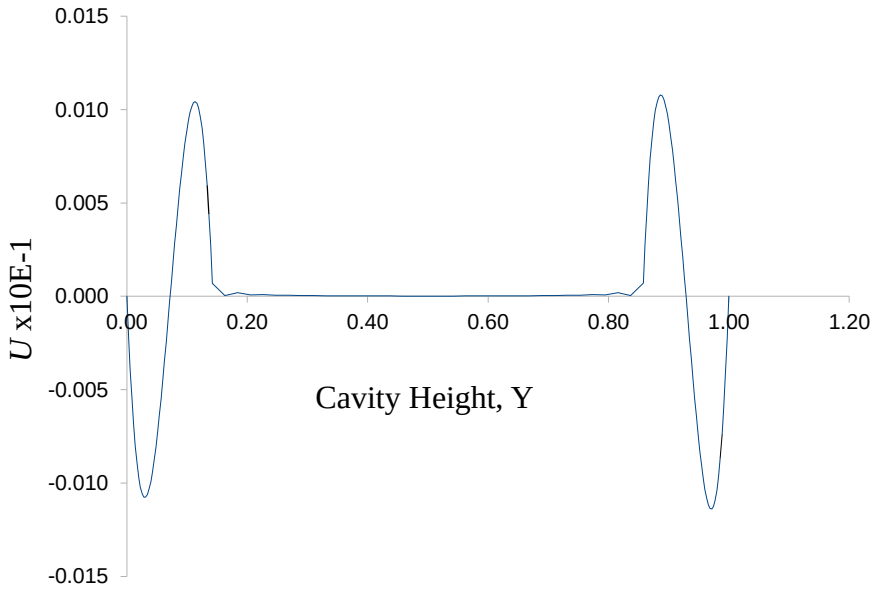

Figure 3.5: The x component of fluid velocity along the Y-axis for the case of heating the system from the bottom surface at ΔT=20K.

From Figure 3.6, it is clear that there is a temperature disturbance in both fluid layers. Also, it is noticeable that there is less temperature distribution within the porous layer than in the fluid layers. This disturbance is due to the swirling motion of the fluid created by convection.

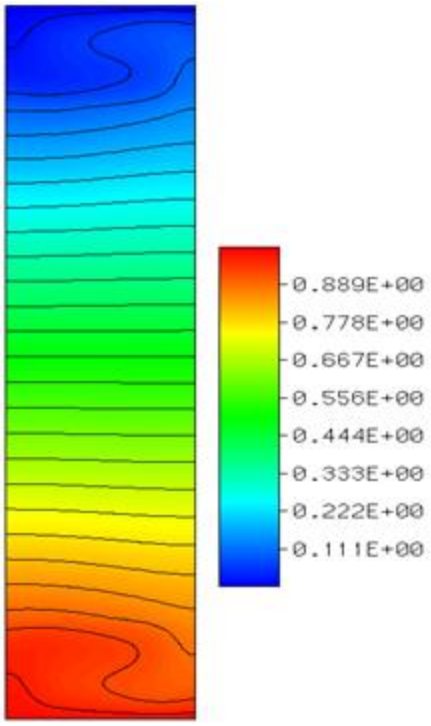

Figure 3.6: Temperature contours for the case of heating the system from below at ΔT=20K.

The numerically calculated averaged Nusselt number (Nu_{avg}) for this model is 0.3965, which is less than unity. The value of the averaged Nusselt number for this model indicates that the dominant mechanism of heat transfer is conduction, because the temperature difference of ΔT=20 K is not sufficient to create a density gradient to increase the velocity of the binary fluid inside the model. If the velocity were increased, then convection would be the dominant mechanism of heat transfer in this case. The convection patterns that appeared in this model are due to the finite geometry of the system and the temperature difference between the horizontal surfaces (top and bottom) and the adjacent vertical surfaces (right and left). To explain the effect of the temperature difference on the convection in the fluids and the porous medium, the temperature disturbance along the vertical axis of the cavity at the center of the horizontal axis is shown in Figure 5.7.

It is noticeable that at the lower temperature difference (ΔT=20K), the system is more stable due to the decreased motion of the fluid. This is further due to the smaller density gradient produced by buoyancy forces in the binary mixture, which causes the hot fluid to rise and displaces the colder fluid that is denser. The characteristic velocity at the system is a function of ΔT, and the Reynolds number (*Re*) is a function of the characteristic velocity as in the following equations:

$$u_0 = \sqrt{g.\beta_T.\Delta T.L} \tag{3.7}$$

$$Re = u_0.\frac{L}{\gamma} \tag{3.8}$$

From the above two equations, it is clear that increasing ΔT will increase the characteristic velocity, which will in turn increase *Re*, which gives us an idea about whether the fluid flow is laminar, streamlined, or turbulent.

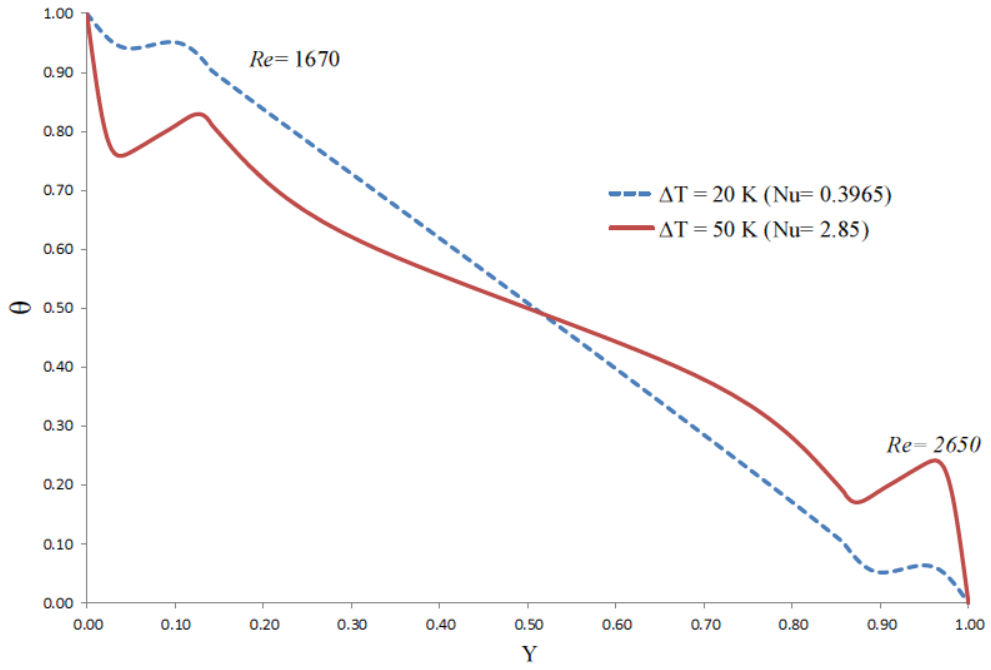

Figure 3.7: Distribution of temperature along the Y-axis at the center of the cavity for different models.

3.3 Natural Convection in a Water-Alcohol Binary Mixture Heated from Above

The model under investigation in this study was previously described in Sections 2.1 and 3.2. In the configuration of heating from above, the first model had a temperature difference of 5 K between the top and bottom horizontal surfaces. Figures 3.8a and 3.8b show the temperature distribution along the Y-axis of the model with a non-dimensional temperature (θ) ranging from 1 to 0. It is noticeable that the temperature distribution is stratified from the top horizontal to the bottom horizontal surface.

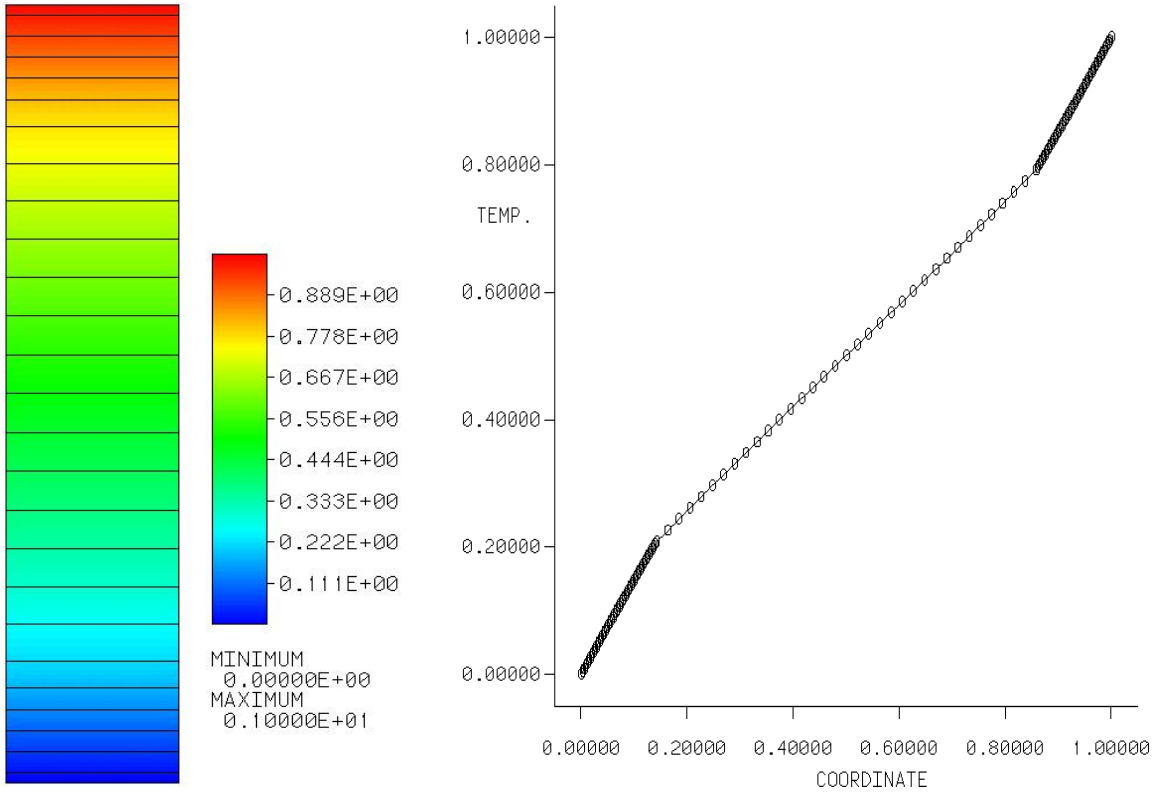

(a) **(b)**

Figure 3.8: Temperature contours (a) and temperature distribution along the Y-axis of the model (b) for the case of heating the system from above at ΔT=5K.

The temperature stratification indicates that the system is stable and there is no density gradient for the binary fluid, which leads to ceased fluid flow inside the system. It also indicates that the heat inside the model transfers via a conduction mechanism. The temperature gradient in the fluid layers is greater than in the porous medium because the fluid velocity in the pure fluid layers is higher than that of the saturated fluid in the porous layer due to the resistance of the porous particles towards the fluid flow. The *x* component of the velocity (*U*) and the streamline contours in this model are shown in Figures 3.9a and 3.9b, respectively.

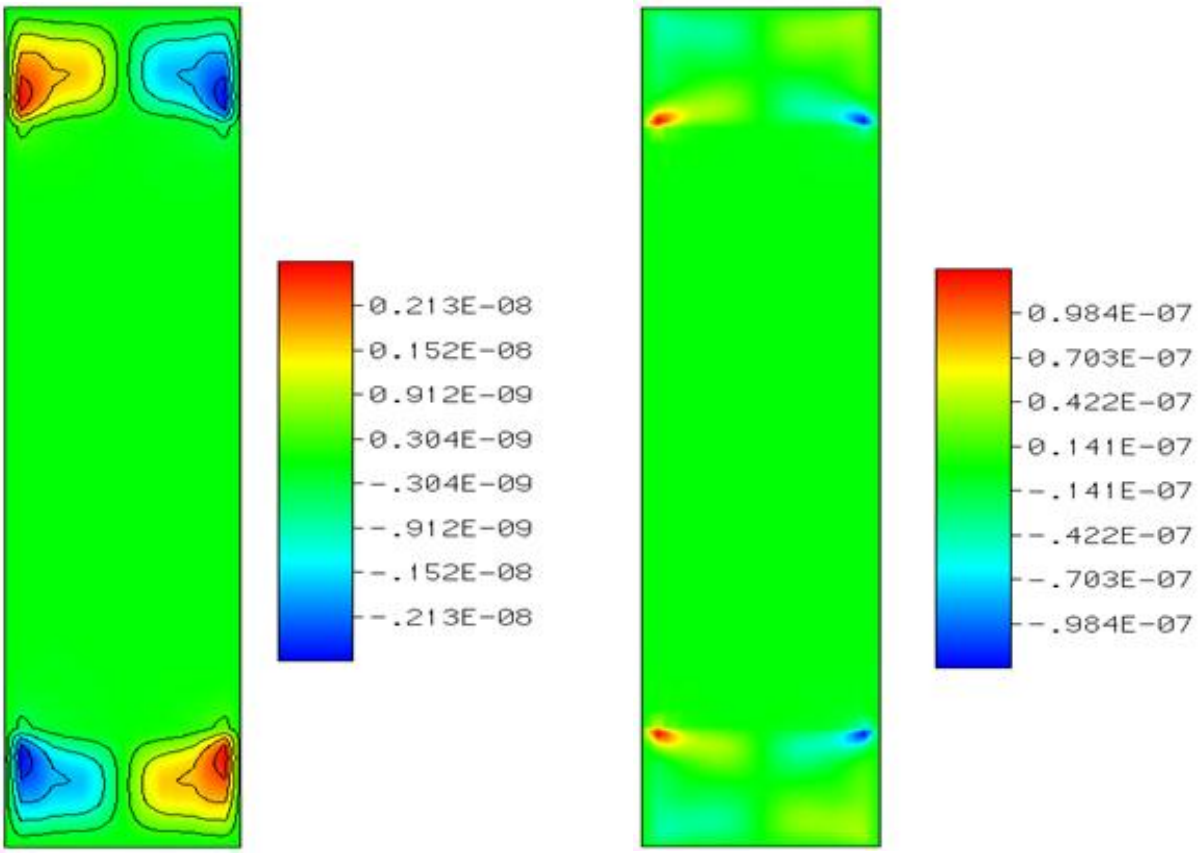

(a) **(b)**

Figure 3.9: The case of heating the system from above at ΔT=5K; (a) contours of stream lines, (b) contours of *U*

To validate these results, the Nusselt number was numerically calculated for this case. The *Nu* is 0.3329, which is less than unity (<1), therefore there is no convective heat transfer and the main mechanism of heat transfer in this model is conduction. The simulations in this model were repeated twice, once with the temperature difference between the top and bottom surfaces at 10 K and the other time at 20 K. Contours of the temperature, streamlines, and x-component of the fluid velocity have been plotted separately for each of these two cases as shown in Figures 3.10 and 3.11. There are no important differences in the temperature contours of these models from the model that used a temperature difference of ΔT = 5 K. For that reason, the original model, with ΔT = 5 K will be utilized to demonstrate the temperature contours for the three cases (refer to Figure 3.12). Likewise for the contours of the streamlines and *U*, there are no major differences from the case of the ΔT = 5 K, except a minor increase in the values of these two contours. The values of these contours, however, do not affect the stability of the system when it is heated from above. Similarly to the first model, *Nu* was numerically calculated for these two cases, and it was found to be equal to 0.3274 and 0.29176 for the case of ΔT = 10 K and ΔT = 20 K, respectively. For both cases, *Nu* is less than unity, which indicates that the conductive heat transfer mechanism is the dominant mode for these models. Multiple patterns in the horizontal direction are noticeable adjacent to the vertical wall, which is due to the temperature difference between the horizontal and the adjacent vertical walls with the heat focused on the top surface. Also, one can notice the low velocity of the fluid motion in the fluid layers. This is due to the opposition in the directions of Rayleigh–Bénard convection with the gravitational force. The temperature gradient along the y-axis of the model resulting from heating the top surface is considered a stabilizing temperature gradient because it works to minimize the fluid movement

from the density gradient. This is different from the bottom-heated case, in which the temperature gradient causes instability in the system.

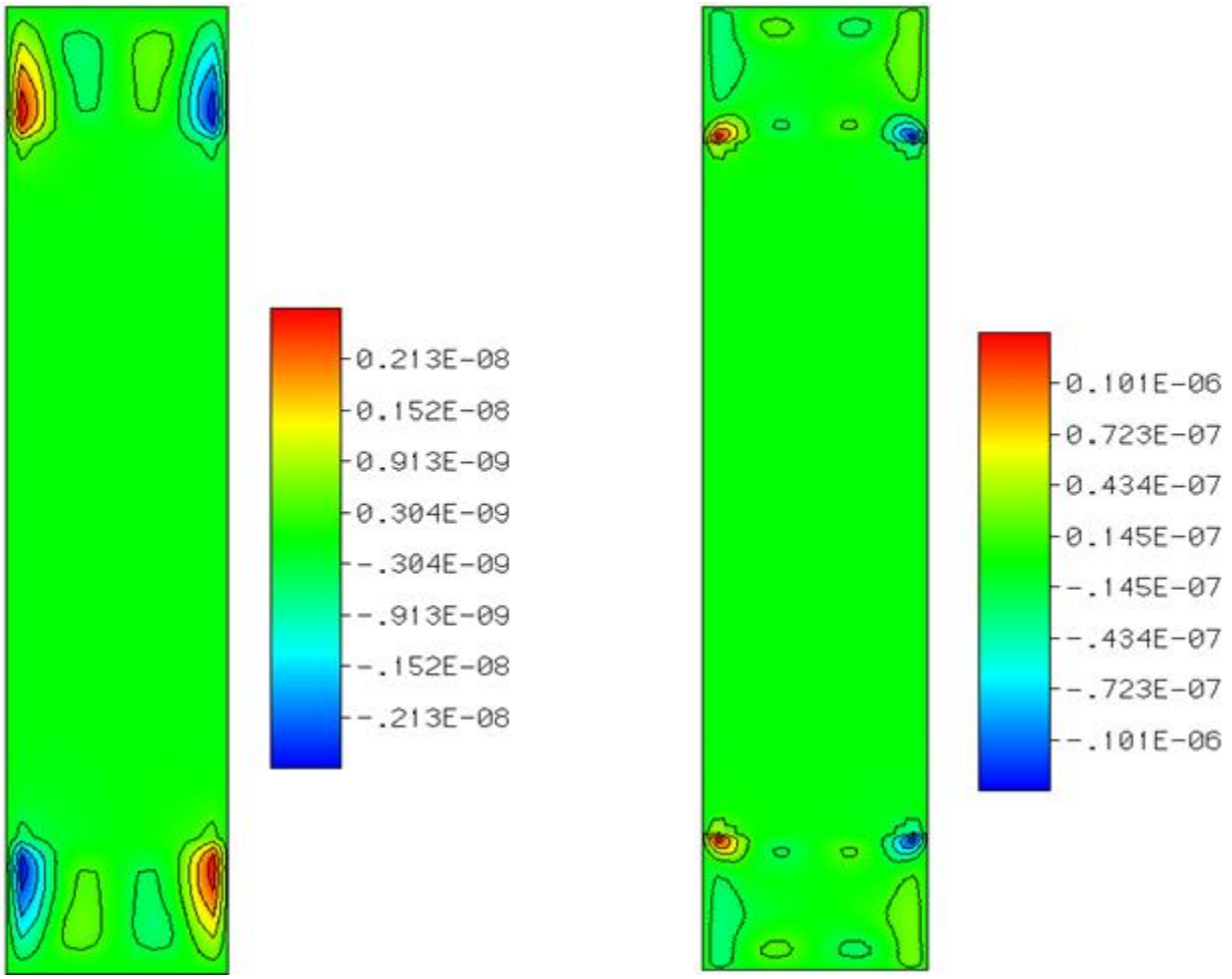

(a) **(b)**

Figure 3.10: The case of heating the system from above at ΔT=10K; (a) contours of stream lines, (b) contours of U

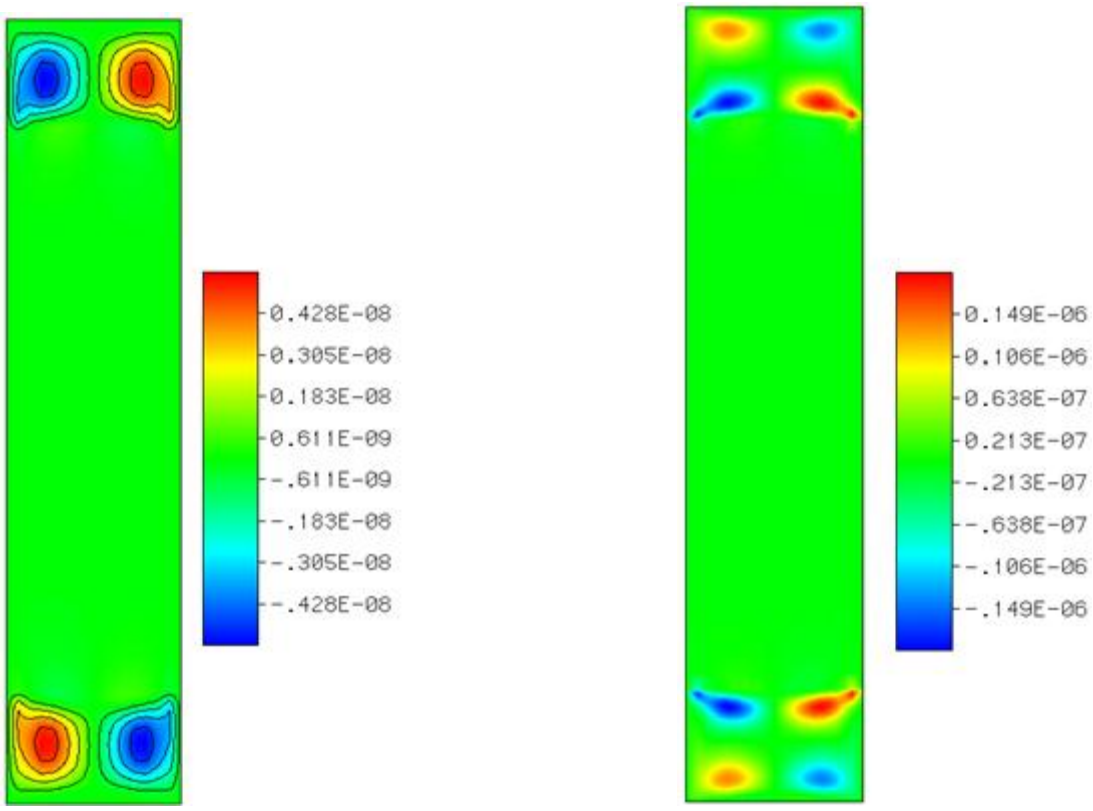

(a) **(b)**

Figure 3.11: The case of heating the system from above at ΔT=20K; (a) contours of stream lines, (b) contours of U

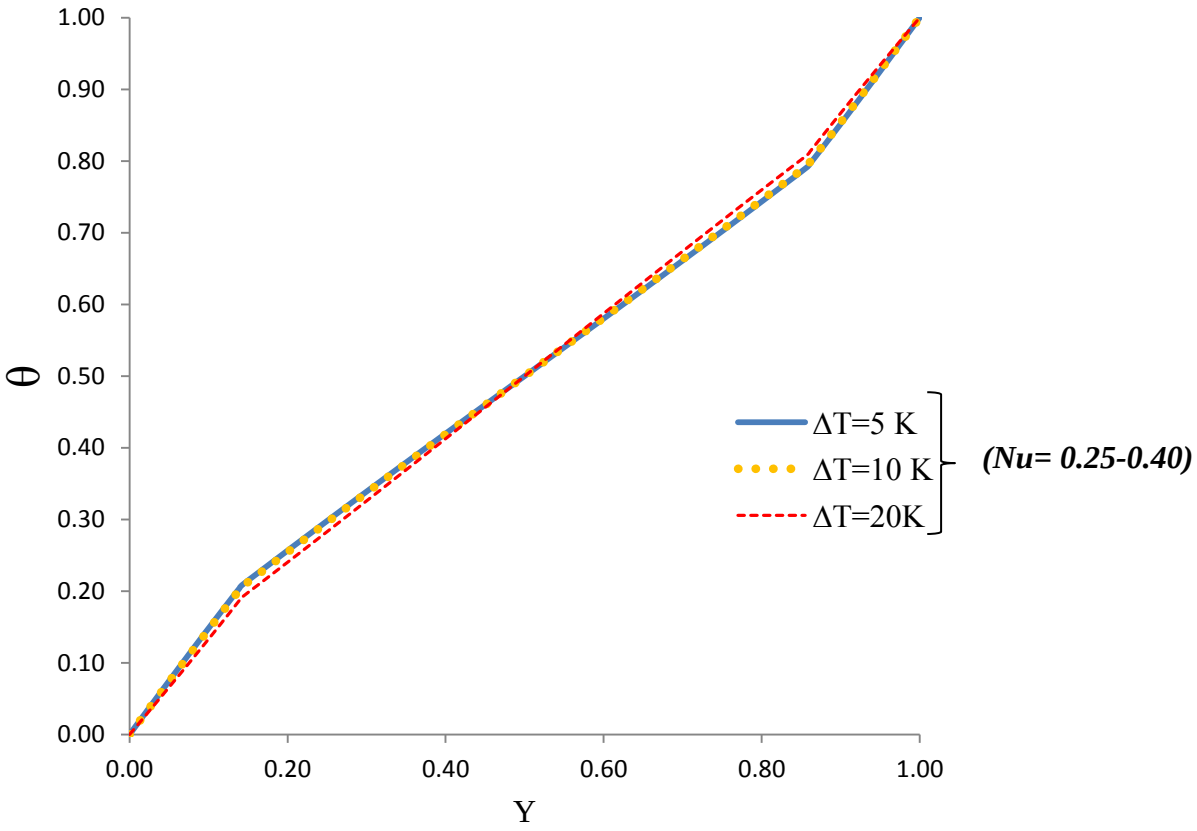

Figure 3.12: Distribution of temperature along the Y-axis at the center of the cavity for different models

3.4 Summary

A numerical study has been carried out to investigate natural convection in a cavity consisting of a porous layer sandwiched between two fluid layers of the same water-alcohol mixture. The cavity was subjected to a heat flux from the top horizontal surface. Three different models were simulated with a temperature difference between the top and bottom horizontal surfaces of 5, 10, and 20 K. For comparison, another two models were simulated with heating from the bottom horizontal surface. The temperature difference between the top and bottom horizontal surfaces was 20 K and 50 K for those two simulations. Contours of temperature, streamlines, and the x-component of the fluid velocity (U) were plotted for all five models. In addition, the average Nusselt number for each case was calculated. The results obtained from this part of the study are summarized as follows:

- Natural convection in a multi-layered system of a porous medium sandwiched between two fluid layers is not possible to be found when the system is heated from the top surface.
- The onset of natural convection in such a system occurs when the system is heated from the bottom surface, and the temperature difference between the top and bottom surfaces is sufficient to produce a density gradient of the saturated fluid, increasing the velocity of the fluid and producing the convection patterns (rolls).
- When heating from the top surface, the heat transfer occurs by the conduction mechanism, and the average Nusselt number is less than unity ($Nu_{avg} < 1$).
- No fluid motion happens when heating the system from the top surface. The system in this case is stable with a stratified temperature profile.

CHAPTER 4

Thermodiffusion in a Binary Fluid System

4.1 Introduction

The tendency of a convection-free mixture to separate under a temperature gradient is called the thermal diffusion process, which is also known as the Soret effect [44]. It was first discovered by the German scientist Carl Ludwig in 1856 and developed later by the Swiss physicist Charles Soret in 1879. The presence of a temperature gradient is the major parameter to describe thermal diffusion in a multi-component mixture (binary or ternary mixtures). Simply, when a binary mixture is under a temperature gradient, a separation of its components occurs caused by one component moving in the direction of the hot side and the other component moving in the direction of the colder side, as shown in Figure 4.1.

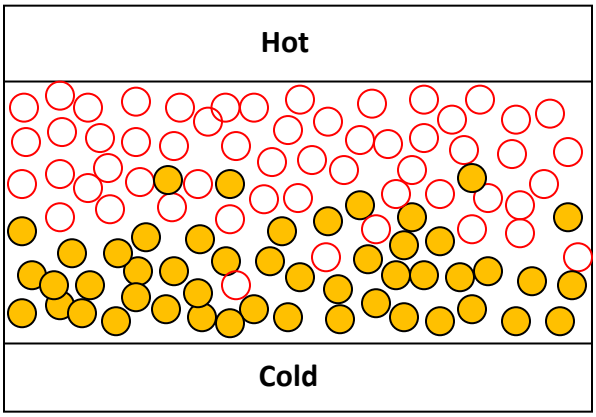

Figure 4.1: Schematic diagram of the thermal diffusion in a binary mixture

The sign of the Soret coefficient of the mixture and the density of the individual components influence this movement or separation of the components. The Soret effect for a binary mixture

can be obtained from Soret coefficient (S_T), which represents the ratio of the thermal diffusion coefficient (D_T) to the molecular diffusion coefficient (D_M). It is given as:

$$S_T = \frac{D_T}{D_M} \tag{4.1}$$

The sign of the Soret effect coefficient is either positive (+) or negative (-), which indicates the direction the components move during the separation. As a rule of thumb, the sign will be positive when the denser component moves in the direction of cold side and negative when the less dense component moves toward the colder side. According to the governing Navier-Stockes (mass balance equation), the mass flux can be presented as per the following equation:

$$J = \underbrace{\rho u_0}_{\mathbf{A}} - \underbrace{\rho D_M \nabla c}_{\mathbf{B}} - \underbrace{\rho \nabla c_0 (1 - c_0) D_T \nabla T}_{\mathbf{C}} \tag{4.2}$$

where the terms A, B, and C represent the convective, diffusive, and thermodiffusive flux, respectively.

For the condition of steady state with no convection, the total mass flux (J) becomes zero and equation (4.2) is expressed as:

$$\nabla C = -\frac{D_T}{D_M} c_0 (1 - c_0) \nabla T \tag{4.3}$$

When the two phenomena of convection and thermodiffusion are combined together in one system, a larger separation of the species in the mixture occurs. In binary mixtures, the density gradient is a function of both of the temperature gradient and mass flux (concentration) gradient, that means:

$$\nabla \rho = \left.\frac{\partial \rho}{\partial C}\right|_T \nabla C + \left.\frac{\partial \rho}{\partial T}\right|_C \nabla T \tag{4.4}$$

The thermal and concentration expansion coefficients can be expressed as:

$$\beta_T = -\frac{1}{\rho_0}\frac{\partial \rho}{\partial T} \tag{4.5}$$

and

$$\beta_C = \frac{1}{\rho_0}\frac{\partial \rho}{\partial C} \tag{4.6}$$

From equations (4.4), (4.5), and (4.6), with the assumption that temperature and concentration vary minimally, the linear variation of the density can be written as:

$$\rho = \rho_0[1 - \beta_C (c - c_0) - \beta_T (T - T_0)] \tag{4.7}$$

Note that β_C is negative if c is for the denser component.

The separation ratio describes the power of the Soret effect for a mixture, and can calculated from the following equation:

$$q = c_0(1 - c_0)\frac{\beta_C}{\beta_T} S_T \tag{4.8}$$

Equation (4.8) represents the ratio of the concentration caused by the density gradient to that which is caused by the temperature gradient in the system. The concentration gradient normally occurs from external boundary conditions, but it is possible for it to exist in a system similar to the one of the current study. The Soret effect is responsible for producing a concentration gradient from the temperature gradient. From equations (4.1) to (4.8), the density gradient for binary fluids can be expressed as:

$$\nabla \rho = \rho_0 \beta_T (1 + q) \nabla T \tag{4.9}$$

Several models and methods have been developed to measure the Soret coefficients of binary systems. Some of these methods are listed below [45]:

- Flow cell: a very thin layer flows in the Poiseuille regime and a sharp edge at the outlet separates the flow in the upper and lower halves. By employing densitometry, a

calculation of the difference in concentration between the two halves will indicate the separation process in this thin layer.

- Diaphragm cell: a porous medium is used to separate the flow into two columns at different temperatures. This creates a differential accumulation of different species at the top and bottom. The Soret coefficient is then calculated from these separation processes that happen in the system.
- Laser-Doppler velocimetry (LDV) technique: an experimental cell consists of two horizontal copper plates that are maintained at different, constant temperatures. The imposed temperature difference is then gradually increased. Enough time is allowed between two successive temperature increments to allow a steady state to be established. The time-dependent velocity amplitude is recorded, and on the onset of convection the critical temperature difference and the dimensional frequency corresponding to the oscillation of the velocity amplitude is used to calculate the Soret coefficient.

4.2 Sign of the Soret Coefficient

According to Fick's law of diffusion, the thermal diffusion flux can be presented as per equation (4.2). When the system containing the binary fluid reaches the condition of steady state, $J = 0$ and the convective term can be eliminated. At this condition, equation (4.2) can be expressed as:

$$0 = 0 - \rho D_M \nabla c - \rho c_0 (1 - c_0) D_T \nabla T \tag{4.10}$$

$$\nabla c = -\frac{c_0 (1 - c_0) D_T \nabla T}{D_M} \tag{4.11}$$

$$\nabla c = - c_0 (1 - c_0) S_T \nabla T \tag{4.12}$$

$$\frac{\nabla c}{\nabla T} = - \ c_0(1 - c_0)S_T \qquad (4.13)$$

Equation (4.13) gives the direction of the species separation according to the sign of the Soret coefficient. If S_T is negative, then the term ($\nabla C/ \nabla T$) is positive, which means that the concentration of one of the components is greater at the hotter surface than at the colder surface. To know which component has a higher concentration close to the hot surface, we need to know the value of β_C, if $\beta_C > 0$, which means the thermal induced density gradient is positive ($\frac{\Delta\rho}{\Delta T} = \beta_C \frac{\Delta C}{\Delta T} > 0$), then the denser species have moved to the hotter side. Therefore, when S_T is negative, the denser component moves in the direction of the hotter side. These equations explain the different signs of the Soret coefficient for a binary mixture of isopropanol and water when the mixing percentage rates (molar fraction) change, as will be explained in Section 4.3.

4.3 Thermodiffusion in a Water-Alcohol Mixture

In the present Section, we will study the thermodiffusion or Soret effect in water and isopropanol binary mixtures, and determine the separation process depending of the sign of the Soret coefficient. As shown in Figure 4.2, the sign of the Soret coefficient of a water-isopropanol binary mixture is strongly dependent on the component ratio. The Soret coefficient is negative ($S_T < 0$) if the water content is greater than 75%, otherwise the Soret coefficient is positive

($S_T > 0$). Therefore, to study the phenomenon of the Soret effect in a binary mixture, we examined two water-isopropanol mixtures having different Soret coefficients. The first case will

deal with a binary mixture of 10% isopropanol and 90% water, having a Prandtl number *Pr* = 10.846 and the Schmidt number was *Sc* = 1620.9. In the second case for the mixture of 50% isopropanol and 50% water, the Prandtl number was higher at *Pr* = 49.165 and the Schmidt number was equal to *Sc* = 23216.667.

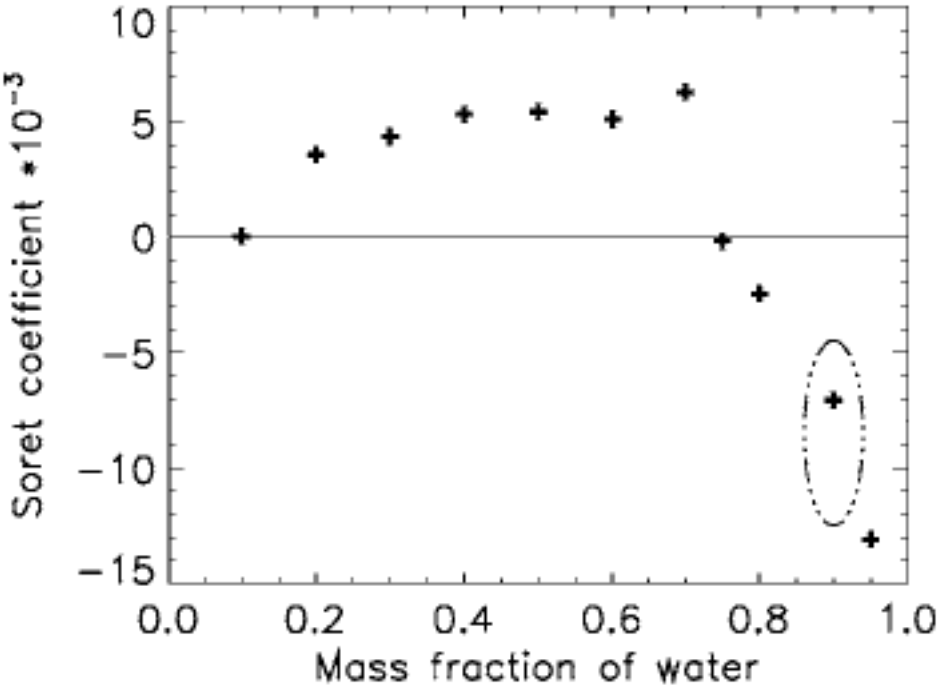

Figure 4.2: Dependence of the Soret coefficient on the mass fraction of water in water-isopropanol mixture (298.15 K) [46]

To activate the Soret effect, both the molecular diffusion coefficient D_M and the thermodiffusion coefficient D_T have been taken into consideration in the mass balance equation and were assumed constant during the calculations despite the changing temperature difference. The model configuration, fluid properties, and porous specifications are the same as were used in chapter 3.

4.3.1 Thermodiffusion in Water-Alcohol Mixture with Negative S_T

The first part of the study was to investigate the separation process and the direction of the component movement when the Soret coefficient of the binary mixture was negative. For this purpose, the mixture of 10% isopropanol and 90% water was selected and modeled in a cavity with a configuration and boundary conditions shown in Figure 4.3.

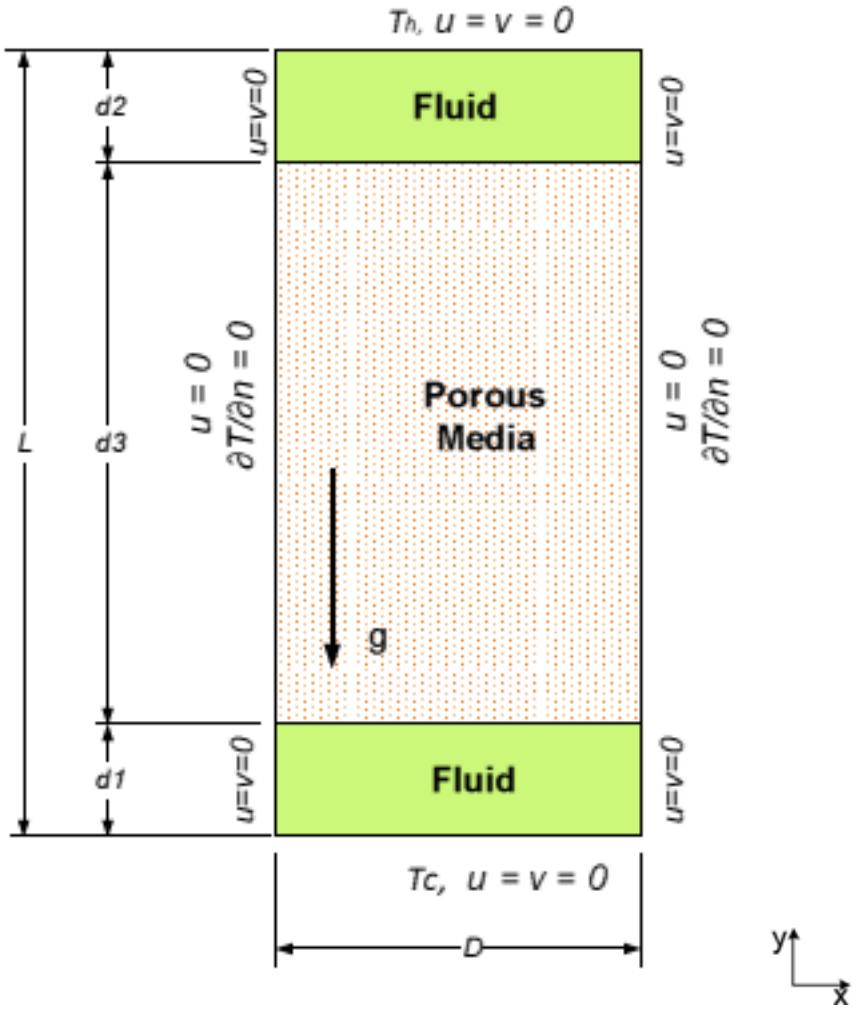

Figure 4.3: Model configuration and boundary conditions for the system under study.

The liquid layers were assumed quiescent, incompressible, Newtonian, and viscous with thermal expansion coefficients of β_T and solutal expansion coefficients of β_C. The width of the closure (D) is 10 mm with a total height (L) of 45 mm. The porous layer has a height (*d3*) of 32.2 mm, while each of the fluid layers has a height (*d1* and *d2*) of 6.40 mm. The physical properties of the liquids are assumed constant. The side (vertical) walls of the closure assumed adiabatic. The temperature of the top wall (T_h) of the closure will be greater than the temperature of the bottom wall (T_c), and the temperature difference (ΔT) between them will be 5, 10, and 20 K. It is assumed that the liquid and the porous layers are in thermal equilibrium. The porous medium has a porosity ϕ = 0.39, which corresponds to glass beads of 3.25 mm diameter. The Darcy number was calculated by using Kozeny-Carmen relation as described in equation (2.1). Three different cases have been selected to study the effect of temperature on the thermodiffusion. The three cases differ in the temperature difference between the hotter top surface and the colder bottom surface. The three temperature differences were 5, 10 and 20 K, keeping the bottom (colder) surface as 298 K for all of the three cases. A full set of plots for temperature, horizontal velocity (U), streamlines, and species separation, were drawn to study each case separately. For the temperature contours, no difference was noticed from the case of natural convection, which was discussed in chapter 3. The temperature in these cases is stratified in the same style and with similar values as for the equivalent case of natural convection (for all the values of ΔT=5, 10 and 20 K). Figure 4.4 illustrates the separation process that occurred in the mixture for each case of ΔT. The concentration of the isopropanol (lighter component of the mixture) is higher near the colder surface (bottom), while the concentration of water (heavier component of the mixture) is higher near the hotter surface (top). This is due to the presence of the thermodiffusion phenomenon, as expected. The streamlines and horizontal velocity (U) are shown in Figures 4.5

and 4.6, respectively. It is clear that there is a small increment in the values of these two parameters over that of the case of natural convection, and there is some noticeable fluid motion and currents in the bottom fluid layer near the colder surface. This motion and current are results of the separation process and the migration of the lighter component (isopropanol) toward the cold side.

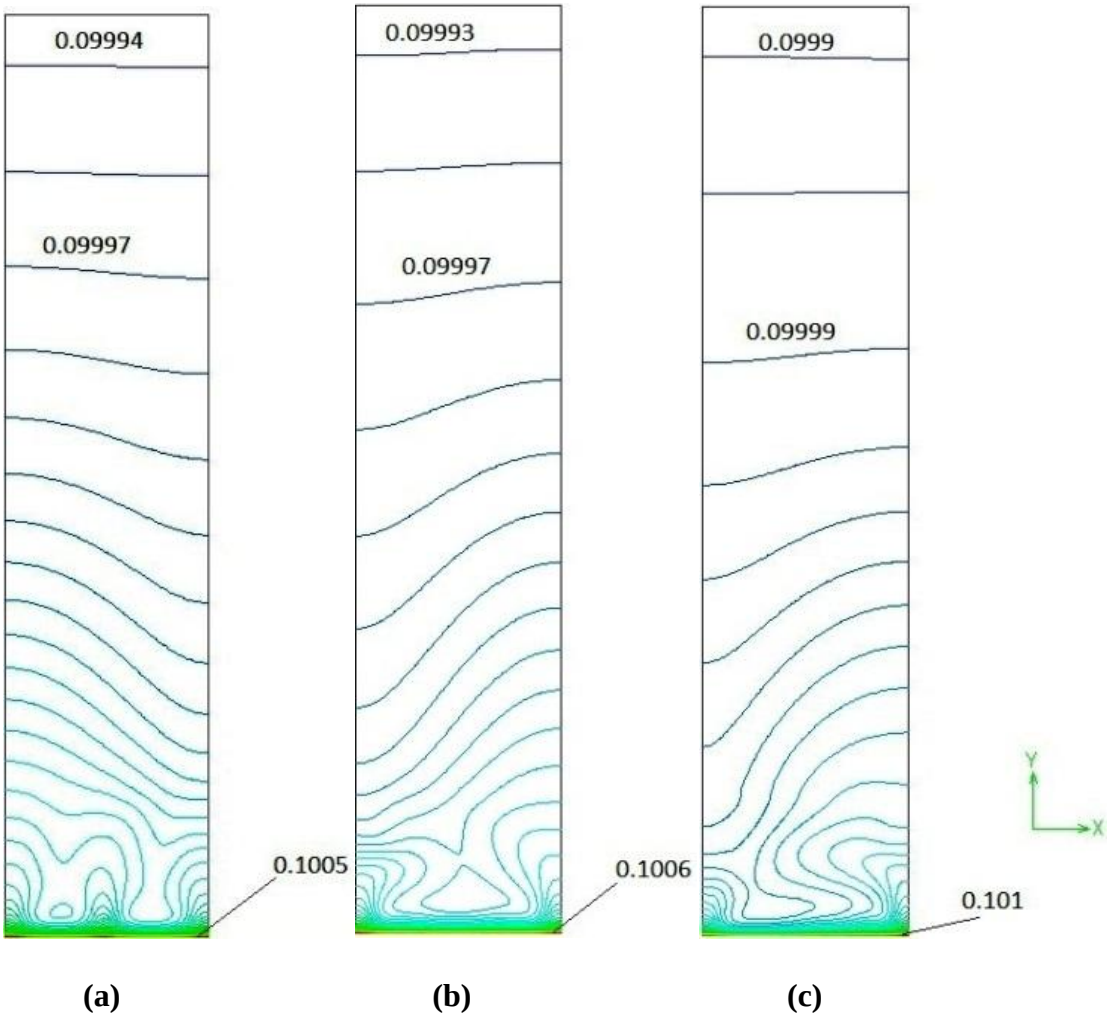

Figure 4.4: Contours of the isopropanol species [(a) ΔT = 5 K, (b) ΔT = 10 K and (c) ΔT = 20 K]

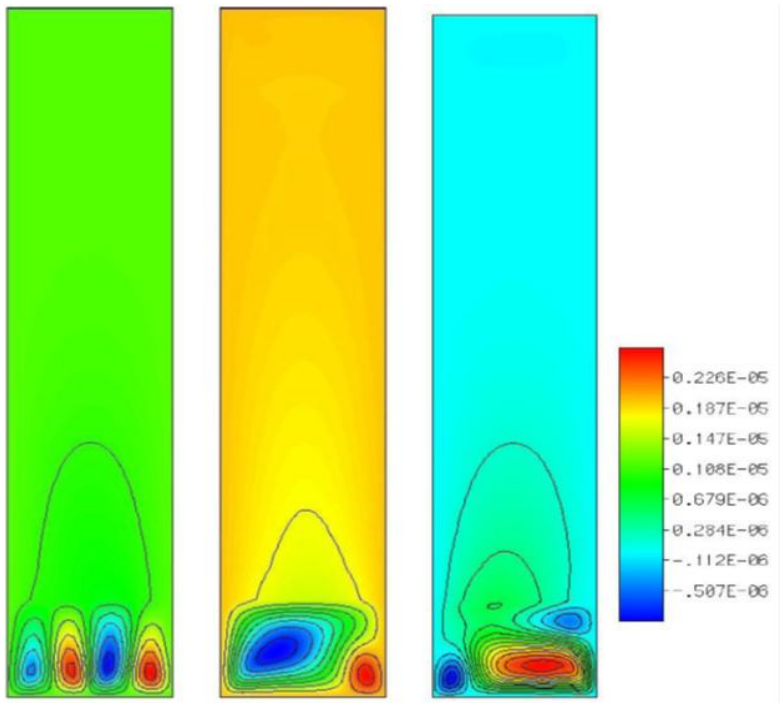

Figure 4.5: Contours of streamlines (a) ΔT=5K, (b) ΔT=10 K and (c) ΔT=20K.

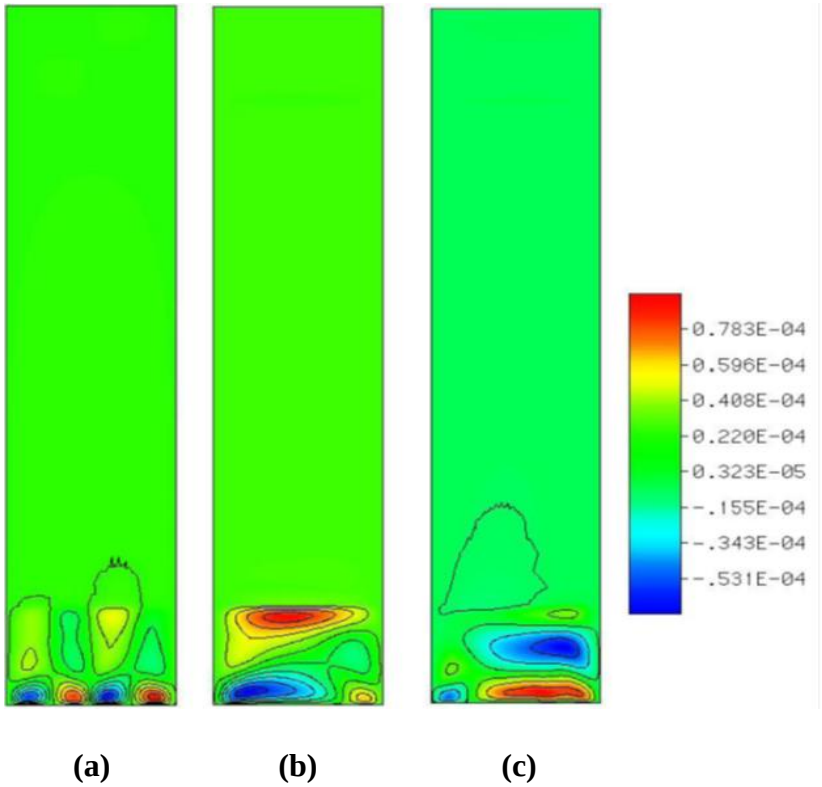

Figure 4.6: Contours of *U;* (a) ΔT=5 K, (b) ΔT=10 K and (c) ΔT=20K.

Because binary mixtures have more components (species), more phenomena can occur than in pure fluids. Therefore, in pure fluids, the temperature gradient is the only reason for producing buoyancy forces, which are responsible for the onset of natural convection. In binary mixtures, on the other hand, the buoyancy forces produced are due to both the temperature and species concentration gradients. Buoyancy convection in binary mixtures is noticeably more complicated than in pure fluids. This is because of the interaction between convection, thermal diffusion, and solutal diffusion. The orientation of temperature and concentration gradients relative to each other plays a major role in determining the dynamics of convection in binary mixtures, and these can be very different from those induced by thermal buoyancy [47]. In the top-heating configuration, the density will not decrease in the same direction as the gravitational force, which will lead to a diffusive regime. Therefore, this diffusion will cause a separation of species in the porous layer. For this particle configuration, eliminating the convection is important to be able to study the thermodiffusion effect. The thermal characteristic time, which represents the time required for heat to diffuse through a distance equal to the characteristic length of the system in order to establish the applied temperature field in that system, can be expressed as:

$$\tau_{th} = \frac{L^2}{\alpha} \tag{4.14}$$

While the mass diffusion characteristic time (diffusive characteristic time) can be written as:

$$\tau_D = \frac{L^2}{D_M} \tag{4.15}$$

In most binary mixtures such water-alcohol, there is a time difference between the thermal characteristic time and diffusive characteristic time in the system. This time difference is due to the slower rate of the mass diffusion of isopropanol than the rate of the heat diffusion in the system caused by the temperature difference between the surfaces. This time difference leads to

the occurrence of some convection patterns. For both of the mixtures used in our study, the mass flow characteristic time (τ_D) is greater than the thermal characteristic time (τ_{th}) (as shown in Appendix C) which causes thermodiffusion to be the major mechanism for the separation of the species in the mixture. The Rayleigh number is considered the criterion for determining whether heat transfer will be in the form of convection or conduction. When heating the system from above, the Rayleigh number will be opposite to the gravitational force (g), which will reduce the convection in the system. In binary fluids, two types of Rayleigh numbers need to be considered: the solutal and thermal Rayleigh numbers. We have calculated both the thermal and solutal Rayleigh numbers for the three layers of our system for the three cases of ΔT of 5, 10 and 20 K for the mixture of 10% isopropanol and 90% water. Table 4.1 shows the values of Ra_S and Ra_T for both of the fluid layers and the porous medium. The calculated Rayleigh numbers indicate that the Ra_T in all the layers of the system under study is opposite to the gravity force, which means that is no convection in the system and diffusion is the only way for heat to be transferred. For all the three cases of ΔT, $Ra_T > Ra_S$ which means that heat diffusion has greater effect than mass diffusion. It is expected that Ra_S at the bottom fluid layer is greater than top fluid layer. This is because $S_T < 0$, which causes the lighter component of the mixture to migrate in the direction of the colder surface (bottom), and because this bottom fluid layer is surrounded by the porous layer from the top, which resists the fluid flow, causing a convective motion to occur in this layer until the concentration has reached steady state. Brand *et al.* [48] first recognized that with the Soret effect it is possible to have oscillatory convection induced by heating from above. They evaluated the range of the existence of an oscillatory instability as a function of the separation ratio (q) and found that if the expansion coefficient (β_C) is negative and the thermodiffusion coefficient is negative, instability could start by sustained oscillations at

onset. The authors concluded that either a stationary instability or an oscillatory instability can occur as the first bifurcation depending on the sign and the magnitude of the Soret coefficient.

Table 4.1: Thermal and solutal Rayleigh numbers for fluid and porous layers for 10% isopropanol and 90 % water

	$\Delta T = 5\ K$	$\Delta T = 10\ K$	$\Delta T = 20\ K$
Top Fluid Layer:			
Ra_{TL}	4327.44	8695.75	17396.75
Ra_{SL}	21.61	31.26	43.21
Porous Layer:			
Ra_{TP}	16	31.6	63.1
Ra_{SP}	4.08	2.40	0.700
Bottom Fluid Layer:			
Ra_{TL}	4331.8	8698.4	17396.75
Ra_{SL}	748.34	1021.35	1459.36

Charrier-Mojtabi *et al.* [49] found that for a cell heated from above, the equilibrium solution is linearly stable if $q > 0$, while a stationary or an oscillatory bifurcation occurs if $q < 0$. Also, Shevtsova *et al* [50] conducted a numerical modeling of Soret-driven convection in a cubic cell filled with 10% isopropanol and 90% water and observed that there is an instability that occurs in the binary mixture with a negative separation ratio while heating from above because of the large differences between viscous, thermal, and diffusion times. In addition, they found that for a relatively low applied temperature difference (ΔT), the lighter and colder liquid is drawn up in the central part of the cell and the heavier liquid flows down along the walls. For finite size systems the situation is reversed at higher ΔT. Figure 4.7 shows the time step sequence for the separation process at ΔT = 20 K. It is apparent that the separation of the species increases with increased processing time, and a larger amount of the lighter component of the mixture migrates

towards the colder side and more of the heavier component migrates toward the hotter side with an increase in time as well. The instability of the system increases with the increasing of the time steps.

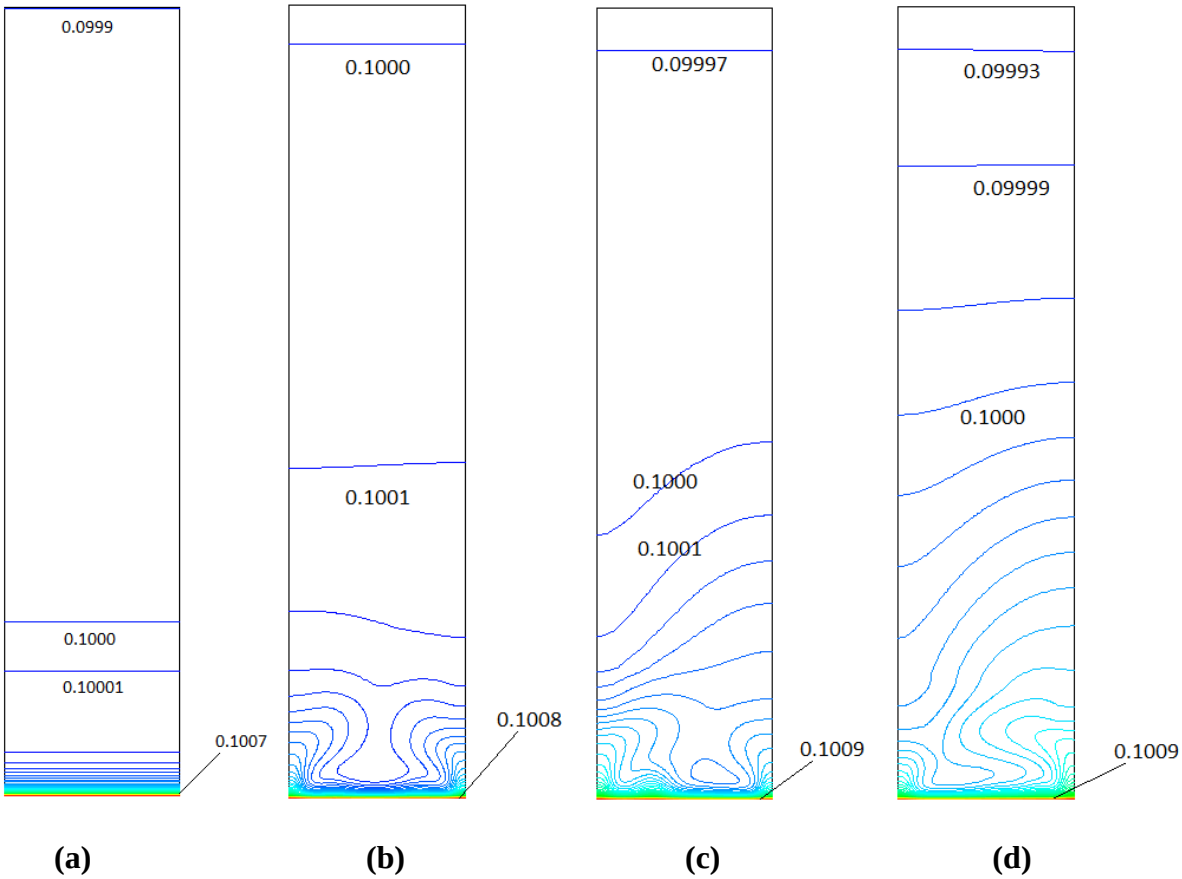

Figure 4.7: Contours of the concentration of isopropanol in a mixture of 10% isopropanol and 90% water at ΔT=20 K at various time steps; (a) 1.25 hr., (b) 12.5 hr., (c) 36.3 hr. and (d) 72 hr.

It is clear from Figure 4.8 that increasing the temperature difference (ΔT) between the top and bottom surfaces of the cavity enhances the process of species separation. This is due to the enhancement of the density gradient from the increased temperature difference in addition to the thermal diffusion flux, which is proportional to the gradient of temperature (equation (4.2)).

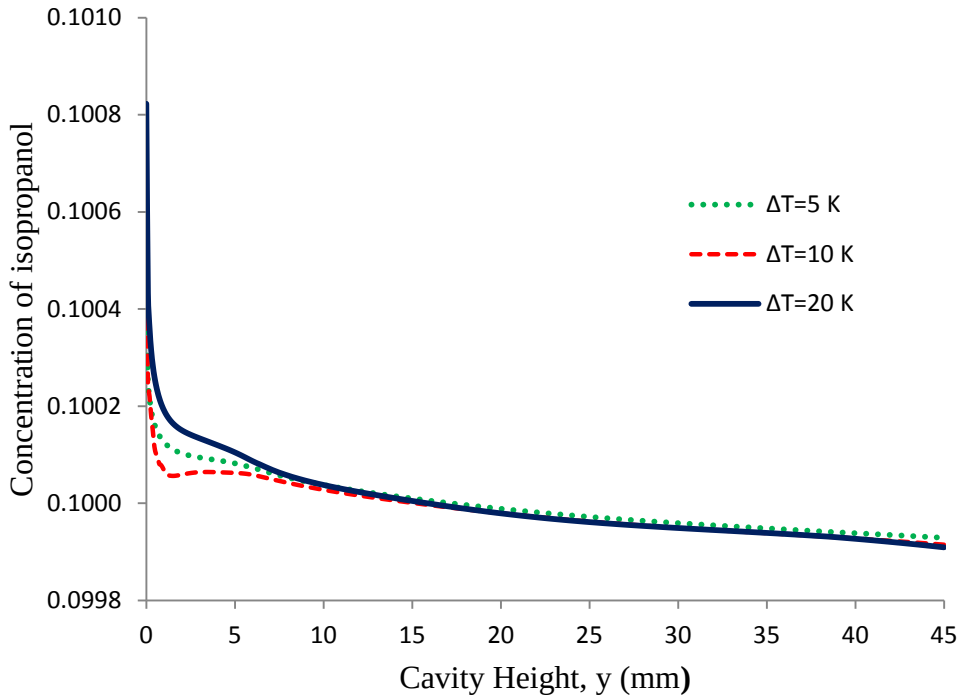

Figure 4.8 Influence of temperature difference on the separation process for 10% isopropanol and 90% water mixture

4.3.2 Thermodiffusion in Water-Alcohol Mixture with Positive S_T

The second part of our study was to investigate the separation process and the direction of the component movement when the Soret coefficient of the binary mixture was positive. For this purpose, the mixture of 50% isopropanol and 50% water was selected and modeled in a cavity with a configuration and boundary conditions similar to the system shown in Figure 4.2. With this type of fluid having a positive Soret coefficient, we still found that there was no major difference from the previous case of that with a negative Soret coefficient, except for the direction of the component separation. As seen in Figure 4.9, the direction of the component separation was opposite to the direction that occurred in the previous case when we modeled a fluid with a negative Soret coefficient. Here, the lighter component of the mixture (isopropanol)

migrated towards the hotter side while the heavier component (water) migrated in the direction of the colder side. This opposition of the migration direction is due to the opposite sign of the Soret coefficient.

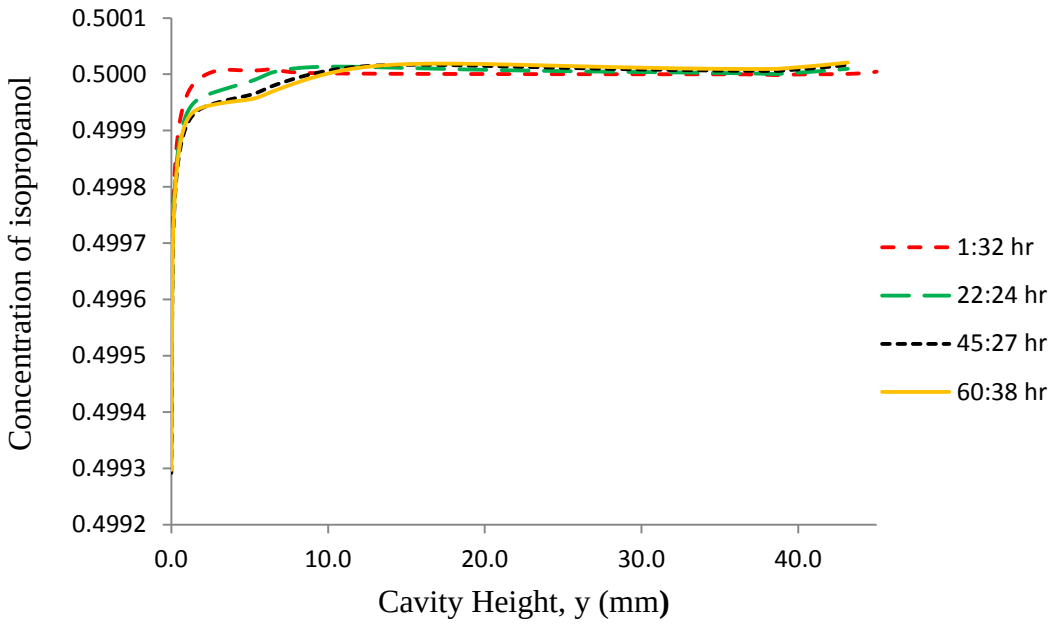

Figure 4.9 Concentration distribution for 50% isopropanol and 50% water mixture (at ΔT=20K) at various time steps

4.4 Summary

A numerical study has been performed to investigate the thermodiffusion (Soret effect) in a cavity consisting of a porous layer sandwiched between two layers of the same water-alcohol binary mixture. The cavity is subjected to heating conditions from the top surface. Three different models have been simulated with a temperature difference between the top and bottom horizontal surfaces of 5, 10 and 20 K. The results obtained from this part of the study can be summarized as follows:

- The first case, performed using a binary mixture of 10% isopropanol and 90% water, was a system with a negative Soret coefficient. The lighter species migrated in the direction of the colder surface while the denser species migrated in the direction of the hotter surface.
- Increasing the temperature difference in the system enhances the separation process. This is due to the greater density gradient caused by the larger temperature difference and the thermal diffusion flux, which is proportional to the gradient of temperature.
- There were some increases in the values of horizontal velocity and streamlines in the bottom fluid layer compared to their values in the case of natural convection. This is an indication for motion in the bottom fluid layer due to the separation process and the migration of the mixture components.
- In the second study case, the binary mixture was changed to a mixture of 50% isopropanol and 50% water, which is a system that has a positive Soret coefficient. The lighter species migrated in the direction of the hotter surface while the denser species migrated in the direction of the colder surface.

CHAPTER 5

Thermodiffusion in Hydrocarbon Binary Fluids

5.1 Introduction

Hydrocarbon fluids are natural compounds composed of hydrogen and carbon. Normal hexane (*n*-hexane / C_6H_{14}) is one of the hydrocarbon fluids. It is a naturally occurring alkane, and it can be extracted from crude oil and natural gas. Hexanes have a wide range of industrial applications and usages, such as textile manufacturing, glues, roofing, extraction of the cooking oils from plants seeds, and many other extracting processes of oils and grease from various items. Another hydrocarbon fluid is toluene (C_7H_8) which is also a naturally occurring chemical, and it is produced with the extraction of crude oil. In the crude oil extraction industry, it is common to find a mixture consisting of these two fluids together. In order to implement our study to the industrial field, it would be useful study a hydrocarbon mixture consisting of 50% *n*-hexane and 50% toluene and simulate the phenomenon of thermal diffusion in this mixture. A numerical study on this mixture was performed as part of the collaboration between Ryerson University (Toronto, Canada) with Université de Pau et des Pays de l'Adour (Pau, France). Figure 5.1 shows the model configuration that was used for this part of the study. The same porous material in previous chapters was used in this study, which are glass beads with diameter of 3.25 mm stacked vertically to make a height (*d3*) of 32.2 mm and 10 mm diameter (*D'*) as the total height and width of the porous layer. The porous layer has been vertically sandwiched between two layers of hydrocarbon fluids. The dimensions of each fluid layer are 21.50 mm in diameter (*D*) and 6.40 mm as a height (*d1* & *d2*) making the total cavity height (*L*) to be 45.0 mm.

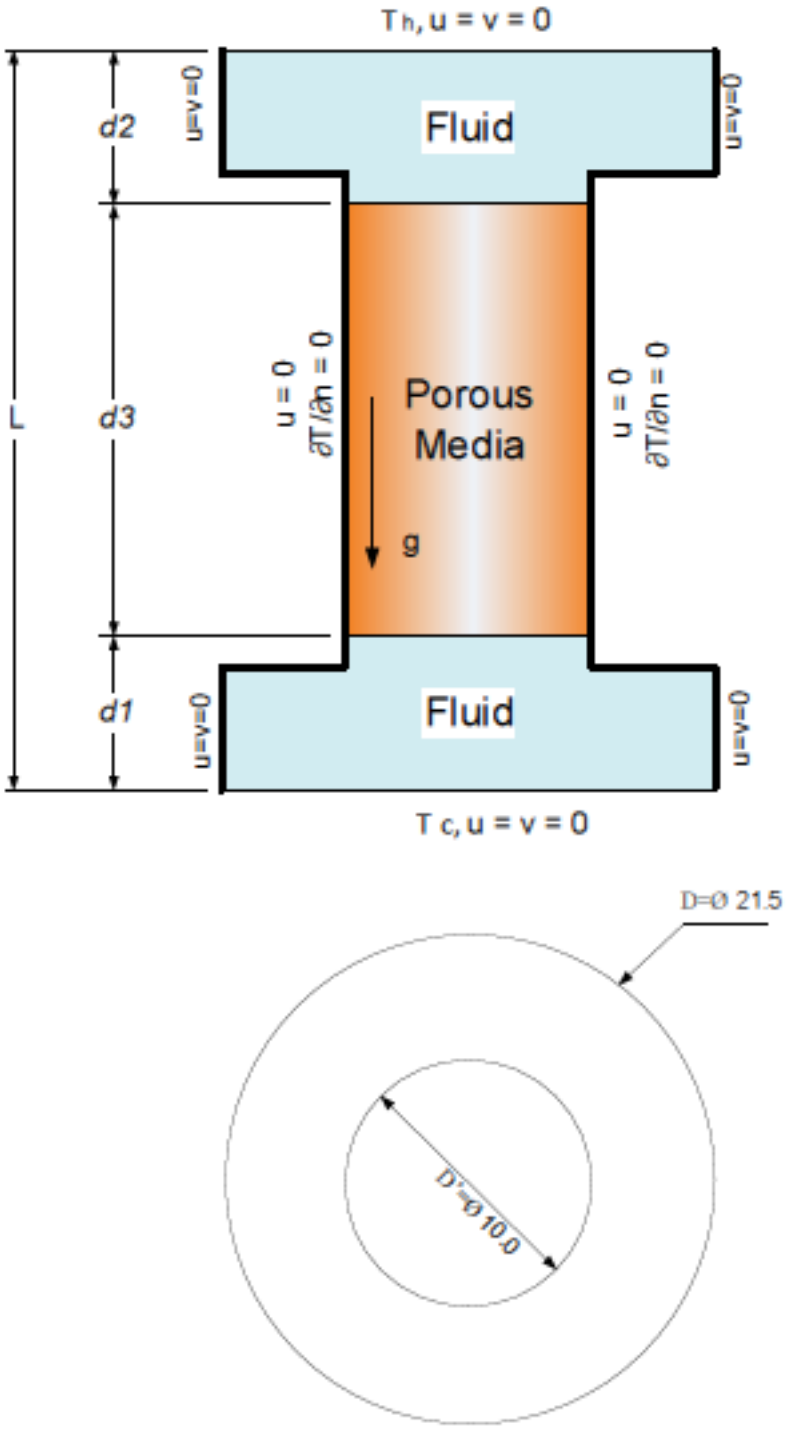

Figure 5.1: Model configuration used for the study of thermal diffusion in hydrocarbon fluids.

5.2 Prediction of Thermodynamic and Transport Properties of the Mixture

Some of the physical properties for the hydrocarbon mixture consisting of 50% toluene and 50% *n*-hexane are shown in Appendix C. Most of these properties have been predicted and calculated with the assistance of the commercial software NIST SUPERTRAPP, which is a computer database for the prediction of thermodynamic and transport properties of fluid mixtures. NIST SUPERTRAPP performs phase equilibrium calculations and provides the thermo-physical properties of all phases and the feed. These results include both equilibrium properties (density, compressibility factor, enthalpy, entropy, *Cp*, *Cp/Cv*) and transport properties (viscosity and thermal conductivity) [51]. To calculate the thermal and concentration expansion coefficients for the mixture in this investigation, we needed to calculate the terms ($\partial\rho/\partial T$) and ($\partial\rho/\partial C$), then substitute them in the following equations:

$$\beta_T = -\frac{1}{\rho_0}\frac{\partial \rho}{\partial T} \tag{5.1}$$

and

$$\beta_C = -\frac{1}{\rho_0}\frac{\partial \rho}{\partial C} \tag{5.2}$$

To calculate the term ($\partial\rho/\partial T$), we predicted the density values at different temperatures by utilizing NIST SUPERTRAPP. The obtained results have been plotted, as shown in Figure 5.2, to obtain the values of the linear trend line the slope of which is the term ($\partial\rho/\partial T$) as per the following equation:

$$y = slope * x + constant \tag{5.3}$$

The calculated value of the slope was -0.9414. Substituting this value in equation (5.1) resulted in β_T for the mixture to be 0.001261 K^{-1}. The same procedure was followed to predict the term ($\partial\rho/\partial C$), but this time the density gradient of the mixture with changing the concentration of the toluene was calculated.

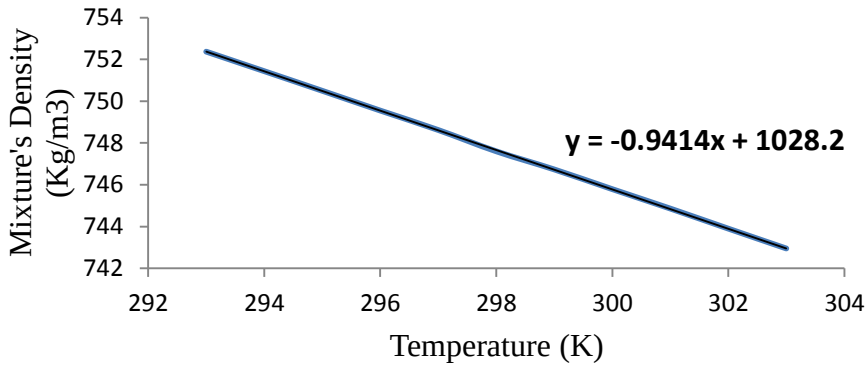

Figure 5.2: Relationship between mixture density as a function of the temperature

Figure 5.3 shows the relationship between density and concentration of the toluene. The value of the slope at this case was 209.66 and when that value was substituted it in equation (5.2) the result provided a value of -0.2881 for β_C.

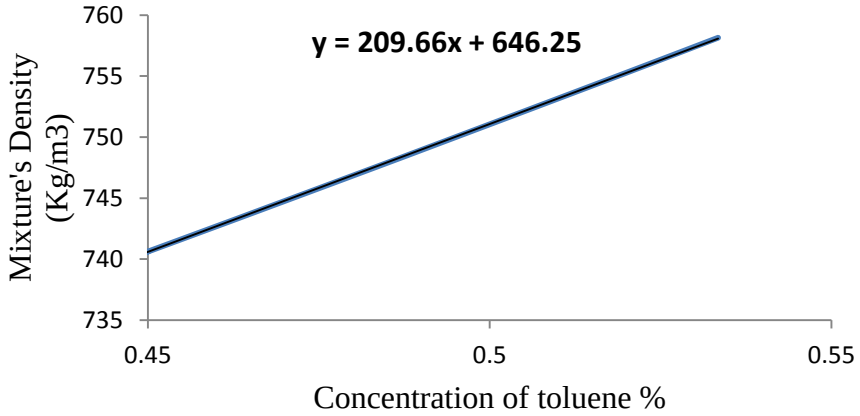

Figure 5.3: Relation between mixture density as a function of the concentration of toluene

5.3 Multi-Dimension Numerical Analysis

5.3.1 Two-Dimensional (2D) Analysis

A two-dimensional simulation analysis was performed as a first step to study the thermodiffusion of a hydrocarbon mixture consisting of 50% toluene and 50% *n*-hexane. The Soret coefficient of this mixture was positive 0.004915 1/K, the dimensionless Prandtl number was Pr = 5.74, and the dimensionless Schmidt number was Sc = 185. Three different cases were conducted for this part of study. These cases differed in the temperature difference applied between the horizontal surfaces (top and bottom) of the model, but all of them had the heating from the top horizontal surface.

A temperature difference of 5 K was applied for the first case. Contours of isotherms, streamlines, U, and species separation of *n*-hexane are shown in Figures 5.4 to Figure 5.7. No major differences are evident from the previous study of the thermal diffusion in a binary alcohol mixture with a positive Soret coefficient. Some minor differences are little disturbances in the temperature contours in the fluid zones, and small increases in the values of the stream functions and U with the appearance of more convection patterns. We believe that these minor differences are due to the special geometry of the model, especially in the fluid zones where there is a diameter reduction from 21.5 mm to 10.0 mm with some sharp edges. The same numerical analysis was performedfor the model twice more, but using a temperature difference of ΔT = 10 K and then ΔT = 20 K. When the temperature was increased, there was a noticeable increase in the species separation of the *n*-hexane in the direction of the hotter horizontal surface (top), as shown in Figures 5.8 and 5.9.

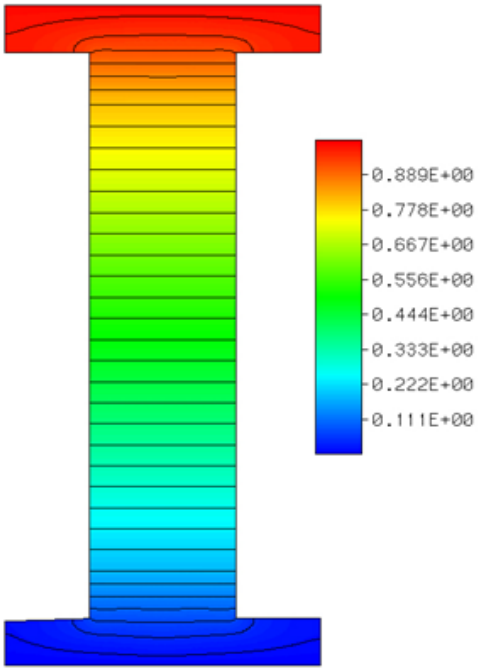

Figure 5.4: Contours of temperature at ΔT=5 K

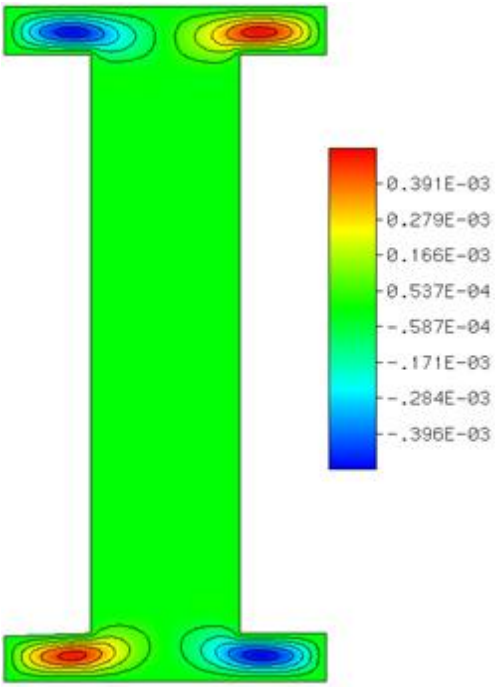

Figure 5.5: Contours of streamlines at ΔT=5 K

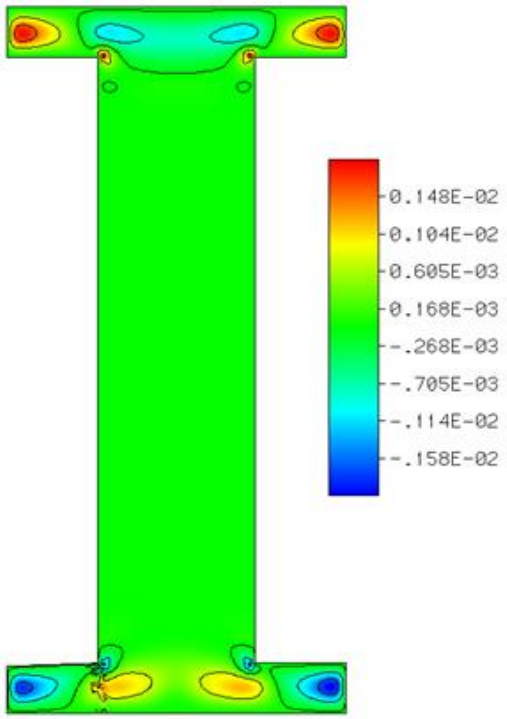

Figure 5.6: Contours of *U* at ΔT=5 K

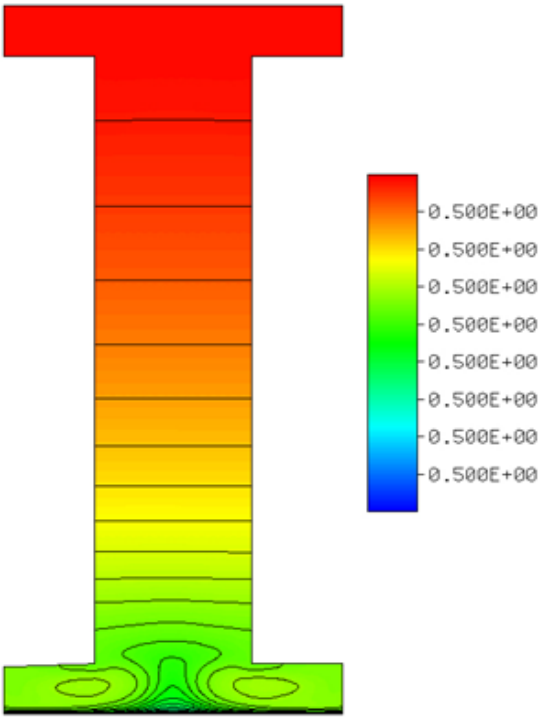

Figure 5.7: Contours of the concentration of *n*-hexane at ΔT=5 K

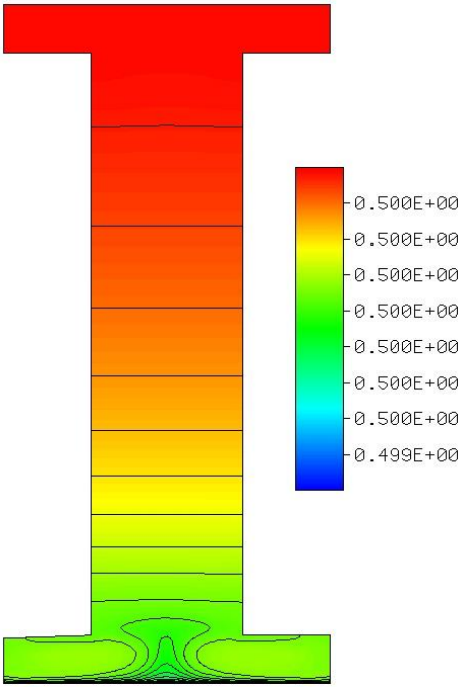

Figure 5.8 Contours of the concentration of *n*-hexane at ΔT=10 K

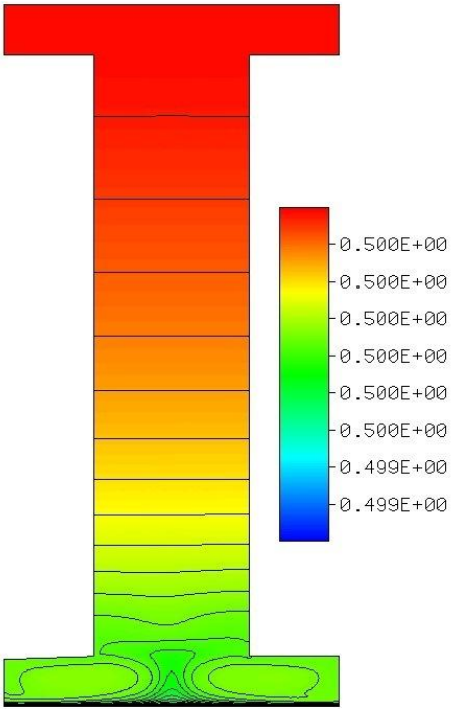

Figure 5.9 Contours of the concentration of *n*-hexane at ΔT=20 K

Figure 5.10 shows the concentration difference of *n*-hexane at various temperature differences between the top and bottom horizontal surfaces. Increasing the temperature difference leads to a greater concentration difference of the lighter *n*-hexane species (density of n-hexane is= 0.655 g/ml and of toluene = 0.87 g/mol) near the hotter surface. The migration of the lighter species to the hotter surface is due to the positive Soret coefficient of this binary hydrocarbon mixture. The effect of increasing the temperature difference on the separation ratio of *n*-hexane has been plotted in Figure 5.11. It is clear that increasing the temperature difference (ΔT) enhaces the seperation of the species.

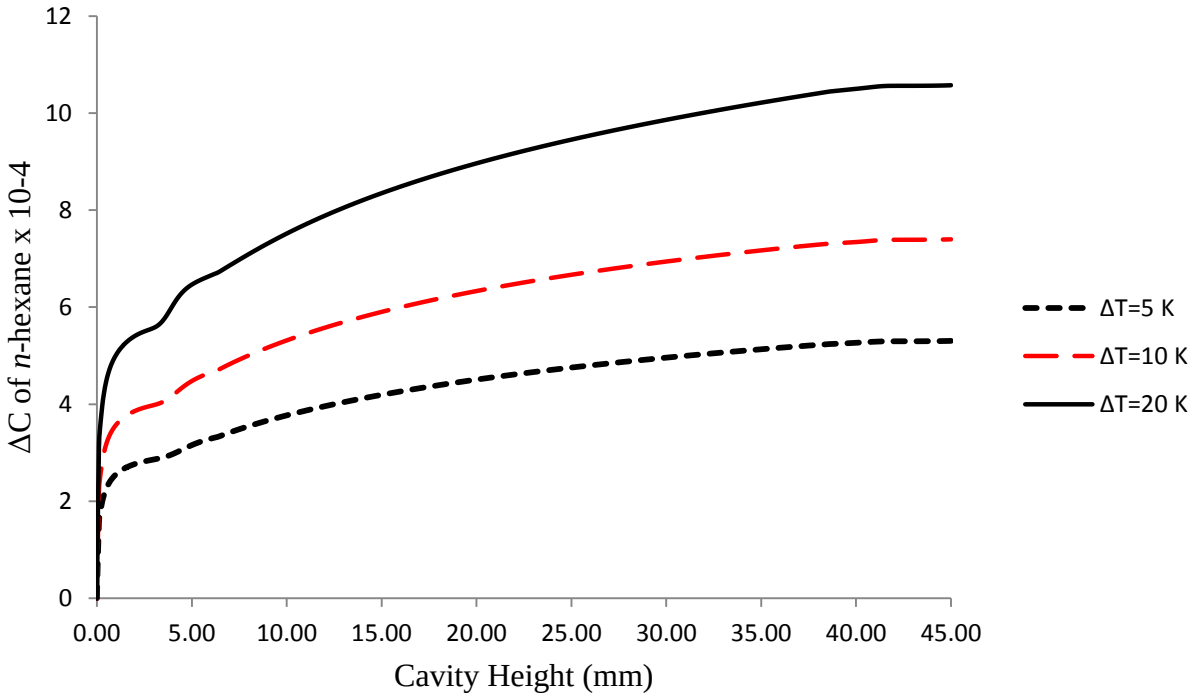

Figure 5.10: Concentration of *n*-hexane vs. the cavity height at various temperature differences between the top and bottom surfaces

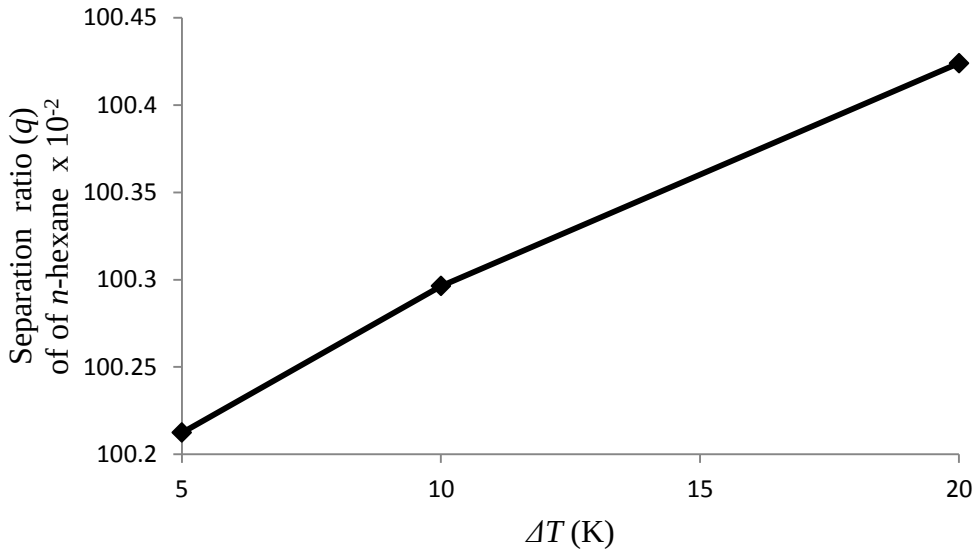

Figure 5.11: Separation ratios (q) of *n*-hexane vs. ΔT between the top and bottom horizontal surfaces

5.3.2 Three-Dimensional (3D) Analysis

In order to obtain a simulation with more accuracy, and to better understand of the phenomenon under study, a three-dimensional simulation has been conducted on the case of this chapter. To generate the mesh for the geometry of our three-dimensional model, which is the most complex part of the CFD (computational fluid dynamics) problem, commercial software called GAMBIT has been utilized. GAMBIT is a commercial software package designed to build and mesh models for computational fluid dynamics and other scientific applications. It receives user input by means of its graphical user interface (GUI) [52]. Over fifteen thousand nodes have been utilized for the three-dimensional model in this study, and I chose to use triangular meshes which contain group of triangles connected together by their sides and edges. After generating the three-dimensional mesh using GAMBIT, the model has been exported to another CFD software

called FLUENT 6.1. FLUENT is a computer programme designed to model incompressible and compressible fluid flow and heat transfer in complex geometries. It provides complete mesh flexibility, solving flow problems with unstructured meshes that can be generated about complex geometries with relative ease. All flow operations such as defining material properties, setting boundary conditions, refining the grids, executing the solution, and viewing and post-processing the results can be performed in FLUENT within a solver [53]. Figure 5.12 illustrates the three-dimensional model configuration and triangular meshes used in this study.

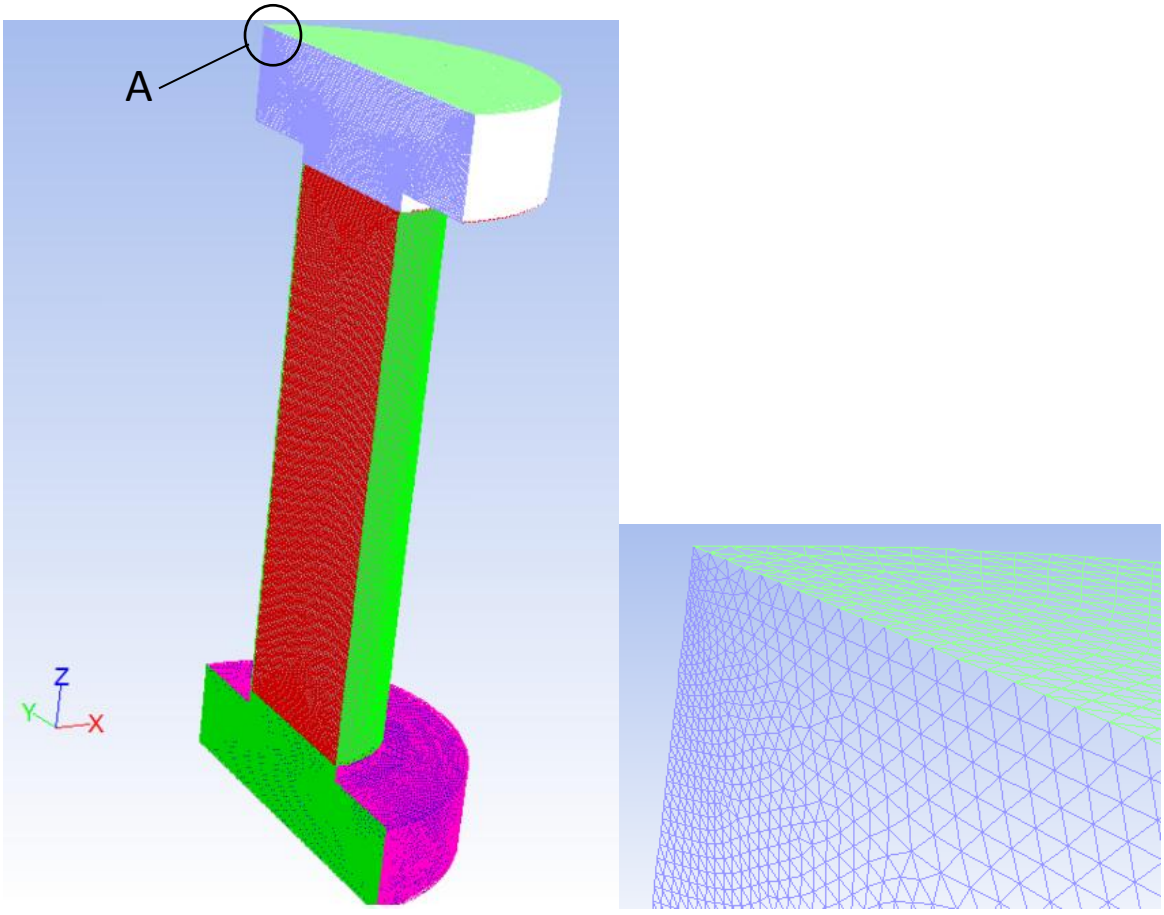

Figure 5.12: Left: 3-D model configuration and, right: Detail (A) shows the meshes used with the 3D model

5.3.3 Results and Discussion of the 3D Analysis

A three-dimensional simulation with the option of double precision at ΔT = 20 K between the top and bottom surfaces was performed. The contours of a number of properties such as temperature density gradient, mole fractions of the components, and species distribution were calculated. To obtain more accurate results for the facet value and to reach a suitable steady-state "converged" condition, the number of iteration was selected carefully. We found that 200 iterations were enough for performing these simulations, since the facet values converged after about 110 iterations as shown in Figure 5.13.

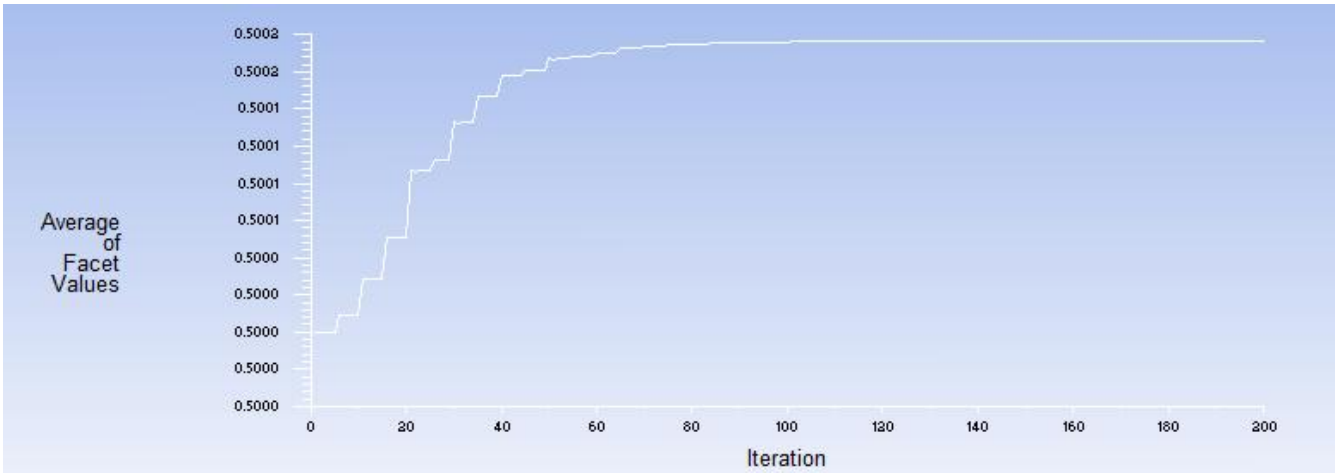

Figure 5.13: Convergence history of mass fraction of *n*-hexane on the top surface

Starting with the mole fraction of the components (as shown in Appendix D), the average molar fraction of toluene was 48.34 % and for *n*-hexane was 51.67 %. The numerical simulations of molar fraction for the same components gave same results as shown in Figure 5.14.

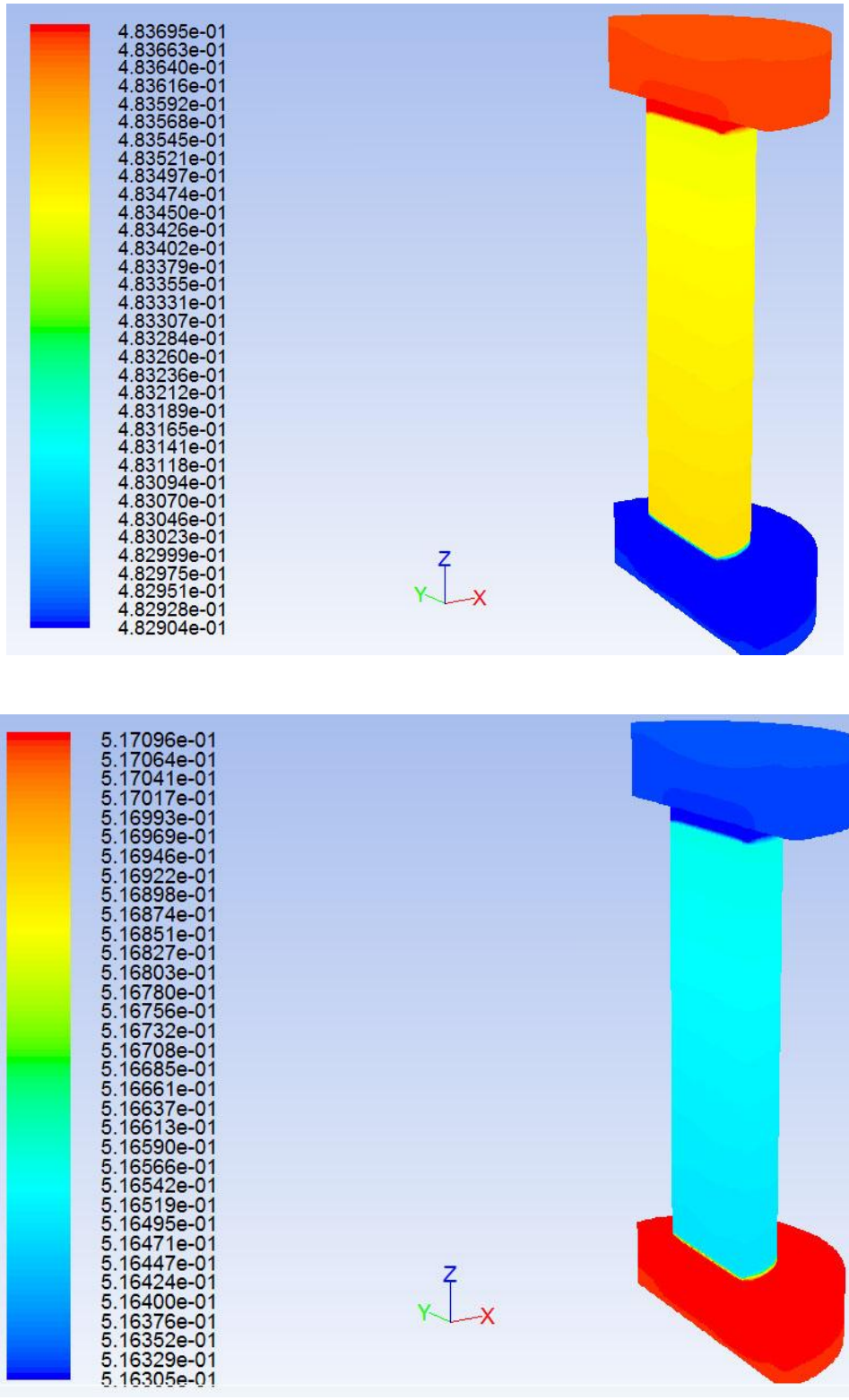

Figure 5.14: Three-dimensional contours of mole fraction for toluene (top) and *n*-hexane (bottom)

The second property that was simulated for this mixture was the distribution of the temperature across the entire cavity. Figure 5.15 shows the temperature gradient along the vertical axis of the cavity. There is close agreement between the three-dimensional model and the two-dimensional model of the temperature distribution as shown in Figure 5.4.

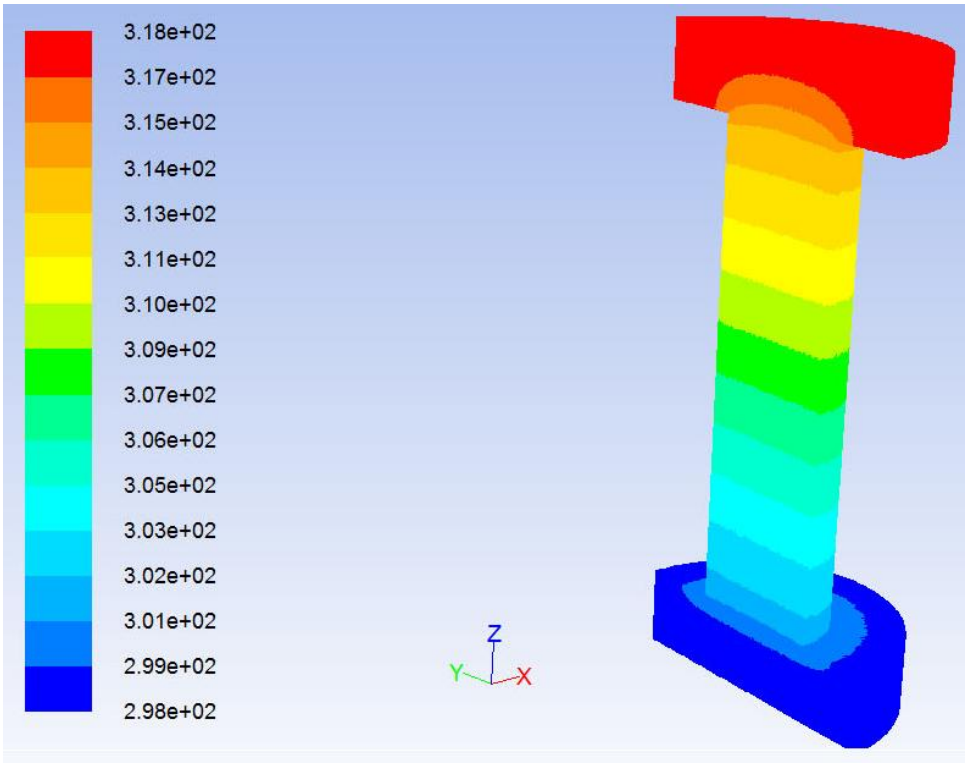

Figure 5.15: Three-dimensional contours of temperature at ΔT=20 K.

The third simulated property was the species concentration. As discussed in Section 5.3.1, and due to the positive Soret coefficient of the mixture in this study, the concentration of *n*-hexane, which is the lighter component, is greater near the hot surface (top) while the concentration of toluene, which is the denser component, is greater near the cold surface (bottom). The opposite

result was seen for the three-dimensional simulation; the denser component moved towards the hot surface and the lighter component moved towards the cold surface, as shown in Figure 5.16.

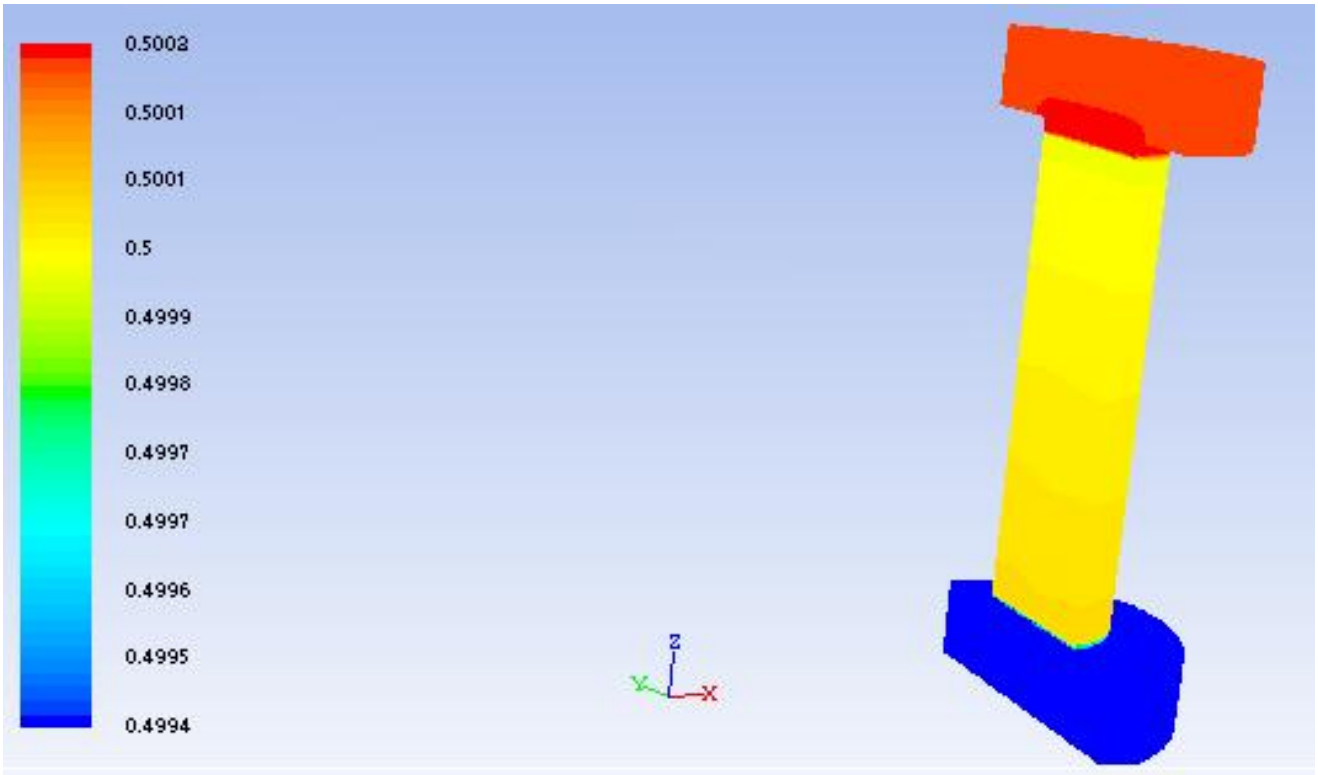

Figure 5.16 Three-dimensional contours of the concentration of *n*-hexane at ΔT=20 K

To validate the results of the concentration of *n*-hexane obtained from both of the two- and three-dimensional simulations, the concentration of *n*-hexane at various points along the vertical axes (Z) of both simulations were selected and plotted against each other, as shown in Figure 5.17. There is good agreement between the results obtained from both simulations.

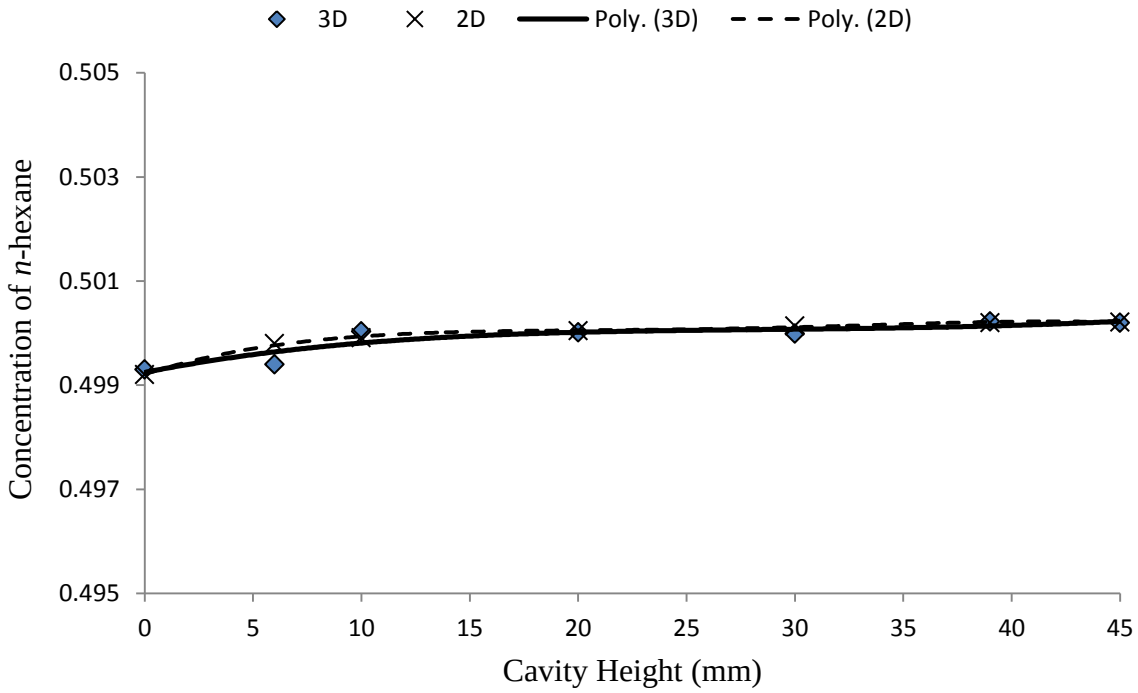

Figure 5.17: The concentration of *n*-hexane at ΔT=20 K obtained from two- and three-dimensional simulations

Lastly, the contours of the mixture density were plotted and are shown in Figure 5.18. It is clear that the density gradient is opposite to the direction of the gravity force, i.e. the density is greater near the bottom surface of the cavity than near the top surface. This density gradient is due to the migration of the mixture components towards the hot and cold surfaces, which explains the lack of natural convection in the cavity when heated from above. This was discussed in detail in chapters 3 and 4 of this thesis.

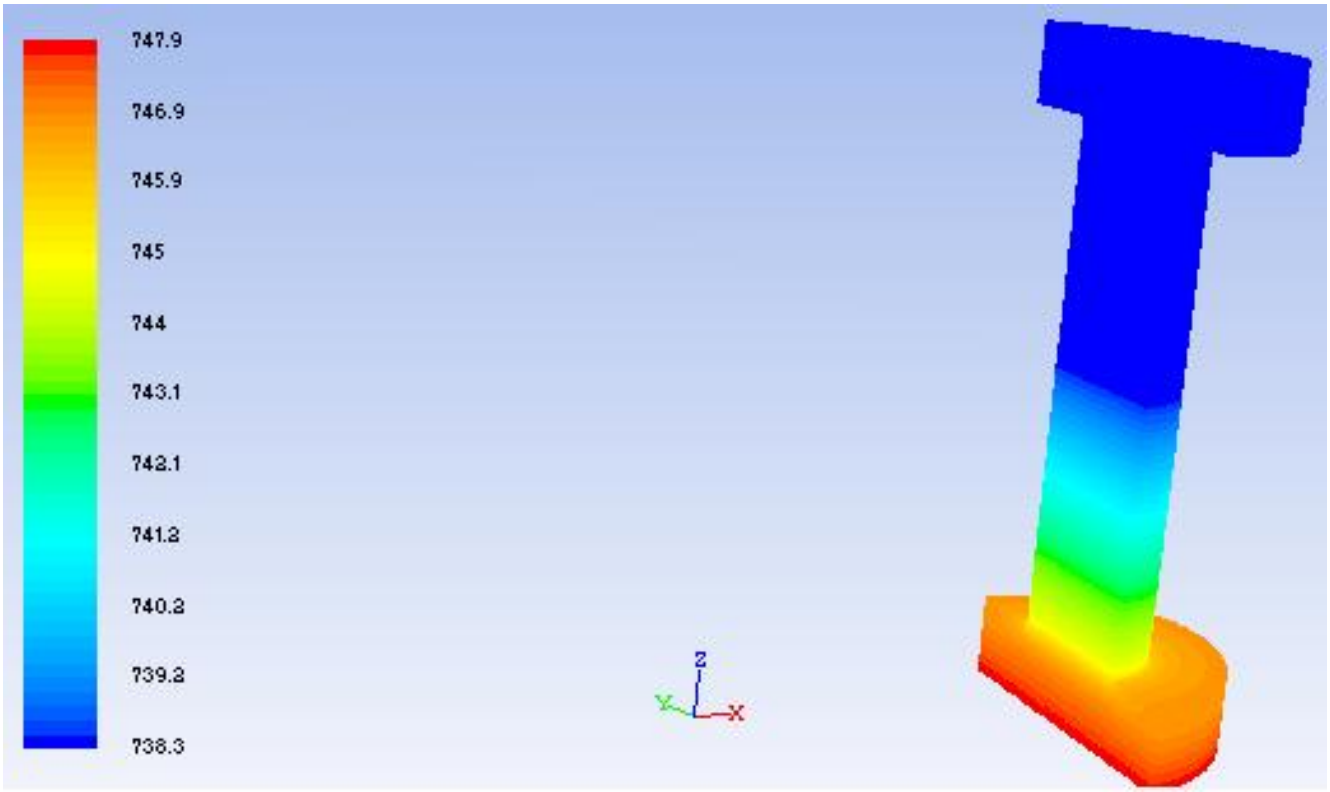

Figure 5.18: Contours of the mixture density at ΔT=20 K.

In Section 4.3.1, Ra_T and Ra_S were calculated for all the three layers of the system under study. The calculations (Table 4.1) showed that $Ra_T > Ra_S$ for the three layers, which means that heat diffusion was a more dominant effect than was mass diffusion. The calculations also showed that Ra_S at the bottom fluid layer is greater than at the top fluid layer, due to the negative Soret coefficient of the mixture studied in Section 4.3.1. For the mixture under study in this chapter (50% toluene and 50% *n*-hexane), Ra_T and Ra_S were calculated for all the three layers. Again, calculations showed that $Ra_T > Ra_S$ for the three layers with a major difference which is that Ra_S in the top fluid layer is greater than at the bottom fluid layer due to the positive Soret coefficient

of the 50% toluene and 50% *n*-hexane mixture. Table 5.1 presents the values of Ra_T and Ra_S calculated for the mixture studied in this chapter.

Table 5.1: Thermal and solutal Rayleigh numbers for fluid and porous layers for 50% toluene and 50% *n*-hexane

	$\Delta T = 5\ K$	$\Delta T = 10\ K$	$\Delta T = 20\ K$
Top Fluid Layer:			
Ra_{TL}	68300	131080	241480
Ra_{SL}	106.75	168.55	215.65
Porous Layer:			
Ra_{TP}	209.70	454.36	838.81
Ra_{SP}	304.42	415.00	594.40
Bottom Fluid Layer:			
Ra_{TL}	68300	131080	241480
Ra_{SL}	11.22	16.11	24.00

5.4 Effect of Porosity on Thermodiffusion in the Presence of Porous Media

In this section, we study the effect of the porosity of a material on thermodiffusion, which plays a crucial role in the study of porous media. Porosity ($\emptyset$) can be defined as the ratio of volume occupied by voids to the total volume of the porous material. Hence, it can be expressed as in the following expression:

$$\emptyset = \frac{V_v}{V_T} \tag{5.4}$$

Mathematically, it can be expressed as a number between (0-1) or as percentage (%). The previously mentioned Kozeny-Carmen relation (Section 2.1) directly relates porosity to the effective permeability:

$$K_e = \frac{d^2}{172.8}\frac{\emptyset^3}{(1-\emptyset)^2} \tag{5.5}$$

The value of porosity that was used in all the previous cases studied in this thesis was 0.39 (or 39%). In order to study the effect of the porosity on the thermodiffusion, another two values of porosity have been taken into consideration. The other two values are 0.25 (25 %) and 0.6 (60%). Figure 5.19 shows the contours of the concentration of the mixture components for the three values of porosity.

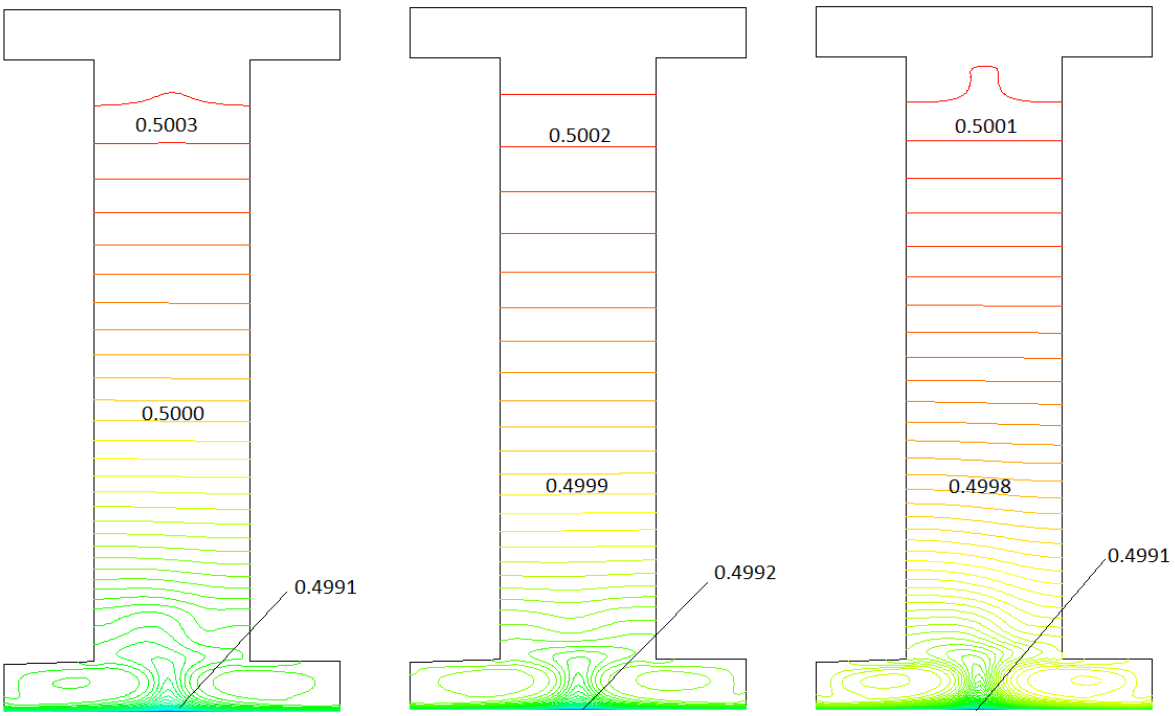

Figure 5.19: Contours of the concentration of *n*-hexane in a mixture of 50% toluene and 50% *n*-hexane at ΔT=20 K with porosities of (a) $\emptyset$ =0.25, (b) $\emptyset$ =0.39 and (c) $\emptyset$ =0.6

It is noticeable that increasing the porosity causes more system destabilization. Increasing the porosity means that the porous material has more voids, which causes less resistance for the fluid to flow and penetrate through the porous layer. Therefore, fluid flow increases and generates a

diffusive regime, which causes more flow mixing that decreases the separation of the mixture components. Increasing the porosity also leads to a decrease in the thermal conductivity of the porous material and reduces the conduction heat transfer, providing greater possibility for convection to occur.

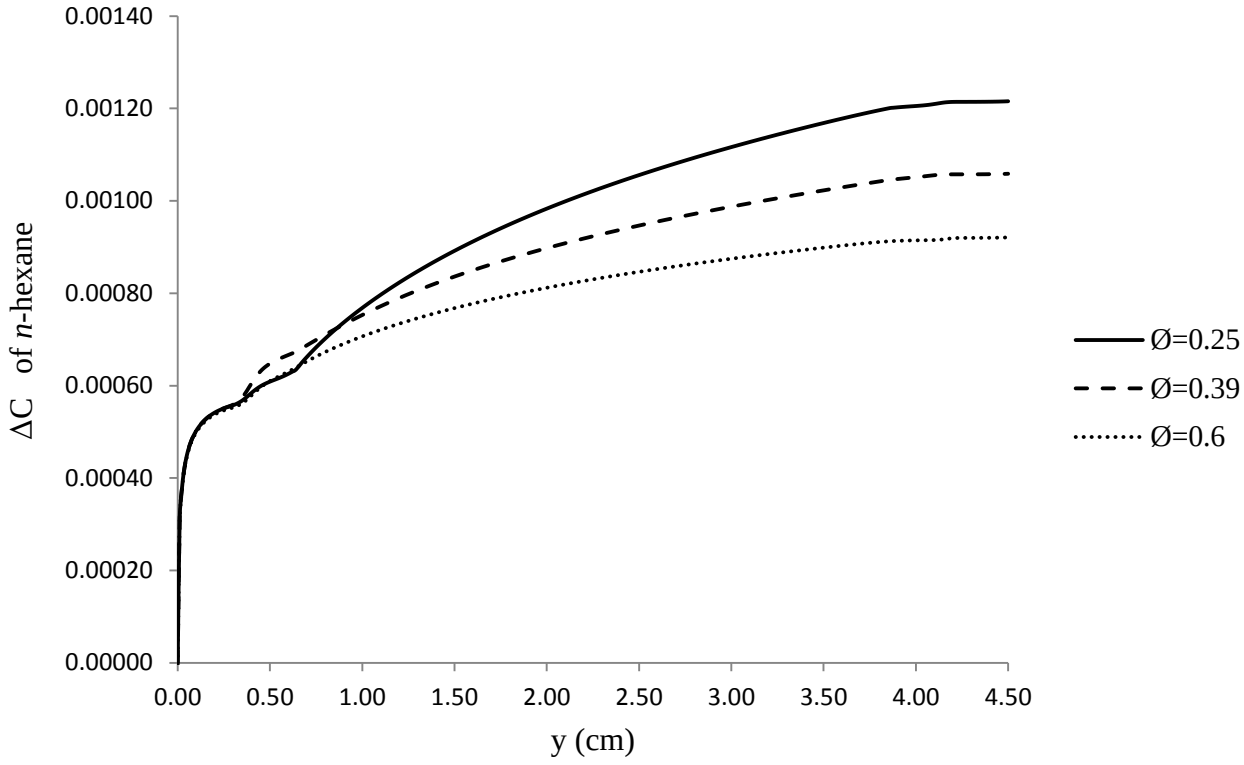

Figure 5.20: Concentration of *n*-hexane vs. the cavity height (*y*) at various values of porosity

5.5 Summary

Two- and three-dimensional numerical studies have been performed to investigate the thermodiffusion (Soret effect) in a cavity that consists of a porous layer sandwiched between two layers of a hydrocarbon binary mixture consisting of 50% toluene and 50% *n*-hexane. The cavity was subjected to a heat flux from the top horizontal surface. Three different models have been simulated with temperature differences between the top and bottom horizontal surfaces of 5, 10, and 20 K. The results obtained from this part of the study can be summarized as follows:

- When the binary mixture has a positive Soret coefficient, the lighter species migrates in the direction of the hotter surface, while the denser species migrates in the direction of the colder surface.
- Increasing the temperature difference in the system enhances the separation process due to the larger density gradient caused by the increase in the temperature difference and the thermal diffusion flux, which is proportional to the gradient of temperature.
- Increasing the porosity of the porous material causes a noticeable reduction in the separation of the mixture components. This is owing to the lesser resistance of the porous material against the fluid flow. Therefore, more fluid mixing occurs in the pore (void) areas.

CHAPTER 6

Conclusions, Contributions, and Future Work

6.1 Conclusions

For the study of natural convection, we found that no motion was noticed when the system was heated from the top surface. The system in this case was stable, with a stratified temperature profile. Therefore, natural convection will not occur when a system consisting of fluid and porous media is heated from above.

For the investigation of thermodiffusion, we found that when the binary mixture has a negative Soret coefficient, the lighter species migrates in the direction of the colder surface while the denser species migrate in the direction of the hotter surface. However, when the binary mixture has a positive Soret coefficient, the lighter species migrates in the direction of the hotter surface while the denser species migrates in the direction of the colder surface. In addition, we consider the following findings major results from the numerical analyses that were conducted in this research:

- Increasing the temperature difference in the system enhances the separation process due to the enhancement of the density gradient with an increase in the temperature difference and the thermal diffusion flux, which is proportional to the gradient of temperature.
- Increasing the porosity of the porous material causes a noticeable reduction in the separation of the mixture components. This is owing to the lesser resistance of the porous material against the fluid flow. Therefore, more fluid mixing occurs in the pore (void) areas.

6.2 Contributions

The main goal of this research was to perform a numerical study to investigate the natural convection and thermodiffusion in a porous layer sandwiched between two liquid layers of water-alcohol mixtures at different concentrations of water. The study was repeated with another model saturated with a binary hydrocarbon mixture. The phenomenon of mass flux in a mixture due to a temperature gradient is called the thermo-solutal, thermodiffusion or Soret effect. This phenomenon has gained the attention of scientists, researchers, and engineers in the last few decades due to its crucial role in many engineering and geophysical applications, such as: mineral migration and mass transfer in living matters, analysis and study of compositional variation in hydrocarbon reservoirs, disposal of nuclear waste material, the migration of a contaminant in saturated soil, isotope separation in gaseous and liquid mixtures. The following are the main contributions of this research:

- We conducted several numerical studies that showed the effect and the importance of heating orientation on the onset of natural convection.
- We conducted numerical analyses to investigate the phenomena of natural convection and themodiffusion in a multi-layered system consisting of a porous medium sandwiched between two layers of binary mixtures. The model configurations used in this study are suitable to many natural and industrial applications. One of these applications is the extraction of oil from deep reservoirs.
- We studied the thermodiffusion in a wider range of associating and hydrocarbon fluids with different signs of the Soret coefficient and different physical properties.
- We investigated the effect of various parameters such as temperature difference, sign of the Soret effect, and porosity on the separation process of the mixture components.

6.3 Future Works

Due to the importance of thermodiffusion (Soret effect) in the presence of porous media, future work may be recommended to address the following issues:

- Repeat the study of the natural convection and thermodiffusion phenomena in a hydrocarbon binary mixture in a high pressure environment to investigate the behaviour of hydrocarbon mixtures in the oil reservoir,
- Further develop the three-dimensional model,
- Extend the present study to investigate the thermodiffusion phenomenon with ternary mixtures and compare the results with this study,
- Study and analyse thermodiffusion with a similar system configuration consisting of a porous medium sandwiched between two layers of binary or ternary mixtures in a microgravity environment,
- Investigate the effect of more parameters on the thermodiffusion in the system configuration that was used in this study. These parameters may include pressure, permeability, and thickness of fluid and porous layers, variable porosity, and aspect ratio.

APPENDIX (A)

Non-Dimensional Analysis of Governing Equations

The following dimensionless variables are substituted into the dimensional equations in order to render them non-dimensional:

$$U = \frac{u}{u_0} \qquad \theta = \frac{T - Tc}{\Delta T} \qquad \tau = \frac{tu_0}{L}$$

$$V = \frac{v}{u_0} \qquad C = \frac{C - C_0}{\Delta C} \qquad N = \frac{\beta_C\, \Delta C}{\beta_T\, \Delta T}$$

$$X = \frac{x}{L} \qquad Re = \frac{\rho_0 u_0 L}{\mu} \qquad Ra_{TL} = \frac{g\beta_T\, \Delta T d_{1,2}^3}{\gamma\alpha}$$

$$Y = \frac{y}{L} \qquad Pr = \frac{\gamma}{\alpha} \qquad Ra_{TP} = \frac{g\beta_T\, \Delta T\, d_3 k}{\gamma\alpha}$$

$$P = \frac{pL}{\mu u_0} \qquad Da = \frac{k}{L^2} \qquad Ra_{SL} = \frac{g\beta_C\, \Delta C d_{1,2}^3}{\gamma\alpha}$$

$$u_0 = \sqrt{g\beta_T \Delta T L} \qquad Sc = \frac{\gamma}{D_M} \qquad Ra_{TP} = \frac{g\beta_C \Delta C\, d_3 k}{\gamma\alpha}$$

(A.1)

A.1 Liquid Layer

A.1.1 Continuity Equation

$$\frac{\partial u}{\partial x} + \frac{\partial v}{\partial y} = 0 \qquad (A.2)$$

Substitute the non-dimensional terms

$$\frac{\partial U}{\partial X} + \frac{\partial V}{\partial Y} = 0 \qquad (A.3)$$

A.1.2 *X*-direction Momentum Balance equation

$$\rho_f \left[\frac{\partial u}{\partial t} + u.\frac{\partial u}{\partial x} + v.\frac{\partial u}{\partial y}\right] = -\frac{\partial p}{\partial x} + \mu \left[\frac{\partial^2 u}{\partial x^2} + \frac{\partial^2 u}{\partial y^2}\right] \qquad (A.4)$$

Substitute the non-dimensional terms:

$$\rho_f \left[\frac{\partial(U.u_0)}{\partial(\frac{\tau.L}{u_0})} + (U.u_0)\frac{\partial(U.u_0)}{\partial(X.L)} + (V.u_0)\frac{\partial(U.u_0)}{\partial(Y.L)}\right] =$$

$$-\frac{\partial(\frac{P.\mu.u_0}{L})}{\partial(X.L)} + \mu\left[\frac{\partial}{\partial(X.L)}.\frac{\partial(U.u_0)}{\partial(X.L)} + \frac{\partial}{\partial(Y.L)}.\frac{\partial(U.u_0)}{\partial(Y.L)}\right]$$

Multiply both sides by the factor of $\frac{L^2}{\mu\, u_0}$ and simplify it to:

$$Re\left[\frac{\partial U}{\partial \tau} + U\frac{\partial U}{\partial X} + V\frac{\partial U}{\partial Y}\right] = -\frac{\partial P}{\partial X} + \left[\frac{\partial^2 U}{\partial X^2} + \frac{\partial^2 U}{\partial Y^2}\right] \qquad (A.5)$$

A.1.3 *Y*-direction Momentum Balance equation

$$\rho_f \left[\frac{\partial v}{\partial t} + u.\frac{\partial v}{\partial x} + v.\frac{\partial v}{\partial y}\right] = -\frac{\partial p}{\partial y} + \mu\left[\frac{\partial^2 v}{\partial x^2} + \frac{\partial^2 v}{\partial y^2}\right] - \rho_0.g\,[\beta T(T - To) - \beta C(C - C_0)] \qquad (A.6)$$

Substitute the non-dimensional terms and take out the common variables to get:

$$\rho_f.\frac{u_0^2}{L}\left[\frac{\partial V}{\partial \tau}+U.\frac{\partial V}{\partial X}+\ V.\frac{\partial V}{\partial Y}\right]=-\frac{\mu.u_0}{L^2}\frac{\partial P}{\partial Y}+\frac{\mu.u_0}{L^2}\left[\frac{\partial^2 V}{\partial X^2}+\ \frac{\partial^2 V}{\partial Y^2}\right]-\rho_0.g\ [\beta_T\Delta T\theta-\beta_C\Delta C.C]$$

Where, $(T - T_0) = \Delta T.\theta$ and $(c\text{-}c_0) = \Delta c.C$

Multiply the both sides of the previous equation by the factor of: $\frac{L^2}{\mu\, u_0}$ and simplify it to:

$$Re\left[\frac{\partial V}{\partial \tau}+U\frac{\partial V}{\partial X}+\ V\frac{\partial V}{\partial Y}\right]=-\ \frac{\partial P}{\partial Y}+\left[\frac{\partial^2 V}{\partial X^2}+\ \frac{\partial^2 V}{\partial Y^2}\right]-\underbrace{\frac{\rho_0.g}{\mu.u_0}[\beta_T\Delta T\theta-\beta_C\Delta C.C]}_{(\text{Ɛ}1)} \quad (\text{A.7})$$

Term (Ɛ1) :

$$\frac{\rho_0.gL^2\beta_T\Delta T\theta}{\mu.u_0}-\frac{\rho_0.gL^2\beta_C\Delta C.C}{\mu.u_0}$$

Multiply term (Ɛ1) by the factor of $\frac{L\rho/\mu}{L\rho/\mu}$ and simplify the same term to be:

$$\frac{Gr_T}{Re}\ [\theta-N.C]$$

Substituting term (Ɛ1) in Eq. (A.7) to get:

$$Re\left[\frac{\partial V}{\partial \tau}+U\frac{\partial V}{\partial X}+\ V\frac{\partial V}{\partial Y}\right]=-\ \frac{\partial P}{\partial Y}+\left[\frac{\partial^2 V}{\partial X^2}+\ \frac{\partial^2 V}{\partial Y^2}\right]-\frac{Gr_T}{Re}[\theta-N.C] \qquad (A.8)$$

A.1.4 Energy balance equation

$$(\rho Cp)_f\left[\frac{\partial T}{\partial t}+u\ \frac{\partial T}{\partial X}\ +v\frac{\partial T}{\partial y}\right]=k_f\left[\frac{\partial^2 T}{\partial x^2}+\frac{\partial^2 T}{\partial y^2}\right] \qquad (A.9)$$

Substitute the non-dimensional parameters to obtain:

$$(\rho Cp)_f\left[\frac{\partial(\Delta T.\theta)}{\partial(\frac{\tau.L}{u_0})}+(U.u_0)\frac{\partial(\Delta T.\theta)}{\partial(X.L)}+(V.u_0)\frac{\partial(\Delta T.\theta)}{\partial(Y.L)}\right]=k_f\left[\frac{\partial^2(\Delta T.\theta)}{\partial(X.L)^2}+\frac{\partial^2(\Delta T.\theta)}{\partial(Y.L)^2}\right]$$

$$(\rho Cp)_f \frac{(\Delta T.u_0)}{L}\left[\frac{\partial\theta}{\partial\tau} + U\frac{\partial\theta}{\partial X} + V\frac{\partial\theta}{\partial Y}\right] = \frac{k_f\,\Delta T}{L^2}\left[\frac{\partial^2\theta}{\partial X^2} + \frac{\partial^2\theta}{\partial Y^2}\right]$$

Multiply both sides by the factor of $\frac{\mathrm{L}^2}{k_f\,\Delta T}$ and simplify it to:

$$(\rho Cp)_f \frac{(L.u_0)}{k_f}\frac{L^2}{k_f\,\Delta T}\left[\frac{\partial\theta}{\partial\tau} + U\frac{\partial\theta}{\partial X} + V\frac{\partial\theta}{\partial Y}\right] = \left[\frac{\partial^2\theta}{\partial X^2} + \frac{\partial^2\theta}{\partial Y^2}\right]$$

Multiply L.H.S by the factor of $\frac{\mu}{\mu}$ and simplify it to:

$$Re.Pr\left[\frac{\partial\theta}{\partial\tau} + U\frac{\partial\theta}{\partial X} + V\frac{\partial\theta}{\partial Y}\right] = \left[\frac{\partial^2\theta}{\partial X^2} + \frac{\partial^2\theta}{\partial Y^2}\right] \qquad (A.10)$$

A.1.5 Mass balance equation

$$\rho_f\left[\frac{\partial c}{\partial t} + u\frac{\partial c}{\partial x} + v\frac{\partial c}{\partial y}\right] = \rho_f D_M\left[\frac{\partial^2 c}{\partial x^2} + \frac{\partial^2 c}{\partial y^2}\right] + \rho_f D_T\left[\frac{\partial^2 T}{\partial x^2} + \frac{\partial^2 T}{\partial y^2}\right] \qquad (A.11)$$

Substitute the non-dimensional parameters to obtain:

$$\rho_f\left[\frac{\partial(c.c)}{\partial(\frac{\tau.L}{u_0})} + (U.u_0)\frac{\partial(\Delta c.c)}{\partial(X.L)} + (V.u_0)\frac{\partial(\Delta c.c)}{\partial(Y.L)}\right] =$$

$$\rho_f D_M\left[\frac{\partial}{\partial(X.L)}\frac{\partial(\Delta c.c)}{\partial(X.L)} + \frac{\partial}{\partial(Y.L)}\frac{\partial(\Delta c.c)}{\partial(Y.L)}\right] + \rho_f D_T\left[\frac{\partial}{\partial(X.L)}\frac{\partial(\Delta T.\theta)}{\partial(X.L)} + \frac{\partial}{\partial(Y.L)}\frac{\partial(\Delta T.\theta)}{\partial(Y.L)}\right]$$

Extract the common variables from both sides of the above equation:

$$\rho_f\frac{\Delta c.u_0}{L}\left[\frac{\partial \mathrm{C}}{\partial\tau} + \mathrm{U}.\frac{\partial \mathrm{C}}{\partial \mathrm{X}} + \mathrm{V}\frac{\partial \mathrm{C}}{\partial \mathrm{Y}}\right] = \rho_f \mathrm{D_M}\frac{\Delta c}{L^2}\left[\frac{\partial^2 C}{\partial X^2} + \frac{\partial^2 C}{\partial Y^2}\right] + \rho_f \mathrm{D_T}\frac{\Delta T}{L^2}\left[\frac{\partial^2\theta}{\partial X^2} + \frac{\partial^2\theta}{\partial Y^2}\right]$$

Multiply both sides of the above equation by the factor of $\frac{L}{\rho_{f.\Delta C.u_0}}$ to obtain:

$$\left[\frac{\partial C}{\partial \tau} + U.\frac{\partial C}{\partial X} + V\frac{\partial C}{\partial Y}\right] = \underbrace{\frac{D_M}{L.u_0}\left[\frac{\partial^2 C}{\partial X^2} + \frac{\partial^2 C}{\partial Y^2}\right]}_{(\text{Ɛ}2)} + \underbrace{\frac{D_T\,\Delta T}{L.u_0\Delta C}\left[\frac{\partial^2 \theta}{\partial X^2} + \frac{\partial^2 \theta}{\partial Y^2}\right]}_{(\text{Ɛ}3)} \qquad (A.12)$$

Now, we need to take the following two steps:

(1) Multiply term (Ɛ2) by $\frac{\gamma}{\gamma}$, then the same term becomes $\frac{1}{Sc.Re}$

(2) Term (Ɛ3) which used at the presence of thermodiffusion convection:

$$\frac{\mathrm{D_T}\,\Delta T}{L.u_0\Delta C} = \frac{\mathrm{D_M}\,S_T\Delta T}{L.u_0\Delta C} = \frac{\mathrm{D_M}\,\alpha}{L.u_0(1)}\ x\ \frac{\gamma}{\gamma} = \frac{\alpha}{Sc.Re}$$

Substitute (Ɛ2) and (Ɛ3) in equation (A.12), we will obtain:

$$\left[\frac{\partial \mathrm{C}}{\partial \tau} + \mathrm{U}\,\frac{\partial \mathrm{C}}{\partial \mathrm{X}} + \mathrm{V}\,\frac{\partial \mathrm{C}}{\partial \mathrm{Y}}\right] = \frac{1}{\mathrm{Re}}.\frac{1}{\mathrm{Sc}}\left[\frac{\partial^2 \mathrm{C}}{\partial \mathrm{X}^2} + \frac{\partial^2 \mathrm{C}}{\partial \mathrm{Y}^2}\right] + \frac{\alpha}{Sc.Re}\left[\frac{\partial^2 \theta}{\partial X^2} + \frac{\partial^2 \theta}{\partial Y^2}\right] \qquad (\mathrm{A.13a})$$

Or

$$\left[\frac{\partial \mathrm{C}}{\partial \tau} + \mathrm{U}\,\frac{\partial \mathrm{C}}{\partial \mathrm{X}} + \mathrm{V}\,\frac{\partial \mathrm{C}}{\partial \mathrm{Y}}\right] = \frac{1}{\mathrm{Re}}.\frac{1}{\mathrm{Sc}}\left[\frac{\partial^2 \mathrm{C}}{\partial \mathrm{X}^2} + \frac{\partial^2 \mathrm{C}}{\partial \mathrm{Y}^2}\right] + \frac{Le}{(Sc.Re)^2}\left[\frac{\partial^2 \theta}{\partial X^2} + \frac{\partial^2 \theta}{\partial Y^2}\right] \qquad (\mathrm{A.13b})$$

A.2 Porous Layer

A.2.1 Continuity Equation

$$\frac{\partial u}{\partial x} + \frac{\partial v}{\partial y} = 0 \qquad (A.14)$$

Substitute the non-dimensional terms

$$\frac{\partial U}{\partial X} + \frac{\partial V}{\partial Y} = 0 \qquad (A.15)$$

A.2.2 *X*-direction Momentum Balance equation

$$\frac{\rho_f}{\emptyset}\left[\frac{\partial u}{\partial t}\right]+\frac{\mu}{k}.u=-\frac{\partial p}{\partial x}+\mu\left[\frac{\partial^2 u}{\partial x^2}+\frac{\partial^2 u}{\partial y^2}\right] \qquad (A.16)$$

Substitute the non-dimensional terms:

$$\frac{\rho_f}{\emptyset}\left[\frac{\partial(\mathrm{U}.u_0)}{\partial(\frac{\tau.L}{u_0})}\right]+\frac{\mu}{k}(\mathrm{U}.u_0)=-\frac{\partial(\frac{P.\mu.u_0}{L})}{\partial(\mathrm{X.L})}+\mu\left[\frac{\partial}{\partial(\mathrm{X.L})}.\frac{\partial(\mathrm{U}.u_0)}{\partial(\mathrm{X.L})}+\frac{\partial}{\partial(\mathrm{Y.L})}.\frac{\partial(\mathrm{U}.u_0)}{\partial(\mathrm{Y.L})}\right]$$

Multiply both sides by the factor of $\frac{\mathrm{L}^2}{\mu\, u_0}$ and simplify it to:

$$\frac{Re}{\emptyset}\left[\frac{\partial U}{\partial \tau}\right]+\frac{U}{Da}=-\frac{\partial P}{\partial X}+\left[\frac{\partial^2 U}{\partial X^2}+\frac{\partial^2 U}{\partial Y^2}\right] \qquad (A.17)$$

A.2.3 *Y*-direction Momentum Balance equation

$$\frac{\rho_f}{\emptyset}\left[\frac{\partial v}{\partial t}\right]+\frac{\mu}{k}v=-\frac{\partial p}{\partial y}+\mu\left[\frac{\partial^2 v}{\partial x^2}+\frac{\partial^2 v}{\partial y^2}\right]-\rho_0.g\,[\beta T(T-To)-\beta C(c-c_0)] \qquad (A.18)$$

Substitute the non-dimensional terms and take out the common variables to get:

$$\rho_f.\frac{u_0^2}{L}\left[\frac{\partial V}{\partial \tau}\right]+\frac{\mu}{k}V.u_0=-\frac{\mu.u_0}{L^2}\frac{\partial P}{\partial Y}+\frac{\mu.u_0}{L^2}\left[\frac{\partial^2 V}{\partial X^2}+\frac{\partial^2 V}{\partial Y^2}\right]-\rho_0.g\,[\beta_T\Delta T\theta-\beta_C\Delta C.C]$$

Where, $(\mathrm{T}-\mathrm{T}_0)=\Delta\mathrm{T}.\theta$ and $(\mathrm{c}-\mathrm{c}_0)=\Delta\mathrm{c}.\mathrm{C}$

Multiply the both sides of the previous equation by the factor of: $\frac{\mathrm{L}^2}{\mu\, u_0}$ and simplify it to:

$$Re\left[\frac{\partial V}{\partial \tau}\right]+\frac{V}{Da}=-\frac{\partial P}{\partial Y}+\left[\frac{\partial^2 V}{\partial X^2}+\frac{\partial^2 V}{\partial Y^2}\right]-\underbrace{\frac{\rho_0.g}{\mu.u_0}[\beta_T\Delta T\theta-\beta_C\Delta C.C]}_{(\mathcal{E}1)} \qquad (A.19)$$

Simplifying Term (Ɛ1):

$$\frac{\rho_0 . gL^2\beta_T \Delta T\theta}{\mu . u_0} - \frac{\rho_0 . gL^2\beta_C \Delta C . C}{\mu . u_0}$$

Multiply term (Ɛ1) by the factor of $\frac{L\rho/\mu}{L\rho/\mu}$ and simplify the same term to be:

$$\frac{Gr_T}{Re}\,[\theta - N.C]$$

Substituting term (Ɛ1) in Eq. (A.19) to get:

$$Re\left[\frac{\partial V}{\partial \tau} + U\frac{\partial V}{\partial X} + V\frac{\partial V}{\partial Y}\right] = -\frac{\partial P}{\partial Y} + \left[\frac{\partial^2 V}{\partial X^2} + \frac{\partial^2 V}{\partial Y^2}\right] - \frac{Gr_T}{Re}[\theta - N.C] \qquad (A.20)$$

A.2.4 Energy balance equation

$$(\rho Cp)_f\left[\frac{\partial T}{\partial t} + u\,\frac{\partial T}{\partial x} + v\,\frac{\partial T}{\partial y}\right] = k_e\left[\frac{\partial^2 T}{\partial x^2} + \frac{\partial^2 T}{\partial y^2}\right] \qquad (A.21)$$

Substitute the non-dimensional parameters to obtain:

$$(\rho Cp)_f\left[\frac{\partial(\Delta T.\theta)}{\partial(\frac{\tau . L}{u_0})} + (U.u_0)\frac{\partial(\Delta T.\theta)}{\partial(X.L)} + (V.u_0)\frac{\partial(\Delta T.\theta)}{\partial(Y.L)}\right] = k_e\left[\frac{\partial^2(\Delta T.\theta)}{\partial(X.L)^2} + \frac{\partial^2(\Delta T.\theta)}{\partial(Y.L)^2}\right]$$

$$(\rho Cp)_f\frac{(\Delta T.u_0)}{L}\left[\frac{\partial\theta}{\partial\tau} + U\frac{\partial\theta}{\partial X} + V\frac{\partial\theta}{\partial Y}\right] = \frac{k_e\,\Delta T}{L^2}\left[\frac{\partial^2\theta}{\partial X^2} + \frac{\partial^2\theta}{\partial Y^2}\right]$$

Multiply both sides by the factor of $\frac{\mathrm{L}^2}{k_f\,\Delta T}$ and simplify it to:

$$(\rho Cp)_f\frac{(L.u_0)}{k_f}\left[\frac{\partial\theta}{\partial\tau} + U\frac{\partial\theta}{\partial X} + V\frac{\partial\theta}{\partial Y}\right] = \frac{k_e}{k_f}\left[\frac{\partial^2\theta}{\partial X^2} + \frac{\partial^2\theta}{\partial Y^2}\right]$$

Multiply L.H.S by the factor of $\frac{\mu}{\mu}$ and simplify it to:

$$Re.Pr\left[\frac{\partial\theta}{\partial\tau}+U\frac{\partial\theta}{\partial X}+V\frac{\partial\theta}{\partial Y}\right]=G\left[\frac{\partial^2\theta}{\partial X^2}+\frac{\partial^2\theta}{\partial Y^2}\right] \qquad (A.22)$$

Where G is the non-dimensional thermal conductivity =

$$\frac{k_e}{k_f}=\frac{\emptyset k_f+(1-\emptyset).k_s}{k_f}$$

A.1.4 Mass balance equation

$$\rho_f\left[\frac{\partial c}{\partial t}+u\frac{\partial c}{\partial x}+v\frac{\partial c}{\partial y}\right]=\rho_f D_M\left[\frac{\partial^2 c}{\partial x^2}+\frac{\partial^2 c}{\partial y^2}\right]+\rho_f D_T\left[\frac{\partial^2 T}{\partial x^2}+\frac{\partial^2 T}{\partial y^2}\right] \qquad (A.23)$$

Substitute the non-dimensional parameters to obtain:

$$\rho_f\left[\frac{\partial(\Delta c.c)}{\partial(\frac{\tau.L}{u_0})}+(U.u_0)\frac{\partial(\Delta c.c)}{\partial(X.L)}+(V.u_0)\frac{\partial(\Delta c.c)}{\partial(Y.L)}\right]=$$

$$\rho_f D_M\left[\frac{\partial}{\partial(X.L)}\frac{\partial(\Delta c.c)}{\partial(X.L)}+\frac{\partial}{\partial(Y.L)}\frac{\partial(\Delta c.c)}{\partial(Y.L)}\right]+\rho_f D_T\left[\frac{\partial}{\partial(X.L)}\frac{\partial(\Delta T.\theta)}{\partial(X.L)}+\frac{\partial}{\partial(Y.L)}\frac{\partial(\Delta T.\theta)}{\partial(Y.L)}\right]$$

Extract the common variables from both sides of the above equation:

$$\rho_f\frac{\Delta C.u_0}{L}\left[\frac{\partial C}{\partial\tau}+U.\frac{\partial C}{\partial X}+V\frac{\partial C}{\partial Y}\right]=\rho_f D_M\frac{\Delta C}{L^2}\left[\frac{\partial^2 C}{\partial X^2}+\frac{\partial^2 C}{\partial Y^2}\right]+\rho_f D_T\frac{\Delta T}{L^2}\left[\frac{\partial^2\theta}{\partial X^2}+\frac{\partial^2\theta}{\partial Y^2}\right]$$

Multiply both sides of the above equation by the factor of $\frac{L}{\rho_{f.\Delta C.u_0}}$ to obtain:

$$\left[\frac{\partial C}{\partial\tau}+U.\frac{\partial C}{\partial X}+V\frac{\partial C}{\partial Y}\right]=\underbrace{\frac{D_M}{L.u_0}}_{(\text{Ɛ}2)}\left[\frac{\partial^2 C}{\partial X^2}+\frac{\partial^2 C}{\partial Y^2}\right]+\underbrace{\frac{D_T\,\Delta T}{L.u_0\Delta C}}_{(\text{Ɛ}3)}\left[\frac{\partial^2\theta}{\partial X^2}+\frac{\partial^2\theta}{\partial Y^2}\right] \qquad (A.24)$$

Now, we need to take the following two steps:

(1) Multiply term (Ɛ2) by $\frac{\gamma}{\gamma}$, then the same term becomes $\frac{1}{Sc.Re}$

(2) Term (Ɛ3) which used at the presence of thermodiffusion convection:

$$\frac{D_T\,\Delta T}{L.u_0\Delta C} = \frac{D_M\,S_T\Delta T}{L.u_0\Delta C} = \frac{D_M\,\alpha}{L.u_0(1)}\;x\;\frac{\gamma}{\gamma} = \frac{\alpha}{Sc.Re}$$

Substitute (Ɛ2) and (Ɛ3) in equation (A.12), we will obtain:

$$\left[\frac{\partial C}{\partial \tau} + U\,\frac{\partial C}{\partial X} + V\,\frac{\partial C}{\partial Y}\right] = \frac{1}{Re}.\frac{1}{Sc}\left[\frac{\partial^2 C}{\partial X^2} + \frac{\partial^2 C}{\partial Y^2}\right] + \frac{\alpha}{Sc.Re}\left[\frac{\partial^2 \theta}{\partial X^2} + \frac{\partial^2 \theta}{\partial Y^2}\right] \qquad (A.25a)$$

Or

$$\left[\frac{\partial C}{\partial \tau} + U\,\frac{\partial C}{\partial X} + V\,\frac{\partial C}{\partial Y}\right] = \frac{1}{Re}.\frac{1}{Sc}\left[\frac{\partial^2 C}{\partial X^2} + \frac{\partial^2 C}{\partial Y^2}\right] + \frac{Le}{(Sc.Re)^2}\left[\frac{\partial^2 \theta}{\partial X^2} + \frac{\partial^2 \theta}{\partial Y^2}\right] \qquad (A.25b)$$

APPENDIX (B)

List of Dimensionless Parameters

Group	Definition	Interpretation
Grashof number (Gr)	$\frac{g.\beta_T.\Delta T.\rho^2 L^3}{\mu^2}$	$\frac{\text{buoyancy forces}}{\text{viscous forces}}$
Lewis number (Le)	α / D_M	$\frac{\text{thermal diffusivity}}{\text{mass diffusivity}}$
Nusselt number (Nu)	$\frac{h.L}{k}$	$\frac{\text{convection heat transfer}}{\text{conduction heat transfer}}$
Prandtl number (Pr)	ν/α	$\frac{\text{momentum diffusivity}}{\text{thermal diffusivity}}$
Rayleigh number (Ra)	$\frac{g.\beta_T.\Delta T.L^3}{\nu\alpha}$	$\frac{\text{buoyancy}}{\text{viscous} \times \text{rate of heat diffusion}}$
Reynolds number (Re)	$\frac{\rho_0.u_0.L}{\mu}$	$\frac{\text{inertial force}}{\text{viscous force}}$
Schmidt number (Sc)	$\gamma/D_M = Le.Pr$	$\frac{\text{momentum diffusivity}}{\text{mass diffusivity}}$

APPENDIX (C)

Physical Properties of Binary Fluids

C.1 Physical Properties of Water-Isopropanol for Two Different compositions*

Property	*Symbol*	*10%isopropanol +90% Water*	*50%Isopropanol +50% Water*
Kinematic Viscosity (m^2/s)	γ	1.41E-06	4.18E-06
Thermal diffusivity (m^2/s)	a	1.30E-07	8.50E-08
Diffusion coefficient (m^2/s)	D_M	8.70E-10	1.80E-10
Density (kg/m3)	ρ	984	905
Soret coefficient (1/K)	S_T	-1.06E-02	5.45E-03
Thermal expansion (1/K)	β_T	3.10E-04	7.70E-04
Solutal expansion	β_C	0.14	-0.25
Prandtl number	Pr	10.846	49.165
Schmidt number	Sc	1620.690	23216.667
thermal characteristic time (s)	τ_{th}	15577	23823.53
Diffusive characteristic time (s)	τ_D	2.328E06	11.25E06
Thermal conductivity (W/m.K)	k	0.522	0.2866
Lewis number	Le	149.3	472.22

(*) Abdur Rahman, Md. (2008), "Thermo-Solutal Convection with Soret Effect", MSc thesis, Ryerson University.

C.2 Physical properties of %50 Toluene and 50% n-Hexane mixture

Property	*Symbol*	*Value*
Kinematic Viscosity (m^2/s)	γ	5.15E-07
Thermal diffusivity (m^2/s)	a	8.963E-08
Diffusion coefficient (m^2/s)	D_M	2.78E-09
Density (kg/m3)	ρ	751.19
Soret coefficient (1/K)	S_T	4.92E-03
Thermal expansion (1/K)	β_T	1.26E-03
Solutal expansion	β_C	-2.88E-01
Prandtl number	Pr	5.74
Schmidt number	Sc	185
thermal characteristic time (s)	τ_{th}	1115.7
Diffusive characteristic time (s)	τ_D	3.6E04
Thermal conductivity (W/m.K)	k	0.128851
Lewis number	Le	32.24
Specific heat (J/Kg.K)	Cp	1923

APPENDIX (D)

Calculations of Mass Fraction for the Mixture of 50% Toluene and 50% n-Hexane

$MW_{toluene}$ = 92.14 g/mol

$MW_{n\text{-}hexane}$ = 86.18 g/mol

$$N_i^* = \frac{M_i}{MW_i}$$

$$N_{toluene}^* = \frac{500\ g}{92.14\frac{g}{mol}} = 5.43\ mol$$

$$N_{n-hexane}^* = \frac{500\ g}{86.14\frac{g}{mol}} = 5.80\ mol$$

$$N_{mixture}^* = \sum_i \frac{M_i}{MW_i}$$

$$N_{mixture}^* = \left(\frac{500\ g}{92.14\frac{g}{mol}}\right) + \left(\frac{500\ g}{86.18\frac{g}{mol}}\right) = 11.23\ mol$$

$$X_i^* = \frac{N_i^*}{N_{mixture}^*}$$

$$X_{toluene}^* = \frac{5.43}{11.23} = 48.34\ \%$$

$$X_{n-hexane}^* = \frac{5.80}{11.23} = 51.67\ \%$$

APPENDIX (E)

Input Files

E.1 Natural Convection

```
Title
Thermodiffusion Convection in Fluid/Porous/Fluid top heated Cavity/top
heating Diffusiion case
fimesh (2-d, imax=3, jmax=7)
expi
/1  2  3
1  0  31
expj
/1  2  3  4  5  6  7
1  0  51  0  85  0  135
/
point
/n i j k x y z
 1 1 1 1 0 0 0
 2 3 1 1 0.222 0 0
 3 1 3 1 0 0.142 0
 4 3 3 1 0.222 0.142 0
 5 1 5 1 0 0.858 0
 6 3 5 1 0.222 0.858 0
 7 1 7 1 0 1 0
 8 3 7 1 0.222 1 0
line
/1st plane
1 2
3 4
5 6
7 8
1 3
3 5
5 7
2 4
4 6
6 8
surface
1 4
3 6
5 8
elements (continuum, quad, node=9, entity="porous")
3 6
elements (continuum, quad, node=9, entity="fluidT")
5 8
elements (continuum, quad, node=9, entity="fluidB")
1 4
```

```
elements(boundary,edge,nodes=3,entity="Top")
7 8
elements(boundary,edge,nodes=3,entity="Bottom")
1 2
bcnode (temperature, constant)
7 8 1
1 2 0
bcnode (velocity, constant)
2 4 0 0
6 8 0 0
1 2 0 0
7 8 0 0
1 3 0 0
5 7 0 0
bcnode (ux, constant)
4 6 0 0
3 5 0 0
/
/
end
fiprep
problem (nonlinear, 2-D, buoyancy, buoyancy=1, transient)
timeint (back, dt=0.00006, nofix=5, nsteps=1500, tend=300000, species=1)
pressure (mixed=1.0e-8, disc)
execution (newjob)
solution (segr=2000, velcon=0.001, normal=40)
option (stress-divergence)
relax
0.12  0.12  0.12  0.0  0.01  0.6
gravity (magn=1)
/
$por=0.39
$perm=4.1e-6
/
cond (set=3, constant=2.1)
permeability (acoef, constant=1, x=$perm, y=$perm, porosity=$por)
/
/physical parameters
/
dens (set=1, constant=1669.7, TYP2, temperature, spec=1)
spec (set=1, constant=10.846)
visc (set=1, constant=1)
cond (set=1, constant=1)
volu (set=1, constant=1, temperature)
volu (set=2, constant=23.36, spec=1)
diff (set=2, constant=3.7e-7, species=1)
/ther (set=1, constant)
/7.84e-08 0 0 0 0 0 0 0 0 0 0 0 0 0 0
renumber (profile)
icnode (temperature, constant=0.5, entity="porous")
icnode (temperature, constant=0.5, entity="fluidT")
icnode (temperature, constant=0.5, entity="fluidB")
icnode (species=1, constant=0.1, entity="porous")
icnode (species=1, constant=0.1, entity="fluidT")
```

```
icnode (species=1, constant=0.1, entity="fluidB")
entity (name="porous", porous, property="1", mdiff=2, sore, species=1,
mexp=2, maper=1, mscond=3)
entity (name="fluidT", fluid, property="1", mdiff=2, sore, species=1,
mexp=2)
entity (name="fluidB", fluid, property="1", mdiff=2, sore, species=1,
mexp=2)
entity(name="Top",plot)
entity(name="Bottom",plot)
print (none)
data (control)
end
create (FISOLV)
```

E.2 Thermodiffusion Convection (Water-Alcohol Binary Mixture):

```
Title
Thermodiffusion Convection in Fluid/Porous/Fluid top heated Cavity/top
heating Diffusiion case
fimesh (2-d, imax=3, jmax=7)
expi
/1  2  3
1  0  31
expj
/1  2  3  4  5  6  7
1  0  51  0  85  0  135
/
point
/n i j k x y z
 1 1 1 1 0 0 0
 2 3 1 1 0.222 0 0
 3 1 3 1 0 0.142 0
 4 3 3 1 0.222 0.142 0
 5 1 5 1 0 0.858 0
 6 3 5 1 0.222 0.858 0
 7 1 7 1 0 1 0
 8 3 7 1 0.222 1 0
line
/1st plane
1 2
3 4
5 6
7 8
1 3
3 5
5 7
2 4
4 6
6 8
surface
1 4
3 6
5 8
elements (continuum, quad, node=9, entity="porous")
3 6
elements (continuum, quad, node=9, entity="fluidT")
5 8
elements (continuum, quad, node=9, entity="fluidB")
1 4
bcnode (temperature, constant)
7 8 1
1 2 0
bcnode (velocity, constant)
2 4 0 0
6 8 0 0
1 2 0 0
```

```
7 8 0 0
1 3 0 0
5 7 0 0
bcnode (ux, constant)
4 6 0 0
3 5 0 0
/
/
end
fiprep
problem (nonlinear, 2-D, buoyancy, buoyancy=1, transient)
timeint (back, dt=0.00006, nofix=5, nsteps=500, tend=300000, species=1)
pressure (mixed=1.0e-8, disc)
execution (newjob)
solution (segr=2000, velcon=0.001, normal=40)
option (stress-divergence)
relax
0.12  0.12  0.12  0.0  0.01  0.6
gravity (magn=1)
/
$por=0.39
$perm=4.1e-6
/
cond (set=3, constant=2.1)
permeability (acoef, constant=1, x=$perm, y=$perm, porosity=$por)
/
/physical parameters
/
dens (set=1, constant=1669.7, TYP2, temperature, spec=1)
spec (set=1, constant=10.846)
visc (set=1, constant=1)
cond (set=1, constant=1)
volu (set=1, constant=1, temperature)
volu (set=2, constant=23.36, spec=1)
diff (set=2, constant=3.7e-7, species=1)
ther (set=1, constant)
7.84e-08 0 0 0 0 0 0 0 0 0 0 0 0 0
renumber (profile)
icnode (temperature, constant=0.5, entity="porous")
icnode (temperature, constant=0.5, entity="fluidT")
icnode (temperature, constant=0.5, entity="fluidB")
icnode (species=1, constant=0.1, entity="porous")
icnode (species=1, constant=0.1, entity="fluidT")
icnode (species=1, constant=0.1, entity="fluidB")
entity (name="porous", porous, property="1", mdiff=2, sore, species=1,
mexp=2, maper=1, mscond=3)
entity (name="fluidT", fluid, property="1", mdiff=2, sore, species=1,
mexp=2)
entity (name="fluidB", fluid, property="1", mdiff=2, sore, species=1,
mexp=2)
print (none)
data (control)
end
create (FISOLV)
```

E.3 Thermodiffusion Convection (Hydrocarbone Binary Mixture)

```
Title
Thermodiffusion Convection in Fluid/Porous/Fluid
/top heating Diffusion case
fimesh(2-d, imax=7, jmax=11)
expi
/1 2 3 4 5 6 7
1 0 31 0 61 0 91
expj
/1 2 3 4 5 6 7 8 9 10 11
1 0 31 0 51 0 151 0 171 0 201
/
point
/n i j k x y z
 1 1 1 1 0 0 0
 2 7 1 1 2.15 0 0
 3 1 3 1 0 0.3.2 0
 4 3 3 1 0.575 0.32 0
 5 5 3 1 1.575 0.32 0
 6 7 3 1 2.15 0.32 0
 7 3 5 1 0.575 0.64 0
 8 5 5 1 1.575 0.64 0
 9 3 7 1 0.575 3.86 0
10 5 7 1 1.575 3.86 0
11 1 9 1 0 4.18 0
12 3 9 1 0.575 4.18 0
13 5 9 1 1.575 4.18 0
14 7 9 1 2.15 4.18 0
15 1 11 1 0 4.5 0
16 7 11 1 2.15 4.5 0
line
/1st Plane
1 2
2 6
6 5
5 8
8 7
7 4
5 4
4 3
3 1
7 9
9 10
10 8
9 12
```

```
12 11
11 15
15 16
16 14
14 13
13 10
12 13
surface
7 10
2 3
4 8
9 13
11 16
elements(continuum,quad,nodes=9,entity="porous")
7 10
elements(continuum,quad,nodes=9,entity="fluidT")
9 13
11 16
elements(continuum,quad,nodes=9,entity="fluidB")
1 6
4 8
elements(boundary,edge,nodes=3,entity="Top")
15 16
elements(boundary,edge,nodes=3,entity="Bottom")
1 2
bcnode(temperature,constant)
15 16 1
1 2 0
bcnode(velocity,constant)
2 6 0 0
5 6 0 0
5 8 0 0
1 2 0 0
1 3 0 0
3 4 0 0
4 7 0 0
9 12 0 0
12 11 0 0
11 15 0 0
15 16 0 0
16 14 0 0
14 13 0 0
13 10 0 0
bcnode(ux, constant)
8 10 0 0
7 9 0 0
/
```

```
/
end
fiprep
problem(nonlinear, 2-D,buoyancy,buoyancy=1,transient)
timeint(back,dt=0.0006,nofix=5,nsteps=1000,tend=6100000,species=
1)
pressure(mixed=1.0e-8,disc)
execution(newjob)
solution(segr=2000,velconv=0.0001,normal=40)
option(stress-divergence)
relax
0.12  0.12  0.12  0.0  0.01  0.6
gravity(magn=1)
/
$por=0.39
$perm=8.3e-9
/
cond(set=3,constant=2.088)
permeability(acoef,constant=1,x=$perm,y=$perm,porosity=$por)
/
/Physical parameters
/
dens (set=1, constant=967, TYP2, temperature, spec=1)
spec (set=1, constant=5.74)
visc (set=1, constant=1)
cond (set=1, constant=1)
volu (set=1, constant=1, temperature)
volu (set=2, constant=11.42, spec=1)
diff (set=2, constant=5.59e-6, species=1)
ther (set=1, constant)
-5.49e-07 0 0 0 0 0 0 0 0 0 0 0 0 0 0
renumber(profile)
icnode(temperature,constant=0.5,entity="porous")
icnode(temperature,constant=0.5,entity="fluidT")
icnode(temperature,constant=0.5,entity="fluidB")
icnode(species=1,constant=0.5,entity="porous")
icnode(species=1,constant=0.5,entity="fluidT")
icnode(species=1,constant=0.5,entity="fluidB")
entity(name="porous",porous,property="1",mdiff=2,sore,species=1,
mexp=2,maperm=1,mscond=3)
entity(name="fluidT",
fluid,property="1",mdiff=2,sore,species=1,mexp=2)
entity(name="fluidB",
fluid,property="1",mdiff=2,sore,species=1,mexp=2)
entity(name="Top",plot)
entity(name="Bottom",plot)
print(none)
```

```
data(control)
end
create(FISOLV)
```

REFERENCES

1. K. Shukla, A. Firoozabadi, “A New Model of Thermal Diffusion Coefficients in Binary Hydrocarbon Mixtures,” Ind. and Eng. Chem. Res. 37 (1998), No. 8, 3331-3342.
2. M.C. Charrier-Mojtabia, B. Elhajjarb, A. Mojtabi, “Analytical and Numerical Stability Analysis of Soret-Driven Convection in a Horizontal Porous Layer,” Physics of Fluids 19 (2007), No. 12, 1-14.
3. D. A. Nield, “Onset of Convection in a Fluid Layer Overlying a Layer of Porous Media,” Journal of Fluid Mechanics 81 (1977), 513-522.
4. C. W. Somerton, I. Catton, “On the Thermal Instability of Superposed Porous and Fluid Layers." Journal of Heat Transfer 104 (1982), Issue 1, 160 (6 pages).
5. M. Z. Saghir, P. Mahendran, M. Hennenberg, “Maragoni and Gravity Driven Convection in a Liquid Layer Overlying a Porous Layer: Lateral and Bottom Heating Conditions.”, Energy Sources Part A 27(2005), Issue: 785022370, 151-171
6. G. Pillastsis, M. E.Tasilm,U. Narusawa, “Thermal Instability of a Fluid-Saturated Porous Medium Bounded by Thin Fluid Layers.”, Journal of Heat Transfer 109 (1987), 677–682.
7. M.E. Taslim, U. Narusawa, “Thermal Stability of Horizontally Superposed Porous and Fluid Layers”, Journal of Heat Transfer 111 (1989), 357–362
8. K. Vafai, R. Thiyagaraja, “Analysis of Flow and Heat Transfer at the Interface Region of a Porous Medium”, International Journal of Heat and Mass Transfer 30 (1987), Issue 7, 1391-1405.
9. K. Vafaim, S.J. Kim, “Fluid Mechanics of the Interface Region between a Porous Medium and a Fluid Layer- An Exact Solution.”, International Journal of Heat and Fluid Flow11 (1990), Issue 3, 254-256
10. B. Alazmi, K. Vafai, “Analysis of Fluid Flow and Heat Transfer Interfacial Conditions Between a Porous Medium and a Fluid Layer.” International Journal of Heat and Mass Transfer 44 (2001), Issue 9, 1735-1749
11. J. C. Umavathi, I.C.Liu, J. Prathap-Kumar, D. Shaik-Meera, “Unsteady Flow and Heat Transfer of Porous Media Sandwiched Between Viscous Fluids.” Applied Mathematics and Mechanics (English Edition) 31(2010), 1497–1516.

12. Min-Hsing Chang, “Thermal Convection in Superposed Fluid and Porous Layers Subjected To a Horizontal Plane Couette Flow.” Phys. Fluids 17, 064106 (2005); doi:10.1063/1.1932312 (7 pages).
13. Min-Hsing Chang, “Thermal Convection in Superposed Fluid and Porous Layers Subjected To a Plane Poiseuille Flow.” Phys. Fluids 18, 035104 (2006); doi:10.1063/1.2182004 (10 pages).
14. Abdul-Fattah A.K. Bukhari, “Convection in a Horizontal Viscous Fluid Layer Sandwiched Between Tow Porous Layers.” Journal of Mathematics 37(2005), 17-30.
15. Falin Chenm“Through Flow Effects on Convective Instability in Superposed Fluid and Porous Layers.” J. Fluid Mech. 231 (1990), 113-133.
16. R. Balasubramanian, R. P. Thangaraj, “Thermal Convection in a Fluid Layer Sandwiched Between Two Porous Layers of Different Permeability.” Acta Mechanica 130 (1998), 1-2, 81-93.
17. N. Rudraiah, R. Sheela, J.K. Shrivashankara Murthy, “Flow Through a Sparsely Packed Porous Layer Sandwiched Between Two Fluid Layers,” Arabian J. Sci. Eng. 12 (4) (1987) 482.
18. V. Prasad and Q. Tian, “An Experimental Study of Thermal Convection in Fluid-Superposed Porous Layers Heated From Below,” Proceedings of the Ninth International Heat Transfer Conference, Vol. 5, pp. 207-212. Hemisphere, Washington, DC (1990).
19. V. Prasad, “Flow Instabilities and Heat Transfer in Fluid Overlying Horizontal Porous Layers,” Experimental Thermal and Fluid Science 6 (1993), 135-146.
20. C. Beckermann, S. Ramadhyani, R. Viskanta, “Natural Convection Flow and Heat Transfer Between a Fluid Layer and a Porous Layer Inside a Rectangular Enclosure,” J. Heat Transfer 109 (1987), Issue 2, 363 (8 pages)
21. P. Nithiarasu , K.N. Seetharamu, T. Sundararajan, “Effect of Porosity on Natural Convective Heat Transfer in a Fluid saturated Porous Medium,” International Journal of Heat and Fluid Flow19 (1998), Issue 1, 56-58.
22. K. Vafai, C. L. Tien, “Boundary and Inertia Effects on Flow and Heat Transfer in Porous Media,” International J. Heat and Mass Transfer 24 (1981), 195-203.

23. A. Raptis, G. Tzivanidis, N. Kafousias, “Free Convection and Mass Transfer Flow Througha Porous Medium Bounded By an Infinite Vertical Limiting Surface With Constant Suction,” Letters in Heat and Mass Transfer 8 (1981), Issue 5, 417-424.
24. Sung Jin Kim ,SeokPil Jang, “Effects of The Darcy number, The Prandtl Number and The Reynolds Number on Local Thermal Non-Equilibrium,” International Journal of Heat and Mass Transfer 45 (2002), 3885–3896.
25. Björn Huke and Manfred, “Convective Patterns in Binary Fluid Mixtures with Positive Separation Ratios,” Lecture Notes in Physics 584, Thermal Non-Equilibrium Phenomena in Fluid Mixtures, Eds. W. Koehler and S. Wiegand, p 334-354 (Springer, Berlin, 2002).
26. Md. Abdur Rahman, M.Z. Saghir**, “**Thermo-solutal Convection in Water-Isopropanol Mixtures in the Presence of Soret Effect,” International Journal of Fluid Mechanics Research 37 (2010), issue3, 237-250.
27. M. Eslamiani, M. M.Z. Saghir, “Dynamic Thermodiffusion Model for Binary Liquid Mixtures,” Physical Review E 80, No. 1, 011201.
28. A. Mansour, A. Amahmid M. Hasnaoui, “Soret Effect on Thermosolutal Convection Developed in a Horizontal Shallow Porous Layer Salted From Below and Subject to Cross Fluxes of Heat,” International Journal of Heat and Fluid Flow 29, 306–314.
29. K. Shukla, K. A Firoozabadi, “A New Model of Thermal Diffusion Coefficients in Binary Hydrocarbon Mixtures,” Ind. And Eng. Chem. Res. 37 (1998), 3331-42.
30. H. Davarzani, M. Marcoux , M. Quintard, “Theoretical Predictions of The Effective Thermodiffusion Coefficients in Porous Media,” International Journal of Heat and Mass Transfer 53 (2010), 1514–1528.
31. L.B. Benano-Melly, J.-P.Caltagirone, B. Faissat , F. Montel , P. Costeseque [*], Modeling Soretcoe • cient measurement experiments in porous media considering thermal and solutal convection, International Journal of Heat and Mass Transfer, Vol. 44, pp 1285-1297.
32. D.E. Melnikov ,V.M.Shevtsova, “Separation of a Binary Liquid Mixture in Compound System: Fluid–Porous–Fluid,” Acta Astronautica 69 (2011), Issues 7-8, 381-386
33. R. Bennacer, A. Mahidjiba, P. Vasseur, H. Beji, R. Duval, “The Soret Effect on Convection in a Horizontal Porous Domain Under Cross Temperature and Concentration

Gradients," Int. J. of Numerical Methods for Heat and Fluid Flow 13 (2003), Issue 2, 199 – 215.

34. A. Mansour, A. Amahmid, M. Hasnaoui, M. Bourich, "Numerical Study of The Multiplicity of Solutions Induced By Thermosolutal Convection in a Square Porous Cavity Heated from Below and Submitted to Horizontal Concentration Gradient in The Presence of Soret Effect," Numerical Heat Transfer, Part A 49 (2006), 69–94.
35. Safia Safi, SmailBenissaad, "Heat and Mass Transfer in Anisotropic Porous Media," Advances in Theoretical and Applied Mechanics 5 (2012), no. 1, 11 – 22.
36. C.G. Jiang, M. Z. Saghir, M. Kawaji, K. Ghorayeb," Two-Dimensional Numerical Simulation of Thermo-Gravitational Convection in a Vertical Porous Column Filled With a Binary fluid mixture," International Journal of Thermal Sciences43 (2004), Issue 11, 1057-1065
37. Pinghua Zhao, C. F. Chen, "Stability Analysis of Double-Diffusive Convection in Superposed Fluid and Porous Layers Using a One-Equation Model," International Journal of Heat and Mass Transfer 44(2001) , 4625-4633.
38. H.C. Brinkman, "A Calculation of Viscous Force Exerted By a Flowing Fluid on a Dense Swarm of Particles," Applied Science Research, 1947; A 1, 27-36.
39. Frank M. White, Fluid Mechanics 6th Edition, McGraw-Hill Series in Mechanical Engineering (2008), pp 287-291.
40. FIDAP software manual, 10.1 Overview.
41. Frank P. Incropera, David P. DeWitt, Fundamentals of Heat and Mass Transfer 4th Edition, John Wiley & Sons, (England, 1996), pp 535.
42. Clayton T. Crowe, Donald F. Elger, John A. Roberson. Engineering Fluid Mechanics 7th edition, John Wiley & Sons (Canada, 2001), pp 94.
43. Sung Jin Kim, Christopher Y. Choi, "Convective Heat Transfer in Porous and Overlying Fluid Layers Heated From Below," International Journal of Heat and Mass Transfer 39 (1996), No. 2, 319-329.
44. M.Z. Saghir, G.G. Hang, Yan M.Y. Chachat, M. Khawaja, S. Pan, Thermodiffusion in Porous Media, in: D. B. Ingham, I. Pop (Eds.), Transport Phenomena In Porous Media III, Elsevier Ltd. (Oxford, 2005), 227-260.

45. M.Z. Saghir, G.G. Hang, Yan M.Y. Chachat, M. Khawaja, S. Pan, Thermodiffusion in Porous Media, in: D. B. Ingham, I. Pop (Eds.), Transport Phenomena In Porous Media III, Elsevier Ltd. (Oxford, 2005), pp 228.
46. V. Shevtsova, D. Melnikov, J.C. Legros, Y. Yan, M.Z. Saghir, T. Lyubimova, G. Sedelnicov, B. Roux, "Influence of Vibrations on Thermodiffusion in Binary Mixture: A Benchmark of Numerical Solutions," Physics of Fluids 19 (2007), 017111.
47. I. Alloui, H. Benmoussa and P. Vasseur, " Soret and Thermosolutal Effects on Natural Convection in a Shallow Cavity Filled With a binary Mixture," International Journal of Heat and Fluid Flow 31 (2010), 191–200.
48. H. Brand, V. Steinberg, "Convective Instabilities in Binary Mixtures in A Porous Medium," Physica A: Statical Mechanics and its Applications 119 (1983), 327–338.
49. M.C. Charrier-Mojtabi, B. Elhajjar, A. Mojtabi, "Analytical And Numerical Stability Analysis of Soret-Driven Convection in a Horizontal Porous Layer," Physics of Fluids 19(2007), 1241041-12410414.
50. V.M. Shevtsova, D.E. Melnikov and J.C. Legros, "Onset of Convection in Soret Driven Instability," Physical Reviews E 73 (2006),047302.
51. M.L. Huber. NIST Thermophysical Properties of Hydrocarbon Mixtures Database (SUPERTRAPP) Version 3.2, Users' Guide (2007).
52. GAMBIT 2.2 user manual, 2004.
53. FLUENT 6.1 User's Guide, 2003.